“Anti-coronaviral activities of natural products and their derivatives’’

Kumulative Dissertation zur Erlangung des Grades

“Doktor der Naturwissenschaften’’

im Promotionsfach Pharmazie

Johannes Gutenberg Universität-Mainz

Vorgelegt von Nasim Shahhamzehei

Mainz, Juni 2025

“Anti-coronaviral activities of natural products and their derivatives’’

Kumulative Dissertation zur Erlangung des Grades

“Doktor der Naturwissenschaften’’

im Promotionsfach Pharmazie

Am Fachbereich Chemie, Pharmazie, Geographie und Geowissenschaften der Johannes Gutenberg Universität-Mainz

Vorgelegt von Nasim Shahhamzehei

Geboren am 27.12.1986 in Iran

Mainz, Juni 2025

Betreuer:

Prof. Dr. Thomas Efferth

Gutachter der Arbeit:

Prof. Dr. Thomas Efferth

Junior-Prof. Dr. Marie-Luise Winz

PD Dr. rer. nat. Marina Jendra

Datum der mündlichen Prüfung

Prüfungskommission:

Prof. Dr. Peter Langguth (Vorsitzender)

Prof. Dr. Thomas Efferth

Junior-Prof. Dr. Marie-Luise Winz

PD Dr. rer. nat. Marina Jendra

Dr. Mohamed Elbadawi (Protokoll)

List of publications

Original articles as first author

1. ***Shahhamzehei N**, Abdelfatah S, Efferth T. *In Silico* and *In Vitro* Identification of Pan-Coronaviral Main Protease Inhibitors from a Large Natural Product Library. Pharmaceuticals. 2022;15(3):1–19. **(IF 4.6)**
2. ***Shahhamzehei N**, Abdelfatah S, Schwarzer-Sperber HS, Sutter K, et al. Identification of nitrile-containing isoquinoline-related natural product derivatives as coronavirus entry inhibitors *in silico* and *in vitro*. Biomedicine and Pharmacotherapy. 2024;180:117517. **(IF 6.9)**
3. ***Shahhamzehei N**, Abdelfatah S, A. Omer E, Riedl M, Meesters C, Schwarzer-Sperber HS, et al. Diketopiperazine/piperidine alkaloid as a potential broad-spectrum coronaviral entry inhibitor identified by supercomputer-based virtual screening from a large natural product-based library. Biomedicine and Pharmacotherapy. 2025; 183:117841. **(IF 6.9)**

*****Articles included in this thesis

Original articles as co-author

1. Nabih HK, Yücer R, Mahmoud N, Dawood M, Elbadawi M, **Shahhamzehei N**, et al. The cytotoxic activities of the major diterpene extracted from Salvia multicaulis (Bardakosh) are mediated by the regulation of heat-shock response and fatty acid metabolism pathways in human leukemia cells. Phytomedicine. 2024;135:156023. **(IF 6.7)**
2. Chen X, Bahramimehr F, **Shahhamzehei** N, Fu H, Lin S, Wang H, et al. Anti-aging effects of medicinal plants and their rapid screening using the nematode Caenorhabditis elegans (Review). Phytomedicine. 2024;129(April):155665. **(IF 6.7)**
3. Khalid SA, Dawood M, Boulos JC, Wasfi M, Drif A, Bahramimehr F, **Shahhamzehei N,** et al. Identification of Gedunin from a Phytochemical Depository as a Novel Multidrug Resistance-Bypassing Tubulin Inhibitor of Cancer Cells. Molecules. 2022;27(18). **(IF 4.6)**
4. Ielo L, Patamia V, Citarella A, Efferth T, **Shahhamzehei N**, Schirmeister T, et al. Novel Class of Proteasome Inhibitors: *In Silico* and *In Vitro* Evaluation of Diverse Chloro(trifluoromethyl)aziridines. Int J Mol Sci. 2022;23(20). **(IF 5.6)**
5. Bahramimehr F, Kurz S, Hai Y, Yücer R, **Shahhamzehei N**. Supercomputer-Based Drug Repurposing to Inhibit Oncostatin M in Crohn ' s Disease. Molecules, (Under revision).

6. A. Omer E, Abdelfatah S, **Shahhamzehei N**, Sutter K, Schwarzer-sperber HS, Schwarzer R, et al. Repurposing of FDA-approved drugs against nsp16 proteins of SARS-CoV-2, SARS-CoV-1, and MERS-CoV in silico and in cell culture. Molecules, (Under revision).
7. Ayoobi A, **Shahhamzehei N**, Lu X, Schwarzer-Sperber HS, Sutter K, Schwarzer R, et al. In Silico and In Vitro Identification of Inhibitors Targeting Functional and Structural SARS-CoV-2 Proteins from a Library of 415 Artemisinin Derivatives. (Submitted).

Conferences

1. **Phytochemical Society of Europe, Natural Drug Discovery Current Approach and Future Perspectives, 12-15 October 2023, Antalya Türkiye.**
   Poster Presentation

   • Potential Coronaviral entry Inhibitors Identified *In Silico* and *In Vitro* from a Large Natural Product Library. Shahhamzehei N, Efferth T.
2. **Phytotherapiekongress 2023 - Phytotherapie im 21. Jahrhundert, 15-17 Jun 2023 Bamberg Germany.**
   Poster Presentation

   • *In-silico*- und *In-vitro*-Identifizierung von pan-coronaviralen Hauptprotease-Inhibitoren aus einer großen Naturstoffbibliothek. Shahhamzehei N, Efferth T. DOI: 10.1055/s-0043-1769557.

Contribution to the articles included in the thesis

1. **Title: *In Silico* and *In Vitro* Identification of Pan-Coronaviral Main Protease Inhibitors from a Large Natural Product Library.**
   Contribution:
   - Conceptualization.
   - Methodology and Conduction of the *in silico* and *in vitro* experiments including PyRx screening, molecular docking, sequence alignment, enzyme inhibition assay, microscale thermophoresis (MST), cell viability assay.
   - Data analysis and curation.
   - Data visualization and presentation of figures except figure 1.
   - Writing the paper.

2. **Title: Identification of nitrile-containing isoquinoline-related natural product derivatives as coronavirus entry inhibitors *in silico* and *in vitro*. Contribution:**
    - Conceptualization.
    - Methodology and Conduction of the *in silico* and *in vitro* experiments including PyRx screening, molecular docking, sequence alignment, plasmid amplification, plasmid extraction and purification, production of SARS-CoV-2 pseudoviruses, luciferase assay, microscale thermophoresis (MST), cell viability assay.
    - Data analysis and curation.
    - Data visualization and presentation of all figures.
    - Writing the paper.

3. **Title: Diketopiperazine/piperidine alkaloid as a potential broad-spectrum coronaviral entry inhibitor identified by supercomputer-based virtual screening from a large natural product-based library.**
   Contribution:
    - Conceptualization.
    - Methodology and Conduction of the *in silico* and *in vitro* experiments including molecular docking, sequence alignment, plasmid amplification, plasmid extraction and purification, production of SARS-CoV-2 pseudoviruses, luciferase assay, microscale thermophoresis (MST), cell viability assay.
    - Data analysis and curation.
    - Data visualization and presentation of figures except figure 1.
    - Writing the paper.

Erklärung.

Hiermit erkläre ich an Eides statt, dass ich diese Arbeit selbstständig verfasst und keine anderen als die angegebenen Quellen und Hilfsmittel verwendet habe.

_____ _____

Ort, Datum

Acknowledgment

I sincerely thank Prof. Dr. Thomas Efferth for his invaluable guidance and support throughout my PhD. His expertise and encouragement have been instrumental in my growth as a researcher. Despite the challenges of the past five years, this journey has been an exceptional experience, shaping me both professionally and personally. I am deeply grateful for the opportunity to join his group and for his unwavering faith in me, which kept me motivated and confident.

My thank is extended to my collaborators, especially, Prof. Dr. Gerhard Bringmann, for his guidance and support and Dr. Roland Schwarzer for performing live SARS-CoV2 investigations.

I would like to thank Prof. Dr. Peter Langguth ,Junior-Prof. Dr. Marie-Luise Winz and PD Dr. rer. nat. Marina Jendra for their time and for being part of my examination committee.

I express my deepest gratitude to my colleagues in the department of pharmaceutical biology for the unique, welcoming, and supportive environment we have put together. For their scientific support and knowledge sharing as well.

My deep gratitude is to my parents Soheyla Ahmadi and Ali Shahhamzehei for their unconditional love, encouragement and support during this journey, and my husband Amirabbas Nematzadeh who has been a constant source of love, strength, understanding, and encouragement.

Last but not least, I have special thanks to my friends in Iran, Germany and United States who have always been a major source of support when things would get discouraging: Dr. Sara Abdelfatah, Dr.Mona Dawood, Dr. Mohamed Elbadawi, Dr. Xiaohua Lu, Dr. Rümeysa Yücer, Ejlal Omar, Faranak Bahramimehr, Assia Drif, and Mahsa Gheysour.

Thanks to Dr. Georg Scheuing Foundation for awarding me a two years scholarship to conduct my PhD studies.

Abstract

The COVID-19 pandemic, caused by SARS-CoV-2, has had a profound impact on global health and economies, highlighting the urgent need for novel, effective antiviral agents. Following its first report in Wuhan, China in 2019, it quickly spread around the world with more than 7 million fatalities and over 777 million reported cases as of February 2025. While vaccines have played a crucial role in decreasing disease severity, the continuous emergence of new mutant strains, particularly the Omicron subvariants, poses a significant challenge. These variants have demonstrated an increased ability to evade immune detection, reducing the efficacy of existing vaccines and antibody therapies. Moreover, the period between disease outbreaks has become shorter, and there is a possibility that more viral epidemics will occur soon. Thus, the identification of pan-coronaviral inhibitors, capable of targeting viral structures essential for replication and host entry, is crucial for pandemic preparedness and long-term antiviral strategies. The present PhD thesis demonstrates that natural product derivatives can serve as pan-coronaviral inhibitors.

The main protease (M^{pro} or $3CL^{pro}$) in coronaviruses represents a promising specific drug target as it is essential for the cleavage of the virus polypeptide and has a unique cleavage site that does not exist in human host proteases. Here we explored potential natural pan-coronavirus drugs using *in vitro* and *in silico* approaches and three coronavirus main proteases as treatment targets. Hypericin, rosmarinic acid, isorhamnetin, and luteolin inhibited M^{pro} of SARS-CoV-2, while hypericin and isorhamnetin inhibited M^{pro} of SARS-CoV-1; hypericin showed inhibitory effects toward M^{pro} of MERS-CoV. Microscale thermophoresis confirmed the binding of these compounds to M^{pro} with high affinity. Cytotoxity results showed that rosmarinic acid and luteolin were not cytotoxic toward MRC-5 cells, whereas hypericin and isorhamnetin showed slightl toxicity. These findings highlight hypericin's potential as a lead compound for further development in antiviral drug discovery as a pan-anti-coronaviral agent by binding to and inhibiting M^{pro} of several human-pathogenic coronaviruses.

The receptor-binding domain (RBD) within the S1 subunit plays a pivotal role in binding to the angiotensin-converting enzyme 2 (ACE2) receptor on host cells, facilitating viral entry, represents a promising target for therapeutic intervention. We demonstrated that a diketopiperazine/piperidine alkaloid and natural isoquinoline derivatives inhibited SARS-CoV-2 pseudovirus and live virus entry in host cells while showing low toxicity. Microscale thermophoresis revealed these compounds strongly bound to the RBDs of SARS-CoV-2,

SARS-CoV-2 XBB, SARS-CoV-1, MERS-CoV, and HCoV-HKU1, with their K_d values increasing as RBD sequence similarity decreased. These findings showed that these compounds, should be considered for further development as potential pan-coronavirus entry inhibitors.

Zusammenfassung

Die COVID-19-Pandemie, die durch SARS-CoV-2 verursacht wurde, hatte tiefgreifende Auswirkungen auf die globale Gesundheit und Wirtschaft und macht deutlich, dass dringend neue, wirksame antivirale Mittel benötigt werden. Nach der ersten Meldung in Wuhan, China, im Jahr 2019 breitete sich die Krankheit schnell auf der ganzen Welt aus und forderte bis Februar 2025 mehr als 7 Millionen Todesopfer und über 777 Millionen gemeldete Fälle. Während Impfstoffe eine entscheidende Rolle bei der Verringerung der Krankheitsschwere gespielt haben, stellt das kontinuierliche Auftreten neuer mutierter Stämme, insbesondere der Omicron-Subvarianten, eine große Herausforderung dar. Diese Varianten haben eine erhöhte Fähigkeit gezeigt, sich der Immunerkennung zu entziehen, was die Wirksamkeit bestehender Impfstoffe und Antikörpertherapien verringert. Außerdem sind die Zeiträume zwischen den Krankheitsausbrüchen kürzer geworden, und es besteht die Möglichkeit, dass bald weitere Virusepidemien auftreten werden. Daher ist die Identifizierung von pan-coronaviralen Inhibitoren, die auf virale Strukturen abzielen, die für die Replikation und den Eintritt in den Wirt wichtig sind, von entscheidender Bedeutung für die Pandemievorsorge und langfristige antivirale Strategien. Die vorliegende Dissertation zeigt, dass Naturstoffderivate als pan-coronavirale Inhibitoren fungieren können.

Die Hauptprotease (M^{pro} oder $3CL^{pro}$) in Coronaviren stellt ein vielversprechendes spezifisches Arzneimittelziel dar, da sie für die Spaltung des Viruspolypeptids unerlässlich ist und eine einzigartige Spaltstelle aufweist, die in menschlichen Wirtsproteasen nicht existiert. Hier haben wir potenzielle natürliche Pan-Coronavirus-Medikamente mit Hilfe von In-vitro- und In-silico-Ansätzen und drei Coronavirus-Hauptproteasen als Behandlungsziele untersucht. Hypericin, Rosmarinsäure, Isorhamnetin und Luteolin hemmten M^{pro} von SARS-CoV-2, während Hypericin und Isorhamnetin M^{pro} von SARS-CoV-1 hemmten; Hypericin zeigte hemmende Wirkungen auf M^{pro} von MERS-CoV. Die mikroskalierte Thermophorese bestätigte die Bindung dieser Verbindungen an M^{pro} mit hoher Affinität. Die Ergebnisse der Zytotoxizität zeigten, dass Rosmarinsäure und Luteolin für MRC-5-Zellen nicht zytotoxisch waren, während

Hypericin und Isorhamnetin eine leichte Toxizität aufwiesen. Diese Ergebnisse unterstreichen das Potenzial von Hypericin als Leitwirkstoff für die weitere Entwicklung von antiviralen Arzneimitteln als pan-anti-coronavirales Mittel, da es an M^{pro} mehrerer humanpathogener Coronaviren bindet und diese hemmt.

Die rezeptorbindende Domäne (RBD) innerhalb der S1-Untereinheit spielt eine zentrale Rolle bei der Bindung an den Angiotensin-Converting Enzyme 2 (ACE2)-Rezeptor auf den Wirtszellen, wodurch das Eindringen des Virus erleichtert wird, und stellt ein vielversprechendes Ziel für therapeutische Maßnahmen dar. Wir konnten zeigen, dass ein Diketopiperazin/Piperidin-Alkaloid und natürliche Isochinolin-Derivate das Eindringen des SARS-CoV-2-Pseudovirus und des lebenden Virus in Wirtszellen hemmen und gleichzeitig eine geringe Toxizität aufweisen. Die mikroskalierte Thermophorese ergab, dass diese Verbindungen stark an die RBDs von SARS-CoV-2, SARS-CoV-2 XBB, SARS-CoV-1, MERS-CoV und HCoV-HKU1 gebunden waren, wobei ihre Kd-Werte mit abnehmender RBD-Sequenzähnlichkeit zunahmen. Diese Ergebnisse zeigten, dass diese Verbindungen für die weitere Entwicklung als potenzielle Pan-Coronavirus-Eintrittsinhibitoren in Betracht gezogen werden sollten.

Table of content

1 Introduction

Natural products provide a rich resource of a variety of bioactive components that have the abilities to inhibit the replication cycle of various types of DNA or RNA viruses (1,2). Several bioactive compounds, including flavonoids, terpenoids, alkaloids, and phenolics, have shown inhibitory effects on key viral targets such as the main protease (M^{pro}), papain-like protease (PL^{pro}), and the receptor binding domain (RBD) of the spike protein. For instance, sanggenon G has demonstrated inhibitory activity against the main protease (M^{pro}) of SARS-CoV2 (3). EGCG, the most active compound extracted from green tea and betulinic acid, is reported to blocks the binding and attachment of the RBD to the ACE2 receptor, reducing the infection rate, inhibiting virus infections (4).

The first project aims to explore potential natural pan-coronavirus compounds using *in silico* and *in vitro* approaches against several coronavirus main protease (M^{pro}) as an ideal drug target due to its specificity and a high degree of structural similarity and conservation of the active site across various coronavirus M^{pro}.

In the second and third project, spike protein as the viral entry mediator were targeted to investigate natural pan-coronavirus entry-inhibitors conducting high-throughput virtual screening, pseudotyped lentiviruses and live viruses.

1.1 Human coronavirus overview

Coronaviruses (CoVs) constitute a highly diverse family of enveloped, positive-sense single-stranded RNA viruses genomes of approximately 26–32 kb, which is currently the largest known genome size for an RNA virus (5). These viruses can infect humans, various mammals, and avian species, including livestock and companion animals. As a result, they pose significant challenges not only to public health but also to veterinary practice and the global economy (6). The highly pathogenic human coronaviruses belong to the subfamily Coronavirinae from the family Coronaviridae, this family, together with the Roniviridae, the Arteriviridae, and the Mesoniviridae, belong to the Nidovirales order (7). The viruses in Coronaviridae subfamily, group into four genera: alpha-coronavirus, beta-coronavirus, gamma-coronavirus, and delta-coronavirus. Whereas alpha-coronaviruses and beta-coronaviruses exclusively infect mammalian species, gamma-coronaviruses and delta-coronaviruses have a wider host range that includes avian species(8). Human and animal coronavirus infections mainly result in respiratory and enteric diseases. Human coronaviruses, such as HCoV-229E and HCoV-OC43,

have long been known to circulate in the population and they, together with the more recently identified HCoV-NL63 and HCoV-HKU1, cause seasonal and usually mild respiratory tract infections associated with symptoms of the common cold (9). Whereas severe acute respiratory syndrome coronavirus (SARS-CoV), Middle East respiratory syndrome coronavirus (MERS-CoV) and SARS-CoV-2, which have emerged in the human population over the past 20 years, are highly pathogenic. By infecting bronchial epithelial cells, pneumocytes and upper respiratory tract cells in humans, SARS-CoV, MERS-CoV and SARS-CoV-2 infections can develop into severe, life-threatening respiratory pathologies and lung injuries (10).

1.1.1 Structural studies of SARS-CoV2

SARS-CoV-2 comprises both structural and non-structural proteins (nsps). The region responsible for encoding replication enzymes contains open reading frames (ORFs), specifically ORF1a and ORF1b. In all coronaviruses (CoVs), the ORF1 downstream regions include specific genes that encode proteins involved in nucleocapsid formation, spike protein synthesis, and viral replication. ORF1a/b, located at the 5′ end, encodes sixteen highly conserved nsps derived from polyproteins pp1a and pp1b. Meanwhile, the structural proteins—envelope protein (E), spike protein (S), nucleocapsid protein (N), and membrane protein (M)—are encoded by ORFs positioned at the 3′ end. The viral envelope consists of three key proteins: M, E, and S. Among them, the M protein facilitates viral assembly and budding by interacting with the nucleocapsid and host membranes. The E protein plays a multifunctional role during infection, contributing to viral morphogenesis, release, and pathogenesis. Additionally, the S protein, a homotrimeric structure on the viral surface, is crucial for host cell receptor recognition and is essential for viral infectivity.(11,12).

1.1.2 SARS-CoV2 life cycle

The SARS-CoV-2 life cycle begins when the receptor-binding domain (RBD) of the S1 subunit of the spike protein interacts with angiotensin-converting enzyme 2 (ACE2), which is expressed on the surface of epithelial cells in the respiratory tract and intestines. Following this initial contact, the virus enters host cells either through direct fusion of viral and cellular membranes or via endocytosis, facilitated by the S2 subunit of the spike protein. The spike protein is initially synthesized as an inactive precursor, requiring cleavage by cellular proteases to induce conformational changes in the S2 subunit, thereby activating the protein for membrane fusion. In the direct fusion pathway, transmembrane protease serine 2 (TMPRSS2)

cleaves the spike protein near ACE2 after the formation of the spike-ACE2 complex, which subsequently triggers membrane fusion and the release of the viral genome into the host cell. Additional proteases, including trypsin, plasmin, and factor Xa, may also contribute to this process (13,14). Alternatively, the virus can enter the host cell via an endocytosis-mediated mechanism, where spike protein activation occurs within endosomes due to the enzymatic action of furin and cathepsins B/L (CatB/L) in endo-lysosomes. This process facilitates the fusion of the viral envelope with the host cell membrane, leading to the release of viral RNA into the cytoplasm (15). The genomic viral RNA in the cytoplasm of infected cells can be translated into two polyproteins, pp1a and pp1ab, which are processed by two viral proteases, 3C-like protease ($3CL^{pro}$), also known as the main protease (M^{pro}), and papain-like protease (PL^{pro}), to generate 16 mature non-structural proteins (NSPs). Among them, NSP12, also known as RNA-dependent RNA polymerase (RdRp), assembles with several NSPs to form a replication and transcription complex (RTC) anchored on double-membrane vesicles (DMVs), responsible for the viral genome replication and transcription. The viral RNA products are localized in the DMVs and transported to the cytosol through a molecular pore complex across the double membrane. Then, structural proteins including spike (S), envelope (E), membrane (M) proteins are translated in the endoplasmic reticulum (ER) and transported to the Golgi apparatus for virion assembly. The viral genomic RNA and the structural protein N are biosynthesized and assembled into the nucleocapsid in the cytoplasm and then associated with the viral structural proteins to produce new virions. In the end, virions are released from the infected cell through exocytosis (**Figure 1)** (16).

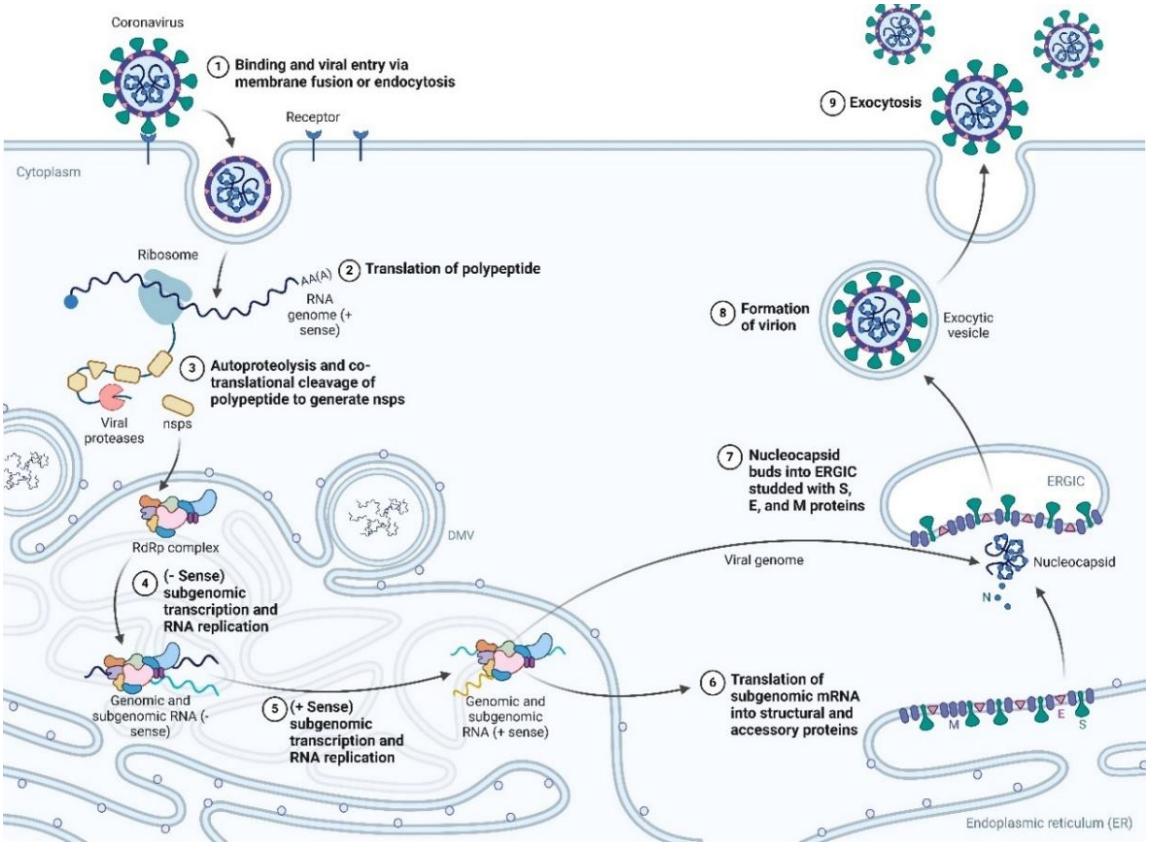

Fig 1 Coronaviruses life cycle (17) (taken from Hartenian E, Nandakumar D, Lari A, Ly M, Tucker JM, Glaunsinger BA. The molecular virology of coronaviruses. Journal of Biological Chemistry. 2020;295(37):12910–34. With permission from The American Society for Biochemistry and Molecular Biology, Inc; © 2020 Hartenian et al. This work is licensed under the Creative Commons Attribution 4.0 International License. To view a copy of this license, visit http://creativecommons.org/licenses/by/4.0/ or send a letter to Creative Commons, PO Box 1866, Mountain View, CA 94042, USA).

1.1.3 Molecular pathogenesis of SARS-CoV-2

Upon infection with the SARS-CoV-2 genome, the host cell activates a rapid and well-coordinated immune response, encompassing both innate and adaptive immunity, which serves as the first line of defense against viral infection (18). Within the endosome, membrane-specific pattern recognition receptors (PRRs), including Toll-like receptors (TLR3, TLR7, TLR8, and TLR9), cytosolic RNA sensors such as RIG-I and MDA5, and secretory PRRs like mannose-binding lectin (MBL) and C-reactive protein (CRP), detect viral RNA as pathogen-associated molecular patterns (PAMPs) (19). Type I interferons (IFNs) play a crucial role in initiating a potent innate immune response against viral infection while also promoting an effective

adaptive immune response. This recognition event triggers a complex signaling cascade involving the recruitment of adaptor proteins such as mitochondrial antiviral-signaling protein (MAVS), IFN-β (TRIF), and stimulator of interferon genes protein (STING), which subsequently activate downstream signaling molecules, including the adaptor molecule MyD88. These interactions lead to the activation of transcription factors such as nuclear factor-κB (NF-κB) and interferon regulatory factor 3 (IRF3), which then translocate into the nucleus. Inside the nucleus, these transcription factors drive the production of type I IFNs (IFN-α/β) and a range of proinflammatory cytokines, particularly IL-6. Consequently, interactions between the virus and host cell generate a multifaceted first-line defense at the site of viral entry. Type I IFN-mediated activation of the JAK-STAT pathway induces the transcription of IFN-stimulated genes (ISGs) under the regulation of the IFN-stimulated response element (ISRE). The accumulation of type I IFNs can suppress viral replication and function as immune modulators, facilitating antigen phagocytosis by macrophages and promoting the elimination of infected cells by natural killer (NK) cells. Therefore, disruptions in IFN production, alterations in the JAK-STAT signaling pathway, or dysregulation of macrophage expression can significantly impact viral survival within the host cell. In general, Th1-mediated immune responses play a central role in adaptive immunity against viral infections. T cell responses are largely dependent on the cytokine microenvironment established by antigen-presenting cells (APCs). CD8+ cytotoxic T lymphocytes (CTLs) are critical for the clearance of virus-infected cells, as they secrete cytotoxic molecules such as granzymes, perforin, and IFN-γ. Meanwhile, CD4+ helper T cells support the overall adaptive immune response by assisting cytotoxic T cells. Additionally, the B cell-mediated humoral immune response plays a protective role by generating neutralizing antibodies, thereby preventing reinfection (20). Recent studies in COVID-19 patients have revealed an elevated presence of plasma cytokines and chemokines, including interleukins (IL-1, IL-2, IL-4, IL-7, IL-10, IL-12, IL-13, and IL-17), IP-10, macrophage colony-stimulating factor (MCSF), monocyte chemoattractant protein-1 (MCP-1), granulocyte colony-stimulating factor (GCSF), hepatocyte growth factor (HGF), IFN-γ, macrophage inflammatory protein-1α (MIP-1α), and tumor necrosis factor-α (TNF-α), which are linked to disease severity (21). Similar to SARS and MERS, the presence of “lymphopenia” and a “cytokine storm” is believed to play a key role in COVID-19 pathogenesis (22). Furthermore, as observed in cancer and other chronic infections, prolonged cytokine storms can induce necrosis or apoptosis of T cells, leading to T cell exhaustion (23). This excessive cytokine release, or "cytokine storm," is a major driver of viral sepsis and inflammation-induced lung injury, which in turn contributes to complications such as acute respiratory

distress syndrome (ARDS), pneumonitis, respiratory failure, septic shock, organ failure, and, in severe cases, death. The severity of COVID-19 is also associated with a significant reduction in circulating B cells, CD8+ T cells, CD4+ T cells, NK cells, eosinophils, monocytes, and basophils (24).

1.1.4 Clinical presentation of COVID-19

In general, common cold coronaviruses (CoVs) primarily cause mild upper respiratory tract (URT) symptoms and occasionally accompanied by gastrointestinal involvement. The most frequently reported symptoms include fever, cough, and difficulty breathing (dyspnea). In contrast, infection with highly pathogenic CoVs, including SARS-CoV-2, leads to severe influenza-like symptoms that may escalate to acute respiratory distress syndrome (ARDS), pneumonia, renal failure, and, in severe cases, death (**Figure 2**). The incubation period for COVID-19 is relatively short, averaging approximately 5-6 days, compared to the 2-11 days observed in SARS-CoV infections. Beyond acute respiratory and gastrointestinal illness, COVID-19 can also result in long-term complications, such as myocardial inflammation. Additionally, while severe COVID-19 cases have been widely associated with older populations, emerging evidence suggests that children and young adults are also susceptible to severe disease manifestations (25,26).

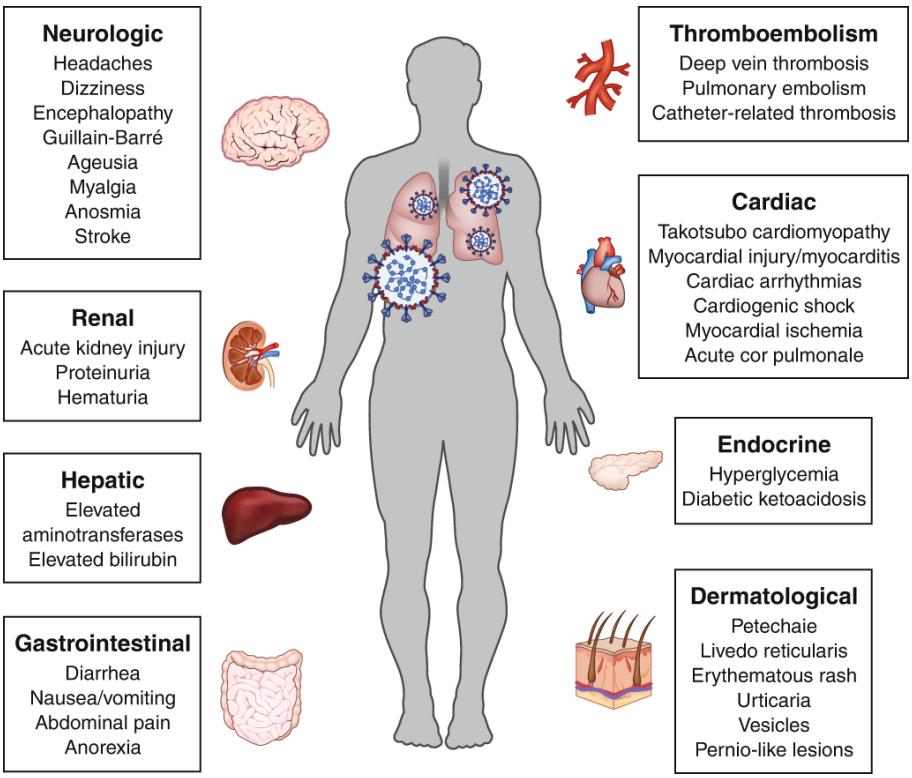

Fig. 2 Clinical symptoms of COVID-19 (26). (Taken from Gupta A, Madhavan M V., Sehgal K, Nair N, Mahajan S, Sehrawat TS, et al. Extrapulmonary manifestations of COVID-19. 2020;26(7):1017–32. With permission from springer nature; license Number 5976500668159.)

1.2 Viral targets for antiviral agents

The development of virus-targeted inhibitors aims to block different stages of the SARS-CoV-2 life cycle, including entry (spike inhibitors), proteolytic processing (main protease inhibitors, papain-like protease inhibitors), RNA synthesis (NSP12 to NSP16 inhibitors) and assembly (nucleocapsid inhibitors) (27).

1.2.1 Spike

The SARS-CoV-2 spike protein is a homotrimeric fusion glycoprotein located on the virion surface and plays a crucial role in viral entry, making it a prime target for antiviral interventions. In most cases, host proteases cleave the spike protein into two subunits: S1, responsible for receptor binding, and S2, which mediates membrane fusion. These subunits are extensively shielded by N-linked and O-linked glycans. Following significant conformational rearrangements, the receptor-binding domain (RBD) of the spike protein binds to angiotensin-converting enzyme 2 (ACE2) on the host cell surface with high affinity approximately 22 times stronger than the binding affinity of the SARS-CoV spike protein for ACE2. Subsequent structural transitions and proteolytic cleavages facilitate the formation of a three-helix bundle in the post-fusion conformation, enabling the fusion of the viral membrane with the host plasma membrane. To disrupt this process, various inhibitors have been developed to block spike-ACE2 interaction or membrane fusion, including neutralizing antibodies, small-molecule inhibitors, and peptide-based inhibitors (28,29).

1.2.1.1 Anti-spike antibodies

Over 300 monoclonal antibodies (mAbs) targeting SARS-CoV-2 have been identified, including bebtelovimab, sotrovimab, regdanvimab, bamlanivimab combined with etesevimab, cilgavimab paired with tixagevimab, casirivimab with imdevimab, and amubarvimab alongside romlusevimab. Many of these mAbs and antibody cocktails have received authorization for early treatment in outpatients with mild to moderate COVID-19. However, with the continuous emergence of SARS-CoV-2 variants, most existing anti-spike antibodies exhibit reduced or no activity against Omicron variants of concern, such as BA.1, BA.1.1, BA.2, BA.4, and BA.5.

This is largely due to the high mutability of the SARS-CoV-2 spike protein, which facilitates the development of drug-resistant mutations (30,31).

1.2.1.2 Anti-spike small molecules and peptides

Small-molecule inhibitors, such as clofazimine and etravirine, have been investigated for their potential to inhibit the SARS-CoV-2 spike protein; however, no results from late-stage clinical trials have been reported to date (32). Additionally, several potent anti-spike peptide inhibitors, derived from the heptad repeat α-helix regions of SARS-CoV-2, SARS-CoV, MERS-CoV, and HIV-1 spike proteins, were first identified by Jiang's group. Among these, EK1, a 36-amino-acid pan-coronavirus fusion peptide inhibitor derived from the heptad repeat 2 region of SARS-CoV-2, is currently undergoing phase I clinical trials for COVID-19 (33–36). Despite their strong antiviral activity and favorable safety profile, peptide inhibitors may be limited by challenges such as low oral bioavailability, metabolic instability, and short circulation time (37).

1.2.2 Main protease (NSP5)

The SARS-CoV-2 main protease (M^{pro}), also known as 3C-like protease, is a cysteine protease responsible for cleaving the pp1a and pp1ab polyproteins, thereby releasing viral non-structural proteins (NSPs) 4 to 16. Inhibiting M^{pro}-mediated proteolytic cleavage prevents the maturation of key viral enzymes such as NSP12 and NSP13, ultimately blocking viral replication. Structurally, the SARS-CoV-2 M^{pro} homodimer exhibits a strong preference for hydrolyzing glutamine residues at the P1 position within the cleavage motif Gln↓(Ser/Ala/Asn) (38). While no known human protease shares the primary cleavage specificity of Mpro, certain human cysteine proteases can cleave at the C-terminal side of glutamine residues, necessitating careful evaluation of potential cross-specificity when designing M^{pro} inhibitors. Each subunit of the M^{pro} homodimer contains a catalytic dyad composed of a nucleophilic cysteine (Cys145) and a histidine residue (His41), which catalyzes the formation of a covalent carbon–sulfur bond between the Cys145 thiolate and the main-chain carbonyl of the substrate's P1 glutamine (39). To date, over 100 M^{pro} inhibitors have been identified, with leading candidates including nirmatrelvir, ensitrelvir, and SIM0417 (40). These inhibitors can be classified into four groups based on their mechanisms of action. Class (i) includes peptidomimetic inhibitors that covalently bind to the M^{pro} catalytic pocket, such as nirmatrelvir, which has demonstrated efficacy against various SARS-CoV-2 variants in cell culture and significantly reduces viral loads in animal models, including mice and hamsters (41). Since nirmatrelvir is primarily

metabolized by human liver cytochrome P450 3A4 (CYP3A4), it is co-administered with ritonavir—an FDA-approved HIV protease inhibitor that lacks direct anti-coronavirus activity—to inhibit CYP3A4-mediated metabolism, thereby enhancing nirmatrelvir's therapeutic concentration (42). The combination of nirmatrelvir and ritonavir, marketed as Paxlovid, received its first Emergency Use Authorization (EUA) in the United States in December 2021, followed by regulatory approvals in multiple countries. It is now recommended as an early treatment option for outpatients with mild-to-moderate COVID-19 who are at high risk of disease progression. However, preliminary studies have indicated occasional COVID-19 rebound following Paxlovid treatment, and naturally occurring mutations, such as E166V in Mpro, may confer resistance to both nirmatrelvir and ensitrelvir. Additionally, Paxlovid is contraindicated in patients with severe renal or hepatic impairment, those with a history of significant hypersensitivity reactions, and individuals taking medications that result in significant drug–drug interactions. Future research should focus on monitoring drug-resistant mutations and potential drug interactions, particularly with CYP3A4 inducers that could impact the safety and efficacy of the nirmatrelvir-ritonavir combination (43). Class (ii) consists of non-peptidomimetic inhibitors that covalently bind to the Mpro catalytic pocket, such as myricetin derivatives, though further optimization is required to improve specificity and minimize off-target effects. Class (iii) includes orthosteric inhibitors that engage the Mpro substrate-binding pocket via non-covalent, reversible interactions, such as ensitrelvir. Notably, ensitrelvir received emergency regulatory approval in Japan in November 2022. However, data from the phase III SCORPIO-HR trial in May indicated that it did not achieve its primary endpoint of a statistically significant reduction in the time to sustained resolution of 15 common COVID-19 symptoms compared to placebo. Class (iv) comprises non-covalent inhibitors that target allosteric sites, primarily aiming to disrupt M^{pro} dimer formation, such as colloidal bismuth subcitrate. Nevertheless, further refinement is needed to enhance their potency and selectivity against M^{pro} (44).

1.2.3 Papain-like protease (part of NSP3)

Papain-like protease (PL^{pro}) is a cysteine protease that plays a dual role in the SARS-CoV-2 life cycle. It cleaves the pp1a and pp1ab polyproteins to release viral non-structural proteins (NSP1, NSP2, and NSP3) while also deubiquitinating host proteins by removing ubiquitin and ubiquitin-like interferon-stimulated gene 15 (ISG15) from signaling proteins, thereby suppressing innate immune responses. The catalytic site of PL^{pro} consists of a classical catalytic triad (Cys111–His272–Asp286) that preferentially cleaves the tetrapeptide motif LXGG↓XX

in adjacent viral proteins (NSP1–NSP2, NSP2–NSP3, NSP3–NSP4) as well as the C-terminal tails of cellular ubiquitin and ISG15. Additionally, a flexible β-hairpin loop, known as blocking loop 2 (BL2), located approximately 15 Å from the catalytic site, regulates substrate access to the active site (45). To date, more than 30 potent PL^{pro} inhibitors have been identified, which can be categorized into three main groups based on their mechanisms of action. Class (i) includes covalent inhibitors that form a C-S thioether bond with the catalytic cysteine, such as VIR250 and VIR251 (46); Class (ii) comprises non-covalent inhibitors that prevent PL^{pro} substrate entry into the catalytic site, including acriflavine and GRL0617 (47); Class (iii) consists of non-covalent inhibitors that bind to allosteric sites, such as HE9, thereby modulating PL^{pro} activity indirectly (48). Inhibition of PL^{pro} not only disrupts viral protein maturation but also restores the host immune response. However, designing selective PL^{pro} inhibitors poses a significant challenge due to its structural similarity to a broad family of human deubiquitinating enzymes (DUBs) and DUB-like proteases, which also recognize ubiquitin or ubiquitin-like proteins. While DUBs and DUB-like proteases are under investigation as therapeutic targets for various human diseases, no inhibitors targeting these enzymes have been approved yet. Future research may focus on optimizing non-covalent PL^{pro} inhibitors from class (ii) to improve selectivity and potency while minimizing cross-reactivity with human homologous DUB and DUB-like proteases (49).

1.2.4 RNA-dependent RNA polymerase (NSP12)

SARS-CoV-2 RNA-dependent RNA polymerase (RdRp), encoded by NSP12, is a highly conserved enzyme essential for viral RNA replication and transcription. RdRp inhibitors are categorized into nucleos(t)ide analogues, such as remdesivir and molnupiravir, and non-nucleos(t)ide analogues, such as suramin, each with distinct mechanisms of action (50). Remdesivir was initially synthesized in 2013 as part of efforts to develop a potent nucleoside inhibitor targeting the respiratory syncytial virus. During the 2014–2016 Ebola virus outbreak, remdesivir demonstrated strong antiviral activity against Ebola, but its clinical application was discontinued due to limited efficacy in infected patients. Following the emergence of COVID-19, remdesivir exhibited promising antiviral effects against SARS-CoV-2 in both preclinical and clinical studies. It is widely accepted that early administration of remdesivir can lower viral loads and enhance recovery in certain COVID-19 patients, particularly in outpatient settings. However, remdesivir is not suitable for oral administration or lung-specific delivery due to its low oral bioavailability and limited stability in human liver microsomes (51,52). Molnupiravir, a mutagenic ribonucleoside analogue, was originally designed to inhibit influenza A and B

viruses. Amid the COVID-19 pandemic, it received its first regulatory approval in the UK in November 2021 and has since been distributed globally. However, findings from the 2022 platform-adaptive PANORAMIC trial indicated that molnupiravir, when combined with standard care, did not significantly reduce COVID-19-related hospitalizations or mortality among high-risk vaccinated adults when administered within five days of symptom onset. Similarly, large-scale real-world studies found no substantial reduction in hospitalization rates among high-risk outpatients with incomplete vaccination. Molnupiravir exerts its antiviral effect by inducing the accumulation of mispaired nucleobases in the viral RNA genome, a process known as lethal mutagenesis or error catastrophe. However, concerns regarding potential mutagenic effects on mammalian cellular DNA synthesis necessitate a thorough safety assessment. Due to possible risks, including fetal toxicity and bone and cartilage damage, molnupiravir is only approved for short-term use (≤5 consecutive days) and is not recommended for pregnant women or individuals under 18 years of age (53–56). Suramin, a non-nucleos(t)ide RdRp inhibitor, interferes with SARS-CoV-2 replication by preventing the viral RNA template strand from binding within the RdRp catalytic site. While suramin has shown antiviral efficacy in Vero E6 cells, it has not been recommended for clinical use due to poor bioavailability and significant adverse effects. The negatively charged suramin molecule binds to multiple human proteins with positively charged surfaces, leading to unwanted interactions that limit its therapeutic application (53–56).

1.2.5 2′-O-methyltransferase (NSP16)

SARS-CoV-2 NSP16, in conjunction with its activator NSP10, forms a heterodimeric 2′-O-methyltransferase complex that modifies viral RNA by converting Cap-0-RNA into Cap-1-RNA, allowing the virus to evade detection by pattern recognition receptors (57). Although compounds such as S-adenosyl-homocysteine (SAH) and SAM derivatives, including sinefungin, exhibit anti-SARS-CoV-2 activity in cell culture, their clinical potential is limited due to poor membrane permeability, attributed to their zwitterionic nature, and high toxicity, which arises from off-target inhibition of human methyltransferases such as cap-specific mRNA (nucleoside-2′-O-)-methyltransferase 1 (CMTR1) (58,59). NSP16 shares structural similarity with CMTR1, which provides an alternative pathway for SARS-CoV-2 RNA methylation (44). An experimental adenine analogue, 3-deazaneplanocin A, has been shown to inhibit SARS-CoV-2 replication by simultaneously targeting both NSP16 2′-O-methyltransferase and human CMTR1. However, its use is associated with adverse effects, including stunted growth and nephrotoxicity in rodent models. In principle, effective inhibition

of SARS-CoV-2 RNA methylation would require the concurrent targeting of NSP16 and CMTR1, but this approach carries a high risk of toxicity, as interfering with human SAM cycle-related enzymes could impair mRNA maturation and disrupt essential cellular functions (60).

1.2.6 Nucleocapsid

The SARS-CoV-2 nucleocapsid is a flexible and multivalent protein with multiple functions including viral genome packaging and suppression of innate antiviral immunity(61). However, it remains a challenge to develop nucleocapsid inhibitors. First, drug-binding pockets in nucleocapsid, unlike those of viral proteases and RdRp, seem to be structurally dynamic, thereby making it difficult for stable drug binding. Second, the nucleocapsid is the most abundant SARS-CoV-2 protein and folds into the intricate ribonucleoprotein complex with viral RNA. Third, current nucleocapsid inhibitors are inferior to protease and RdRp inhibitors regarding antiviral potency and binding affinity. Despite active research in the past 30 years, no antiviral nucleocapsid inhibitor has been approved (44,62).

1.3 Treatment strategies for COVID-19

To date, more than ten antiviral agents, including small molecules and monoclonal antibodies, have been approved for the treatment of COVID-19 (63). The therapeutic window for antiviral agents is likely restricted to the viral phase of SARS-CoV-2 infection, making early administration crucial for outpatients with mild-to-moderate COVID-19 to prevent disease progression to severe stages (44). However, most currently available antiviral treatments, with the exception of oral nirmatrelvir–ritonavir and molnupiravir (64), require injection and are typically administered in hospitals or infusion centers. This limitation reduces their feasibility in outpatient settings and resource-limited environments. During the early stages of COVID-19, the use of anti-inflammatory drugs and immunomodulators may be harmful, as they can suppress immune responses and lead to increased viral loads. However, in hospitalized patients with severe or critical COVID-19, a combination of antiviral agents with supportive interventions such as immunomodulators, anticoagulants, and anti-inflammatory drugs may provide synergistic benefits (65). Nevertheless, potential drug-drug interactions should be carefully assessed, as many antiviral and non-antiviral drugs are frequently co-administered, particularly in severely ill patients with pre-existing conditions (66). A major challenge in the development of effective antiviral treatments is the emergence of drug-resistant variants, which often result from amino acid substitutions in drug-binding pockets (67). In particular, the rise of Omicron variants has led to resistance against many monoclonal antibodies, rendering their

clinical use no longer recommended (68). While the traditional approach of developing antiviral drugs targeting specific pathogens often referred to as the 'one bug, one drug' strategy has been successful, it may not be sufficient to address the growing diversity of viruses that pose significant threats to human health. Given the increasing frequency of emerging and re-emerging viral zoonoses, along with the vast number of undiscovered mammalian viruses that could serve as potential reservoirs for future outbreaks, the conventional virus-specific model of antiviral drug development is unlikely to yield timely and effective treatments. These challenges highlight the urgent need for pan-genus and pan-family antivirals capable of targeting multiple viruses within a single viral family, offering broader protection against a wide range of pathogens (69).

1.4 Long COVID and antiviral therapy

Many patients have experienced prolonged health effects following SARS-CoV-2 infection, commonly referred to as post-COVID-19 conditions or long COVID. According to the World Health Organization (WHO) update in December 2022, long COVID is clinically defined by the presence of symptoms such as chronic fatigue syndrome, respiratory complications, and cognitive dysfunction that persist for at least three months after the initial infection and last for at least two months without any alternative explanation (70). Evidence from various studies has indicated viral persistence, characterized by the continued presence of viral RNA or protein fragments for months or even years in multiple organ systems, including the gastrointestinal tract, brain, kidneys, and blood vessels. Additionally, research has detected subgenomic RNA, a marker of viral replication, in solid tissues months after the initial infection (71). A recent study has further demonstrated that SARS-CoV-2 viral RNA can persist in tissues alongside sustained T-cell activation for up to two years in individuals who had mild acute COVID-19. These immune abnormalities appear to correlate with long COVID symptoms (72). Collectively, these findings suggest that ongoing viral replication or transcriptional activity may contribute to the persistence of active SARS-CoV-2 reservoirs, leading to long-term immune disturbances at the tissue level. This raises the possibility that targeting viral persistence with antiviral therapies could be a viable strategy for both preventing and treating long COVID. Initial observational studies have provided promising evidence supporting this approach. Data from non-hospitalized individuals with mild to moderate COVID-19 and at least one risk factor for severe disease suggest that the use of SARS-CoV-2 antivirals, such as ritonavir-boosted nirmatrelvir and molnupiravir, during the acute phase of infection may help reduce the risk of developing long COVID (71). Furthermore, findings from the PANORAMIC

trial indicate that treatment with molnupiravir improved long-term health outcomes compared to usual care. Patients receiving molnupiravir reported reduced symptom severity, lower healthcare utilization, and better quality of life at both three and six months post-infection (73).

2 Objectives of the thesis

The ongoing threat posed by coronaviruses, including SARS-CoV-2, SARS-CoV-1, and MERS-CoV, has highlighted the urgent need for effective therapeutic strategies. The high mutation rate and emergence of new variants necessitate the development of broad-spectrum antiviral agents, or pan-coronaviral inhibitors, that can combat a range of coronavirus strains and potentially prevent future pandemics. The discovery of pan-coronaviral inhibitors is crucial due to the unpredictable nature of coronavirus outbreaks and the rapid emergence of new variants. Broad-spectrum inhibitors offer a proactive approach to pandemic preparedness, reducing the time required to develop treatments for novel strains and natural products with their structural diversity provide a valuable resource for discovering such inhibitors, contributing to global health security.

This thesis aims to explore and develop natural product-derived inhibitors targeting critical proteins involved in coronavirus replication and entry. By leveraging computational and experimental approaches, this research seeks to identify compounds that can serve as pan coronaviral agents.

This thesis comprises three projects, in the first project the goal was to identify natural products that inhibit the main protease (M^{pro}) of SARS-CoV-2, SARS-CoV-1, and MERS-CoV, through a combination of computational and experimental approaches. In the first phase, a virtual screening was conducted on a large natural product library to identify potential inhibitors of M^{pro} and molecular docking simulations were performed to predict binding affinity. In the second phase, in vitro assays were carried out to validate the inhibitory potential of the selected compounds. A FRET-based enzymatic assay was used to measure M^{pro} inhibition, while cell-based cytotoxicity assays in MRC-5 cells evaluated compound safety and to confirm interactions with M^{pro}, microscale thermophoresis (MST) were utilized. Through this integrative approach, the study aims to discover novel M^{pro} inhibitors from natural sources and provide valuable insights into their antiviral potential, contributing to the development of natural pan- coronaviral agents.

The second project goal was to identify natural pan-coronaviral entry inhibitors. To achieve this, a high-throughput virtual screening approach was employed to evaluate over 210,000

natural product-based compounds from the ZINC database against the receptor-binding domain (RBD) of the spike protein of SARS-CoV-2, its variant of concern, SARS-CoV-1, and MERS-CoV. The most promising candidates were selected for further validation. For entry inhibition studies, lentiviruses bearing the spike protein of SARS-CoV-2 were produced to establish a pseudovirus-based entry assay, allowing the assessment of viral entry inhibition by selected compounds using luciferase assay. The inhibition potential of these compounds was further tested in live-virus assays using a SARS-CoV-2 clinical isolate. Microscale thermophoresis (MST) was used to measure the binding affinities of the lead compounds to the RBDs of multiple coronaviruses, while resazurin-based cytotoxicity assays determined the safety profile of the candidates. Additionally, sequence alignment studies were conducted to correlate compound efficacy with sequence homology of the viral RBDs.

And finally, the third project focused on identify novel small-molecule inhibitors targeting coronavirus entry by focusing on nitrile-containing natural product derivatives. Nitrile-containing compounds have demonstrated promising pharmacological properties, making them valuable candidates for drug development. To achieve this, we employed a structure-based virtual screening approach to identify potential inhibitors of the SARS-CoV-2 spike receptor-binding domain (RBD). The top candidates were subjected to in vitro validation using pseudovirus and live-virus neutralization assays to assess their efficacy in blocking viral entry. Additionally, we performed microscale thermophoresis (MST) to evaluate the binding affinities of selected compounds to the RBDs of multiple coronaviruses, including SARS-CoV-2, SARS-CoV-2 XBB, SARS-CoV-1, MERS-CoV, and HCoV-HKU1. Additionally, sequence alignment studies were conducted to correlate compound efficacy with sequence homology of the viral RBDs.

3 Results and Discussion

3.1 Identification of pan-Coronaviral natural product targeting main protease

Initially, a large-scale virtual screening was performed on 39,442 natural-product-like compounds from the ZINC database and 121 preselected medicinal plants with known antiviral activity. Molecular docking studies identified 12 promising candidates. Subsequent *in vitro* enzymatic assays revealed that hypericin, rosmarinic acid, isorhamnetin, and luteolin were the most active natural products among the 12 compounds preselected by our bioinformatical approach against SARS-CoV-2 M^{pro}. Further experiments demonstrated that hypericin and isorhamnetin also inhibited SARS-CoV-1 M^{pro}, while hypericin exhibited inhibitory activity

against MERS-CoV M^{pro}, suggesting its potential as a pan-coronaviral inhibitor. Microscale thermophoresis (MST) confirmed the binding of these four compounds to M^{pro} with high affinity. A cell viability assay using MRC-5 lung fibroblasts showed that rosmarinic acid and luteolin were non-toxic, whereas hypericin and isorhamnetin displayed mild cytotoxicity. The therapeutic indices indicated that hypericin had the highest potential as a broad-spectrum antiviral agent. The study highlights the significance of natural products in drug discovery, demonstrating that hypericin could serve as a promising lead compound for further drug development against coronaviruses. These findings reinforce the importance of targeting viral proteases for antiviral therapy and suggest that natural products offer viable candidates for broad-spectrum coronavirus inhibitors. Future studies should focus on optimizing the potency and selectivity of these compounds through further chemical modifications and *in vivo* validation.

Further reading: Appendix I

***In Silico* and *In Vitro* Identification of Pan-Coronaviral Main Protease Inhibitors from a Large Natural Product Library**

Nasim Shahhamzehei , Sara Abdelfatah and Thomas Efferth

3.2 Identification of pan-coronaviral entry inhibitors from a large natural product-based library

A total of 210,541 natural product-derived small molecules from the ZINC database were screened against the receptor-binding domains (RBDs) of SARS-CoV-2, its variants (including XBB.1), SARS-CoV, and MERS-CoV. The most promising candidate, a diketopiperazine/piperidine alkaloid (compound 28), demonstrated strong inhibitory potential in both computational and experimental analyses.

In vitro pseudovirus inhibition assays in HEK-ACE2 and Vero E6 host cells showed that compound 28 significantly blocked viral entry, with an IC_{50} value of 1.96 μM for SARS-CoV-2 pseudovirus and 5.02 μM for live SARS-CoV-2 infection. Further microscale thermophoresis (MST) experiments confirmed that compound 28 binds strongly to the RBDs of multiple coronaviruses, with binding affinities decreasing as sequence similarity decreased. Cell viability assays showed that compound 28 had low cytotoxicity, indicating a favorable therapeutic profile.

Molecular docking studies revealed that compound 28 interacts with key amino acid residues within the RBD of the spike protein, potentially blocking the virus from binding to the ACE2 receptor. The presence of N-heterocycles in its structure, including diketopiperazine and piperidine rings, appears to contribute to its binding efficiency. Given its broad activity across multiple coronaviruses and its strong binding affinity to the spike protein, this diketopiperazine/piperidine alkaloid represents a promising pan-coronaviral entry inhibitor and a potential lead for further drug development.

Further reading: Appendix II

Diketopiperazine/piperidine alkaloid as a potential broad-spectrum coronaviral entry inhibitor identified by supercomputer-based virtual screening from a large natural product-based library.

Nasim Shahhamzehei, Sara Abdelfatah, Ejlal A. Omer, Max Riedl, Christian Meesters, Hannah S. Schwarzer-Sperber, Kathrin Sutter, Gerhard Bringmann, Roland Schwarzer, and Thomas Efferth

3.3 Identification of of nitrile-containing natural product derivatives as potential broad-spectrum entry inhibitors of coronaviruses.

A virtual screening of 143 sulfur- and nitrile-containing natural product-derived compounds was conducted against the receptor-binding domain (RBD) of the SARS-CoV-2 spike protein, identifying 18 top candidates with strong predicted binding affinities. These compounds were subjected to *in vitro* testing to evaluate their efficacy in inhibiting viral entry.

Among the tested compounds, compounds 9, 14, and 15 demonstrated significant inhibition of SARS-CoV-2 pseudovirus and live virus entry into HEK-ACE2 and Vero E6 cells, with low micromolar IC_{50} values. These compounds also exhibited low cytotoxicity towards MRC-5, Vero E6, and HEK-ACE2 cell lines, suggesting a favorable therapeutic profile. Microscale thermophoresis (MST) confirmed strong binding of all three compounds to the RBDs of SARS-CoV-2, SARS-CoV-2 XBB.1 (Omicron variant), SARS-CoV-1, MERS-CoV, and HCoV-HKU1, with binding affinities correlating with the degree of sequence similarity among these coronaviruses. Molecular docking studies further revealed that compounds 9, 14, and 15 interacted with hotspot residues essential for RBD-ACE2 interaction, providing structural insights into their inhibitory mechanisms. Compound 15 was identified as the most potent inhibitor, showing the highest binding affinity and antiviral activity. The findings suggest that these nitrile-containing natural product derivatives have strong potential as pan-coronaviral entry inhibitors, warranting further investigation for drug development.

Further reading: Appendix III

Identification of nitrile-containing isoquinoline-related natural product derivatives as coronavirus entry inhibitors *in silico* and *in vitro*

Nasim Shahhamzehei, Sara Abdelfatah, Hannah S. Schwarzer-Sperber, Kathrin Sutter, Rümeysa Yücer, Gerhard Bringmann, Roland Schwarzer, and Thomas Efferth

4 Conclusion:

The COVID-19 pandemic has reinforced the critical need for effective antiviral therapeutics, particularly broad-spectrum inhibitors capable of targeting multiple coronaviruses. Given the ability of coronaviruses to mutate rapidly and evade immune responses, the identification of conserved viral structures remains a priority in antiviral drug development. This thesis focused on the discovery and characterization of natural product-derived inhibitors targeting the main protease (M^{pro}) and receptor-binding domain (RBD) of the spike protein, two essential viral components involved in replication and host cell entry.

Both *in silico* and *in vitro* investigations demonstrated that hypericin is a promising candidate as a novel pan-coronaviral inhibitor, effectively binding to and inhibiting the main protease (M^{pro}) of several human-pathogenic coronaviruses. Additionally, isorhamnetin exhibited inhibitory activity against the M^{pro} of SARS-CoV-2 and SARS-CoV-1, while luteolin showed inhibitory effects specifically against SARS-CoV-2 M^{pro}. Furthermore, the generally low toxicity profiles of natural products provide an additional advantage, further supporting the therapeutic potential of the compounds investigated in this study. However, these results should be further validated through animal models and subsequent clinical trials.

A N-heterocyclic compound ((2R,8S)-6-(1-benzylpiperidin-4-yl)-2-naphthalen-1-yl-3,6,17 triazatetracyclo [8.7.0.03,8.011,16] heptadeca-1(10),11,13,15-tetraene-4,7-dione)) derived from natural products identified as a promising broad-spectrum entry inhibitor against coronaviruses, demonstrating strong antiviral activity combined with a low toxicity profile. The selective identification of an active compound containing an N-heterocyclic structure, despite the extensive diversity of screened candidates from the ZINC database, underscores the effectiveness and specificity of our computational and experimental selection approach. Notably, this compound significantly protected cells from infection with both SARS-CoV-2 pseudoviruses and live virus strains. Additionally, Microscale thermophoresis (MST) assays

confirmed that the compound binds with high affinity to the receptor-binding domains (RBDs) of SARS-CoV-2, its variant SARS-CoV-2 XBB.1, as well as SARS-CoV, MERS-CoV, and HCoV-HKU1. Further preclinical studies, including *in vivo* assessments, are essential to fully confirm the therapeutic potential of this compound.

Three Nitrile-containing isoquinoline natural product-derived compounds ((4-imino-2-[3-methoxy-4-(propan-2-yloxy)phenyl]-6,7,11,12-tetrahydro-4H,10H-[1,4]dioxepino[2,3-g]pyrido[2,1 a]isoquinoline-3-carbonitrile), (4-imino-2-(3-methoxyphenyl)-6,7-dihydro-4H [1,3]dioxolo[4,5-g]pyrido[2,1-a]isoquinoline-3-carbonitrile), (2-(1,3-benzodioxol-5-yl)-4-imino-9,10-dimethoxy-6,7-dihydro-4H-pyrido[2,1-a]isoquinoline-3-carbonitrile)) identified as promising broad-spectrum coronavirus. These compounds showed entry inhibition, targeting the receptor-binding domain (RBD) of the spike protein of SARS-CoV-2 pseudovirus and live virus infections while maintaining low cytotoxicity. Microscale thermophoresis (MST) assays confirmed that the compound binds with high affinity to the receptor-binding domains (RBDs) of SARS-CoV-2, its variant SARS-CoV-2 XBB.1, as well as SARS-CoV, MERS-CoV, and HCoV-HKU1. further preclinical studies, including *in vivo* assessments, are essential to fully confirm the therapeutic potential of this compound.

5 References

1. Lin LT, Hsu WC, Lin CC. Antiviral natural products and herbal medicines. J Tradit Complement Med. 2014;4(1):24–35.

2. Sagaya Jansi R, Khusro A, Agastian P, Alfarhan A, Al-Dhabi NA, Arasu MV, et al. Emerging paradigms of viral diseases and paramount role of natural resources as antiviral agents. Science of the Total Environment. 2021;759:143539.

3. Wasilewicz A, Kirchweger B, Bojkova D, Abi Saad MJ, Langeder J, Bütikofer M, et al. Identification of Natural Products Inhibiting SARS-CoV-2 by Targeting Viral Proteases: A Combined in Silico and in Vitro Approach. J Nat Prod. 2023;86(2):264–75.

4. Mhatre S, Naik S, Patravale V. A molecular docking study of EGCG and theaflavin digallate with the druggable targets of SARS-CoV-2. Comput Biol Med. 2021;129(November 2020):104137.

5. V'kovski P, Kratzel A, Steiner S, Stalder H, Thiel V. Coronavirus biology and replication: implications for SARS-CoV-2. Vol. 19, Nature Reviews Microbiology. Nature Research; 2021. p. 155–70.

6. Tiwari R, Dhama K, Sharun K, Iqbal Yatoo M, Malik YS, Singh R, et al. COVID-19: animals, veterinary and zoonotic links. Veterinary Quarterly. 2020;40(1):169–82.

7. Malik JK, Kumar A, Soni H. Epidemiology of Novel Corona Virus (Covid-19): A Review. Journal of Clinical/Pharmaco-Epidemiology Research. 2020;2(2):5–13.

8. Cui J, Li F, Shi ZL. Origin and evolution of pathogenic coronaviruses. Nat Rev Microbiol. 2019;17(3):181–92.

9. Harrison CM, Doster JM, Landwehr EH, Kumar NP, White EJ, Beachboard DC, et al. Evaluating the Virology and Evolution of Seasonal Human Coronaviruses Associated with the Common Cold in the COVID-19 Era. Microorganisms. 2023;11(2).

10. Zhu Z, Lian X, Su X, Wu W, Marraro GA, Zeng Y. From SARS and MERS to COVID-19: A brief summary and comparison of severe acute respiratory infections caused by three highly pathogenic human coronaviruses. Respir Res. 2020;21(1):1–14.

11. Kakavandi S, Zare I, VaezJalali M, Dadashi M, Azarian M, Akbari A, et al. Structural and non-structural proteins in SARS-CoV-2: potential aspects to COVID-19 treatment or prevention of progression of related diseases. Cell Communication and Signaling. 2023;21(1):1–31.

12. Gorkhali R, Koirala P, Rijal S, Mainali A, Baral A, Bhattarai HK. Structure and Function of Major SARS-CoV-2 and SARS-CoV Proteins. Bioinform Biol Insights. 2021;15(Figure 1).

13. Yang H, Rao Z. Structural biology of SARS-CoV-2 and implications for therapeutic development. Nat Rev Microbiol. 2021;19(11):685–700.

14. Trougakos IP, Stamatelopoulos K, Terpos E, Tsitsilonis OE, Aivalioti E, Paraskevis D, et al. Insights to SARS-CoV-2 life cycle, pathophysiology, and rationalized treatments that target COVID-19 clinical complications. J Biomed Sci. 2021;28(1):1–18.

15. Rahbar Saadat Y, Hosseiniyan Khatibi SM, Zununi Vahed S, Ardalan M. Host Serine Proteases: A Potential Targeted Therapy for COVID-19 and Influenza. Front Mol Biosci. 2021;8(August):1–13.

16. Malone B, Urakova N, Snijder EJ, Campbell EA. Structures and functions of coronavirus replication–transcription complexes and their relevance for SARS-CoV-2 drug design. Nat Rev Mol Cell Biol. 2022;23(1):21–39.

17. Hartenian E, Nandakumar D, Lari A, Ly M, Tucker JM, Glaunsinger BA. The molecular virology of coronaviruses. Journal of Biological Chemistry. 2020;295(37):12910–34.

18. Catanzaro M, Fagiani F, Racchi M, Corsini E, Govoni S, Lanni C. Immune response in COVID-19: addressing a pharmacological challenge by targeting pathways triggered by SARS-CoV-2. Signal Transduct Target Ther. 2020;5(1).

19. O'Connell P, Aldhamen YA. Systemic innate and adaptive immune responses to SARS-CoV-2 as it relates to other coronaviruses. Hum Vaccin Immunother. 2020;16(12):2980–91.

20. Zhu Q, Xu Y, Wang T, Xie F. Innate and adaptive immune response in SARS-CoV-2 infection-Current perspectives. Front Immunol. 2022;13(November):1–15.

21. Montazersaheb S, Hosseiniyan Khatibi SM, Hejazi MS, Tarhriz V, Farjami A, Ghasemian Sorbeni F, et al. COVID-19 infection: an overview on cytokine storm and related interventions. Virol J. 2022;19(1):1–15.

22. Ansariniya H, Seifati SM, Zaker E, Zare F. Comparison of Immune Response between SARS, MERS, and COVID-19 Infection, Perspective on Vaccine Design and Development. Biomed Res Int. 2021;2021.

23. Karki R, Kanneganti TD. The 'cytokine storm': molecular mechanisms and therapeutic prospects. Trends Immunol. 2021;42(8):681–705.

24. Wang J, Jiang M, Chen X, Montaner LJ. Cytokine storm and leukocyte changes in mild versus severe SARS-CoV-2 infection: Review of 3939 COVID-19 patients in China and emerging pathogenesis and therapy concepts. J Leukoc Biol. 2020;108(1):17–41.

25. Harrison AG, Lin T, Wang P. Mechanisms of SARS-CoV-2 Transmission and Pathogenesis. Trends Immunol. 2020;41(12):1100–15.

26. Gupta A, Madhavan M V., Sehgal K, Nair N, Mahajan S, Sehrawat TS, et al. Extrapulmonary manifestations of COVID-19. Nat Med. 2020;26(7):1017–32.

27. Poduri R, Joshi G, Jagadeesh G, Kaur U, Acharya K, Mondal R, et al. Drugs targeting various stages of the SARS-CoV-2 life cycle: Exploring promising drugs for the treatment of Covid-19. 2020;(January):19–21.

28. Almehdi AM, Khoder G, Alchakee AS, Alsayyid AT, Sarg NH, Soliman SSM. SARS-CoV-2 spike protein: pathogenesis, vaccines, and potential therapies. Infection. 2021;49(5):855–76.

29. Zhang J, Xiao T, Cai Y, Chen B. Structure of SARS-CoV-2 spike protein. Curr Opin Virol. 2021;50:173–82.

30. 13.pdf file:///C:/Users/User/Desktop/research paper download/monoclonal antibody. Monoclonal antibody therapies against SARS-CoV-2. Ann Oncol. 2020;(January):19–21.

31. Almagro JC, Mellado-Sánchez G, Pedraza-Escalona M, Pérez-Tapia SM. Evolution of Anti-SARS-CoV-2 Therapeutic Antibodies. Int J Mol Sci. 2022;23(17).

32. Xiang R, Yu Z, Wang Y, Wang L, Huo S, Li Y, et al. Recent advances in developing small-molecule inhibitors against SARS-CoV-2. Vol. 12, Acta Pharmaceutica Sinica B. Chinese Pharmaceutical Association and Institute of Materia Medica, Chinese Academy of Medical Sciences; 2022. 1591–1623 p.

33. Xia S, Lan Q, Zhu Y, Wang C, Xu W, Li Y, et al. Structural and functional basis for pan-CoV fusion inhibitors against SARS-CoV-2 and its variants with preclinical evaluation. Signal Transduct Target Ther. 2021;6(1).

34. Liu S, Xiao G, Chen Y, He Y, Niu J, Escalante CR, et al. Interaction between heptad repeat 1 and 2 regions in spike protein of SARS-associated coronavirus: Implications for virus fusogenic mechanism and identification of fusion inhibitors. Lancet. 2004;363(9413):938–47.

35. Lu L, Liu Q, Zhu Y, Chan KH, Qin L, Li Y, et al. Structure-based discovery of Middle East respiratory syndrome coronavirus fusion inhibitor. Nat Commun. 2014;5.

36. Shibo Jiang KLNS& ARN. HIV-1 inhibition by a peptide. Nature. 1993 Sep 9;(Nature 365, 113).

37. Verma S, Goand UK, Husain A, Katekar RA, Garg R, Gayen JR. Challenges of peptide and protein drug delivery by oral route: Current strategies to improve the bioavailability. Drug Dev Res. 2021;82(7):927–44.

38. Ullrich S, Nitsche C. The SARS-CoV-2 main protease as drug target. Bioorg Med Chem Lett. 2020;30(17):127377.

39. Li X, Song Y. Structure and function of SARS-CoV and SARS-CoV-2 main proteases and their inhibition: A comprehensive review. Vol. 260, European Journal of Medicinal Chemistry. 2023.

40. Zag A, Czopek A, Fryc M, Jo J. Inhibitors of SARS-CoV-2 Main Protease (Mpro) as Anti-Coronavirus Agents. 2024;

41. Shawky AM, Almalki FA, Alzahrani HA, Abdalla AN, Youssif BGM, Ibrahim NA, et al. Covalent small-molecule inhibitors of SARS-CoV-2 Mpro: Insights into their design, classification, biological activity, and binding interactions. Eur J Med Chem. 2024;277(July):116704.

42. Hu Y, Lewandowski EM, Tan H, Zhang X, Morgan RT, Zhang X, et al. Naturally Occurring Mutations of SARS-CoV-2 Main Protease Confer Drug Resistance to Nirmatrelvir. ACS Cent Sci. 2023;9(8):1658–69.

43. Hashemian SMR, Sheida A, Taghizadieh M, Memar MY, Hamblin MR, Bannazadeh Baghi H, et al. Paxlovid (Nirmatrelvir/Ritonavir): A new approach to Covid-19 therapy? Biomedicine and Pharmacotherapy. 2023;162(February):114367.

44. Li G, Hilgenfeld R, Whitley R, De Clercq E. Therapeutic strategies for COVID-19: progress and lessons learned. Nat Rev Drug Discov. 2023;22(6):449–75.

45. Osipiuk J, Azizi SA, Dvorkin S, Endres M, Jedrzejczak R, Jones KA, et al. Structure of papain-like protease from SARS-CoV-2 and its complexes with non-covalent inhibitors. Nat Commun. 2021;12(1):1–9.

46. Rut W, Lv Z, Zmudzinski M, Patchett S, Nayak D, Snipas SJ, et al. Activity profiling and crystal structures of inhibitor-bound SARS-CoV-2 papain-like protease: A framework for anti–COVID-19 drug design. Sci Adv. 2020;6(42):1–12.

47. Ton AT, Pandey M, Smith JR, Ban F, Fernandez M, Cherkasov A. Targeting SARS-CoV-2 papain-like protease in the postvaccine era. Trends Pharmacol Sci. 2022;43(11):906–19.

48. Srinivasan V, Brognaro H, Prabhu PR, de Souza EE, Günther S, Reinke PYA, et al. Antiviral activity of natural phenolic compounds in complex at an allosteric site of SARS-CoV-2 papain-like protease. Commun Biol. 2022;5(1):1–12.

49. Puhl AC, Godoy AS, Noske GD, Nakamura AM, Gawriljuk VO, Fernandes RS, et al. Discovery of PLpro and Mpro Inhibitors for SARS-CoV-2. ACS Omega. 2023;8(25):22603–12.

50. Wang Y, Anirudhan V, Du R, Cui Q, Rong L. RNA-dependent RNA polymerase of SARS-CoV-2 as a therapeutic target. J Med Virol. 2021;93(1):300–10.

51. Vargas DF, Larghi EL, Kaufman TS. Evolution of the Synthesis of Remdesivir. Classical Approaches and Most Recent Advances. ACS Omega. 2021;6(30):19356–63.

52. Liang C, Tian L, Liu Y, Hui N, Qiao G, Li H, et al. A promising antiviral candidate drug for the COVID-19 pandemic: A mini-review of remdesivir. Eur J Med Chem. 2020;201:112527.

53. Kabinger F, Stiller C, Schmitzová J, Dienemann C, Kokic G, Hillen HS, et al. Mechanism of molnupiravir-induced SARS-CoV-2 mutagenesis. Nat Struct Mol Biol. 2021;28(9):740–6.

54. Masyeni S, Iqhrammullah M, Frediansyah A, Nainu F, Tallei T, Emran T Bin, et al. Molnupiravir: A lethal mutagenic drug against rapidly mutating severe acute respiratory syndrome coronavirus 2—A narrative review. J Med Virol. 2022;94(7):3006–16.

55. Hadj Hassine I, Ben M'Hadheb M, Menéndez-Arias L. Lethal Mutagenesis of RNA Viruses and Approved Drugs with Antiviral Mutagenic Activity. Viruses. 2022;14(4).

56. Waters MD, Warren S, Hughes C, Lewis P, Zhang F. Human genetic risk of treatment with antiviral nucleoside analog drugs that induce lethal mutagenesis: The special case of molnupiravir. Environ Mol Mutagen. 2022;63(1):37–63.

57. Strategies T. NSP16 2-O-MTase in Coronavirus Pathogenesis: Possible Prevention and Treatments Strategies. 2021;

58. Kremling V, Falke S, Fernández-García Y, Ehrt C, Kiene A, Klopprogge B, et al. SARS-CoV-2 methyltransferase nsp10-16 in complex with natural and drug-like purine analogs for guiding structure-based drug discovery. 2024;

59. Bobiļeva O, Bobrovs R, Kaņepe I, Patetko L, Kalniņš G, Šišovs M, et al. Potent SARS-CoV-2 mRNA Cap Methyltransferase Inhibitors by Bioisosteric Replacement of Methionine in SAM Cosubstrate. ACS Med Chem Lett. 2021;12(7):1102–7.

60. Bergant V, Yamada S, Grass V, Tsukamoto Y, Lavacca T, Krey K, et al. Attenuation of SARS-CoV -2 replication and associated inflammation by concomitant targeting of viral and host cap 2'-O-ribose methyltransferases . EMBO J. 2022;41(17):1–23.

61. El-Maradny YA, Badawy MA, Mohamed KI, Ragab RF, Moharm HM, Abdallah NA, et al. Unraveling the role of the nucleocapsid protein in SARS-CoV-2 pathogenesis: From viral life cycle to vaccine development. Int J Biol Macromol. 2024;279(P2):135201.

62. Zenchenko AA, Drenichev MS, Mikhailov SN. Nucleoside Inhibitors of Coronaviruses. Curr Med Chem. 2021;28(26):5284–310.

63. Aboul-Fotouh S, Mahmoud AN, Elnahas EM, Habib MZ, Abdelraouf SM. What are the current anti-COVID-19 drugs? From traditional to smart molecular mechanisms. Virol J. 2023;20(1):1–20.

64. Saravolatz LD, Depcinski S, Sharma M. Molnupiravir and Nirmatrelvir-Ritonavir: Oral COVID Antiviral Drugs. Clin Infect Dis. 2023;76(1):165–71.

65. Zhou Q, Zhao S, Gan L, Wang Z, Peng S, Li Q, et al. Use of non-steroidal anti-inflammatory drugs and adverse outcomes during the COVID-19 pandemic: A systematic review and meta-analysis. EClinicalMedicine. 2022;46:101373.

66. Taburet AM, Singlas E. Drug interactions with antiviral drugs. Clin Pharmacokinet. 1996;30(5):385–401.

67. Prüβ BM. Variants of SARS CoV-2: mutations, transmissibility, virulence, drug resistance, and antibody/vaccine sensitivity. Frontiers in Bioscience - Landmark. 2022;27(2).

68. Iketani S, Ho DD. SARS-CoV-2 resistance to monoclonal antibodies and small-molecule drugs. Cell Chem Biol. 2024;31(4):632–57.

69. Totura AL, Bavari S. Broad-spectrum coronavirus antiviral drug discovery. Vol. 14, Expert Opinion on Drug Discovery. Taylor and Francis Ltd; 2019. p. 397–412.

70. Davis HE, McCorkell L, Vogel JM, Topol EJ. Long COVID: major findings, mechanisms and recommendations. Nat Rev Microbiol. 2023;21(3):133–46.

71. Al-Aly Z. SARS-CoV-2 antivirals and post-COVID-19 condition. Lancet Infect Dis. 2024;3099(24):9–11.

72. Peluso MJ, Ryder D, Flavell RR, Wang Y, Levi J, LaFranchi BH, et al. Tissue-based T cell activation and viral RNA persist for up to 2 years after SARS-CoV-2 infection. Sci Transl Med. 2024;16(754):1–16.

73. Harris V, Holmes J, Gbinigie-Thompson O, Rahman NM, Richards DB, Hayward G, et al. Health outcomes 3 months and 6 months after molnupiravir treatment for COVID-19 for people at higher risk in the community (PANORAMIC): a randomised controlled trial. Lancet Infect Dis. 2024;25(January).

6 Appendices

pharmaceuticals

MDPI

Article

In Silico and In Vitro Identification of Pan-Coronaviral Main Protease Inhibitors from a Large Natural Product Library

Nasim Shahhamzehei, Sara Abdelfatah and Thomas Efferth *

Department of Pharmaceutical Biology, Institute of Pharmaceutical and Biomedical Sciences, Johannes Gutenberg University, Staudinger Weg5, 55128 Mainz, Germany; nshahham@uni-mainz.de (N.S.); saabdelf@uni-mainz.de (S.A.)

* Correspondence: efferth@uni-mainz.de; Tel.: +49-6131-3925751; Fax: +49-6131-3923752

Abstract: The main protease (M^{pro} or $3CL^{pro}$) in coronaviruses represents a promising specific drug target as it is essential for the cleavage of the virus polypeptide and has a unique cleavage site that does not exist in human host proteases. In this study, we explored potential natural pan-coronavirus drugs using in vitro and in silico approaches and three coronavirus main proteases as treatment targets. The PyRx program was used to screen 39,442 natural-product-like compounds from the ZINC database and 121 preselected phytochemicals from medicinal plants with known antiviral activity. After assessment with Lipinski's rule of five, molecular docking was performed for the top 33 compounds of both libraries. Enzymatic assays were applied for the top candidates from both in silico approaches to test their ability to inhibit SARS-CoV-2 M^{pro}. The four compounds (hypericin, rosmarinic acid, isorhamnetin, and luteolin) that most efficiently inhibited SARS-CoV-2 M^{pro} in vitro were further tested for their efficacy in inhibiting M^{pro} of SARS-CoV-1 and MERS-CoV. Microscale thermophoresis was performed to determine dissociation constant (Kd) values to validate the binding of these active compounds to recombinant M^{pro} proteins of SARS-CoV-2, SARS-CoV-1, and MERS-CoV. The cytotoxicity of hypericin, rosmarinic acid, isorhamnetin, and luteolin was assessed in human diploid MRC-5 lung fibroblasts using the resazurin cell viability assay to determine their therapeutic indices. Sequence alignment of M^{pro} of SARS-CoV-2 demonstrated 96.08%, 50.83%, 49.17%, 48.51%, 44.04%, and 41.06% similarity to M^{pro} of other human-pathogenic coronaviruses (SARS-CoV-1, MERS-CoV, HCoV-NL63, HCoV-OC43, HCoV-HKU1, and HCoV-229E, respectively). Molecular docking showed that 12 out of 121 compounds were bound to SARS-CoV-2 M^{pro} at the same binding site as the control inhibitor, GC376. Enzyme inhibition assays revealed that hypericin, rosmarinic acid, isorhamnetin, and luteolin inhibited M^{pro} of SARS-CoV-2, while hypericin and isorhamnetin inhibited M^{pro} of SARS-CoV-1; hypericin showed inhibitory effects toward M^{pro} of MERS-CoV. Microscale thermophoresis confirmed the binding of these compounds to M^{pro} with high affinity. Resazurin assays showed that rosmarinic acid and luteolin were not cytotoxic toward MRC-5 cells, whereas hypericin and isorhamnetin were slightly cytotoxic. We demonstrated that hypericin represents a potential novel pan-anti-coronaviral agent by binding to and inhibiting M^{pro} of several human-pathogenic coronaviruses. Moreover, isorhamnetin showed inhibitory effects toward SARS-CoV-2 and SARS-CoV-1 M^{pro}, indicating that this compound may have some pan-coronaviral potential. Luteolin had inhibitory effects against SARS-CoV-2 M^{pro}.

Keywords: infectious diseases; natural products; pan-inhibitor; virtual drug screening

Citation: Shahhamzehei, N.; Abdelfatah, S.; Efferth, T. In Silico and In Vitro Identification of Pan-Coronaviral Main Protease Inhibitors from a Large Natural Product Library. *Pharmaceuticals* **2022**, *15*, 308. https://doi.org/10.3390/ph15030308

Academic Editor: Daniela De Vita

Received: 8 February 2022
Accepted: 26 February 2022
Published: 3 March 2022

1. Introduction

Coronaviruses are enveloped, positive-sense, single-stranded RNA viruses with different hosts occurring in avians and mammals. This family is divided into four genera: α-, β-, γ-, and δ-coronaviruses. Among them, seven coronaviruses are pathogenic to humans, i.e., HCoV-229E and HCoV-NL63, which belong to the α-coronaviruses, and HCoV-OC43, HKU1, SARS-CoV-1, MERS-CoV, and the novel coronavirus nominated as SARS-CoV-2,

which belong to the β-coronaviruses [1,2]. SARS-CoV-1, MERS-CoV, and SARS-CoV-2 are highly pathogenic and cause viral pneumonia in patients. Meanwhile, the other four coronaviruses (HCoV-229E, HCoV-NL63, HCoV-OC43, and HKU1) usually infect the upper human respiratory system and cause the common cold (5–30%) [3]. However, they can also cause severe or lethal diseases in patients who are children, elderly, or immunodeficient [4].

The period between disease outbreaks has become shorter, and there is a possibility that more viral epidemics will occur soon. As vaccines provoke immunological memory against specific antigens, it is probable that the current therapeutic strategies targeting SARS-CoV-2 and its mutant variants may be inefficient against future coronaviruses that emerge in the human population. This threat is supported by data showing that vaccines formulated against SARS-CoV-1 antigens do not effectively protect from infections related to other SARS-like coronaviruses that are currently circulating in bat populations [5]. However, novel bat coronaviruses have sequence homologies of more than 90% to SARS-CoV-2 [6,7]. Hence, it is likely that more still-undetected bat coronaviruses with high similarity to SARS-CoV-2 exist and that some of them may have the potential for starting the outbreak of the next coronavirus epidemic or pandemic. It is common sense among the virological community that COVID-19 may not be the last pandemic and that more will threaten us in the future [8,9]. Consequently, there is an urgent need to identify and develop pan-anti-coronaviral drugs to be better prepared for the next coronavirus pandemic compared with our preparation for the current one.

Sequence comparison studies showed that SARS-CoV-2 shares approximately 79% sequence similarity with SARS-CoV-1 and approximately 50% with MERS-CoV [10]. Moreover, SARS-CoV-2 has a similar genome organization compared to β-coronaviruses with 14 open reading frames (ORFs). The large reading frame, ORF-1ab, encodes two polyproteins, pp1a and pp1ab, that are cleaved into 16 nonstructural proteins (nsp1-16, also termed replicase complex) by the main protease (at 11 positions), implying its important role in viral replication. This main protease is located in nsp5 and the papain-like protease (PL^{pro}) in nsp3. The rest of ORF-1ab encodes nine accessory proteins and four structural proteins, i.e., spike (S), envelope (E), membrane (M), and nucleocapsid (N) [11,12]. The coronavirus main protease (M^{pro}, also termed $3CL^{pro}$) is a cysteine protease with cysteine^{145} and histidine^{41} in its active site [10]. Its structure is composed of two monomers, and each of them consists of three domains. Domain I (residues 8–101) and domain II (residues 102–184) are catalytic domains and have an antiparallel β-barrel. Domain III (residues 201–303) is responsible for enzyme dimerization and has five α-helices [13,14]. M^{pro} has a unique cleavage site at conserved Leu-Gln↓ (Ser/Ala/Gly) [15,16]. This feature is absent in closely related human host proteases, and the side effects of M^{pro} inhibitors in human patients are limited. Therefore, the main protease represents an ideal target for developing anti-coronaviral drugs [17].

Natural products provide a rich resource for novel antiviral compounds. They are an extensive source of oral drugs based on Lipinski's rule of five [18]. Furthermore, they are evolutionarily optimized for interaction with different proteins and biological targets, which explains their high relevance for a variety of therapeutic purposes. Natural products have been used in traditional medicine for centuries, which provides insights regarding efficacy and safety. While many natural products have been extracted, only a few have been marketed as drugs. Therefore, further identification of their active compounds is useful for the treatment of viral infections and the management of outbreaks [19,20].

In this investigation, we aimed to explore potential pan-coronavirus compounds using in vitro and in silico approaches against several coronavirus M^{pro}. We studied 39,442 natural-product-like compounds from the ZINC database and 121 preselected natural products from medicinal plants with known antiviral activity [21–27] by virtual drug screening using SARS-CoV-2 M^{pro} as a target to identify lead compounds that may be further developed as pan-coronaviral drugs. Then, the top 12 compounds identified in silico were investigated for the inhibition of SARS-CoV-2 M^{pro} in vitro. The top four compounds from this experiment were used to calculate IC_{50} values for the orthologous main

proteases of SARS-CoV-1 and MERS-CoV. Finally, microscale thermophoresis was used as a biochemical assay to verify the binding of these compounds to recombinant M^{pro}.

2. Results

2.1. In Silico Studies

By using a ZINC library of 39,442 natural-product-like compounds and a second natural product library of 121 compounds that were preselected from medicinal plants with known antiviral activity, we performed virtual screening with PyRx. A total of 89 hits from the ZINC natural-product-like library and 32 hits from the antiviral natural product library were selected on the basis of their lowest PyRx-based binding energies to SARS-CoV-2 M^{pro}. These compounds were assessed using the Lipinski rules, and compounds with a molecular weight $\leq$ 500 and an octanol–water partition coefficient of log $p \leq 5$ were considered for further investigation, i.e., 21 candidate compounds from the ZINC database and 12 candidates from the antiviral natural product library. These 33 compounds were subjected to molecular docking with AutoDock 4.2.6. The lowest binding energy values (LBEs) and predicted inhibition constants (pKi's) of the 12 candidates from the antiviral natural product library that were used for subsequent experiments are shown in Table 1. Figure 1 depicts the structures of these 12 compounds and the known M^{pro} inhibitor, GC376, which was used as a positive control. To identify similarities between the main protease of seven human coronaviruses, we performed protein alignments. The results revealed 96.08%, 50.83%, 49.17%, 48.51%, 44.04%, and 41.06% identity of SARS-CoV-2 M^{pro} to SARS-CoV-1, MERS-CoV, HCoV-NL63, HcoV-OC43, HcoV-HKU1, and HcoV-229E, respectively (Table 2). Figure 2 shows the highly conserved amino acid residues between the seven human coronaviruses.

Table 1. Results of virtual screening with PyRx and molecular docking with AutoDock 4.2.6 of 12 selected compounds and GC376 as positive control binding to SARS-CoV-2 main protease.

Compound	PyRx Binding Affinity (kcal/mol)	Lowest Binding Energy (kcal/mol)	Predicted Ki (nM)
Hypericin	−8.70	−12.44 ± <0.01	0.762 ± 1.34
Curcumin	−7.90	−12.48 ± 0.04	0.679 ± 11.7
Isoliquiritin	−7.60	−11.69 ± 0.02	2.64 ± 0.11
Quercetin	−9.20	−10.72 ± 0.03	13.90 ± 0.80
Rosmarinic acid	−7.80	−9.98 ± 0.08	42.62 ± 3.25
Delphinidin	−8.50	−9.23 ± <0.01	170.92 ± 0.06
Cyanidin	−8.20	−9.13 ± <0.01	203.87 ± 0.04
Isorhamnetin	−8.20	−9.06 ± <0.01	237.99 ± 11.59
Luteolin	−8.10	−9.01 ± <0.01	247.73 ± 1.21
Kaempferol	−8.00	−8.77 ± <0.01	375.12 ± 0.05
Berberine	−8.10	−8.07 ± <0.01	1210 ± 0.01
Naringenin	−7.80	−8.00 ± 0.04	1370 ± 0.1
GC376 (positive control)	−8.00	−12.58 ± 0.29	0.70 ± 0.42

Table 2. Percent identity of SARS-CoV-2 M^{pro} with six human-pathogenic β-coronaviruses (complete protein sequence).

Human Coronavirus	% Identity with SARS-CoV-2
SARS-CoV-1	96.08
MERS-CoV	50.83
HcoV-NL63	49.17
HcoV-OC43	48.51
HcoV-HKU1	44.04
HcoV-229E	41.06

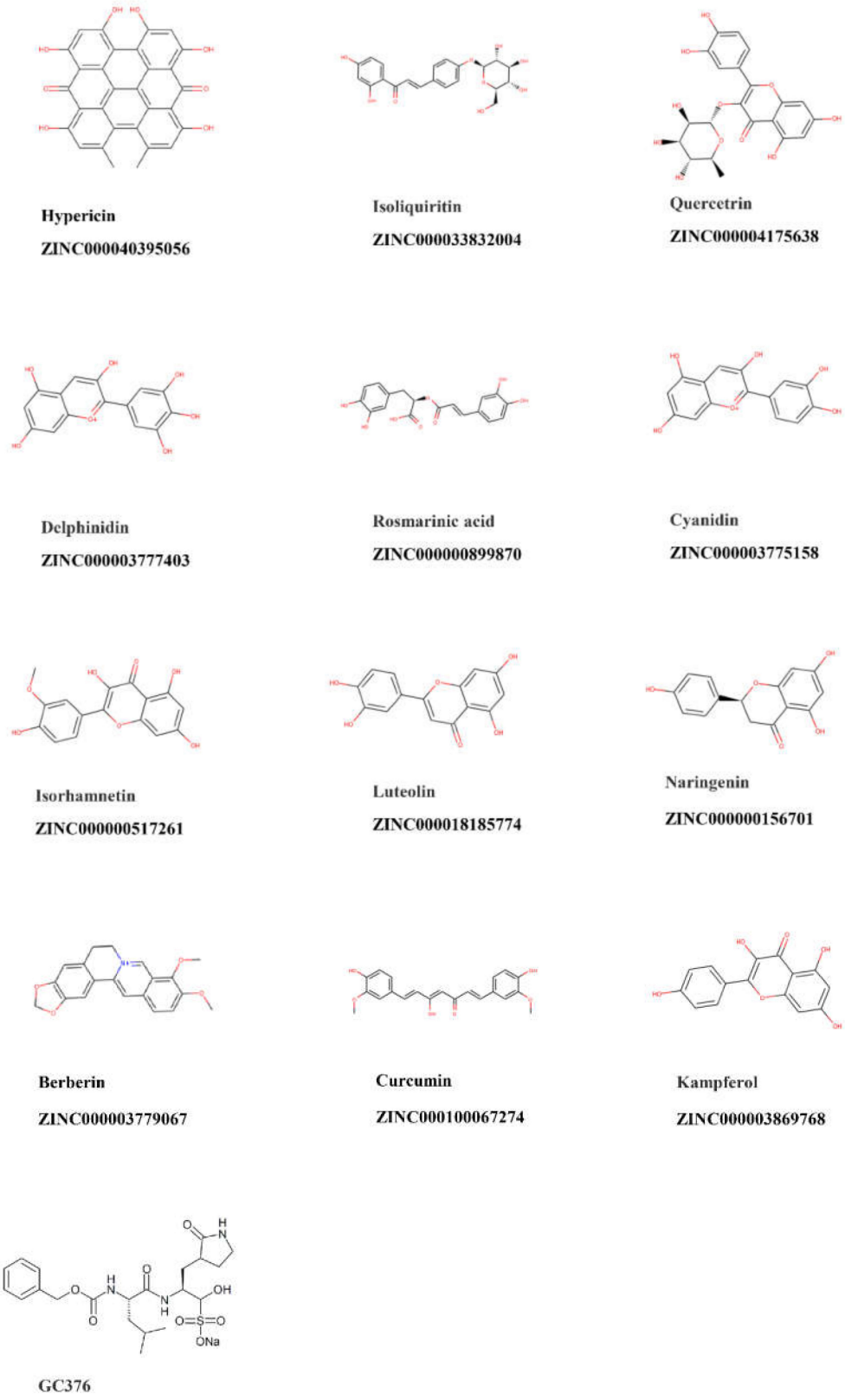

Figure 1. Chemical structures of the top 12 compounds with the lowest binding energy to SARS-CoV-2 main protease.

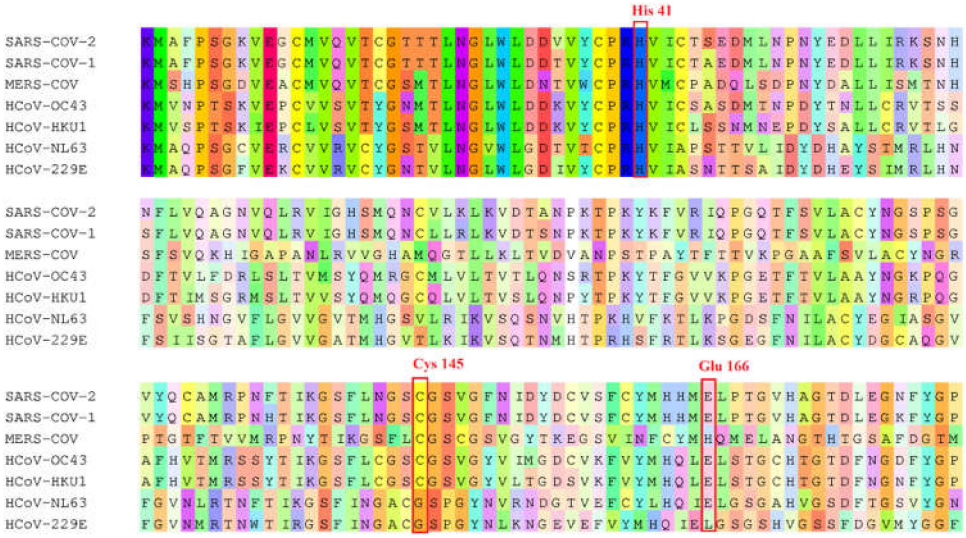

Figure 2. Sequence alignments of the main protease (binding site sequence) among SARS-CoV-2, SARS-CoV-1, MERS-CoV, HcoV-OC43, HcoV-HKU1, HcoV-NL63, and HcoV-299E. Catalytic residues are indicated by the red box.

2.2. Inhibition of M^{pro} Enzyme Activity

We performed in vitro enzymatic assays to validate whether the compounds selected from the in silico studies inhibit the activity of M^{pro} of SARS-CoV-2. As expected, hypericin, rosmarinic acid, isorhamnetin, and luteolin were the most active natural products among the 12 compounds preselected by our bioinformatical approach. These compounds inhibited enzymatic activity by more than 50% (Figure 3). Therefore, these four compounds were subjected to subsequent dose-response experiments to calculate the concentration of each compound required to inhibit M^{pro} activity by half (IC_{50}). The percentage of activity versus the log concentration of the inhibitors was used to calculate the IC_{50} values (Figure 4A–C). The IC_{50} values for hypericin, rosmarinic acid, isorhamnetin, and luteolin for SARS-CoV-2 CL^{pro} were 23.30, 9.43, 8.42, and 11.81 µM, respectively. The IC_{50} values for the inhibition of M^{pro} of SARS-CoV-1 by hypericin and isorhamnetin were 19.43 and 13.13 µM, respectively. Rosmarinic acid and luteolin inhibited the enzymatic activity of M^{pro} of SARS-CoV-1 only at the highest concentration of 100 µM by 31% and 44%, respectively. The IC_{50} value for the inhibition of MERS-CoV M^{pro} by hypericin was 49.65 µM. At a concentration of 100 µM, rosmarinic acid, luteolin, and isorhamnetin inhibited MERS-CoV M^{pro} activity to 14.9%, 21.3%, and 26.3%, respectively (Table 3).

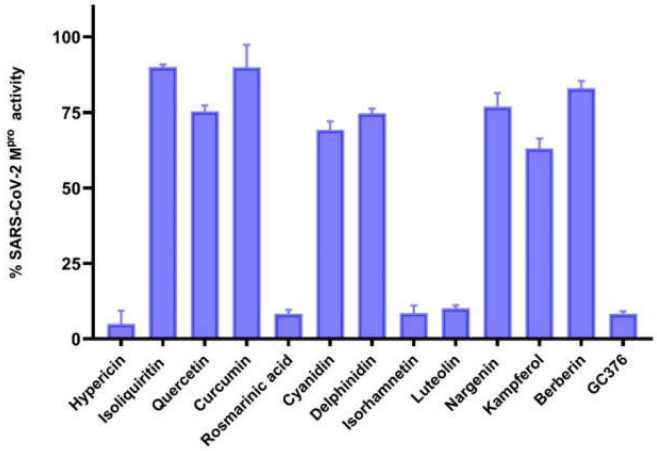

Figure 3. Percent activity of SARS-CoV-2 main protease in the presence of 12 compounds (100 µM). GC376 was used as a positive control. The results are expressed as mean value ± standard deviation.

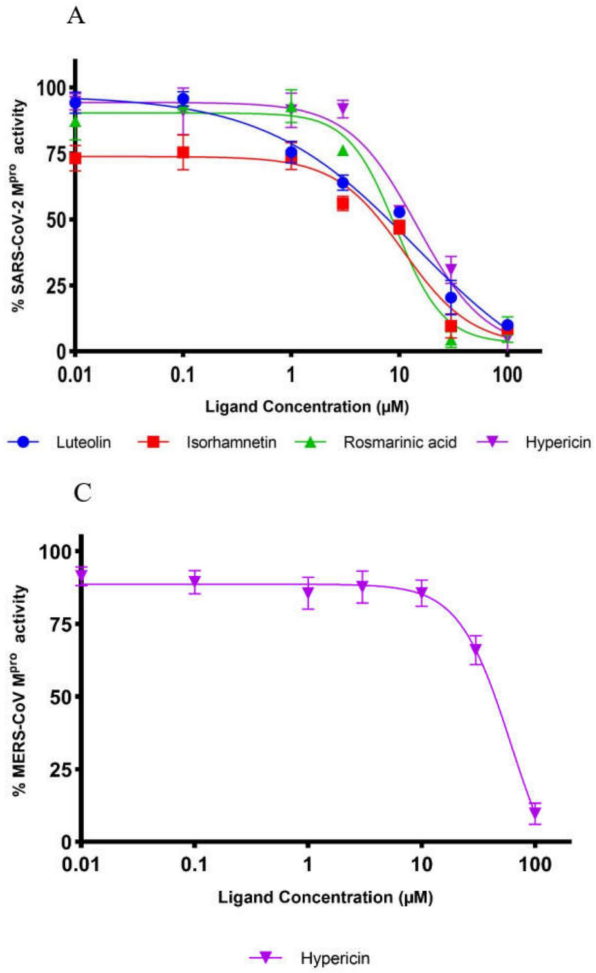

Figure 4. Dose-dependent inhibition of (**A**) SARS-CoV-2, (**B**) SARS-CoV-1, and (**C**) MERS-CoV main protease activity. Triplicate experiments were performed for each compound, and the IC_{50} values are presented as mean ± standard deviation (SD).

Table 3. IC_{50} values of selected compounds that inhibited M^{pro} of SARS-CoV-2, SARS-CoV-1, and MERS-CoV.

Compound	IC_{50} Value (μM) (mean ± SD)		
	SARS-CoV-2 M^{pro}	**SARS-CoV-1 M^{pro}**	**MERS-CoV M^{pro}**
Hypericin	23.30 ± 1.21	19.43 ± 3.11	49.65 ± 5.41
Rosmarinic acid	9.43 ± 0.46	n.a.	n.a.
Isorhamnetin	8.42 ± 1.15	13.13 ± 1.78	n.a.
Luteolin	11.81 ± 1.27	n.a.	n.a.

2.3. Microscale Thermophoresis

Microscale thermophoresis is a sensitive technique used to determine the binding between unlabeled molecules and labeled macromolecules (i.e., proteins). The labeled recombinant M^{pro} of SARS-CoV-2, SARS-CoV-1, and MERS-CoV were titrated against different concentrations of the selected compounds (Figure 5A–C). Hypericin, rosmarinic acid, isorhamnetin, and luteolin were bound in vitro to SARS-CoV-2 M^{pro} with Kd values of 7.73, 15.47, 4.379, and 13.417 μM, respectively. This was also the case with M^{pro} of the other coronavirus family members. SARS-CoV-1 M^{pro} was inhibited with Kd values of 25.49 μM by hypericin and 3.60 μM by isorhamnetin. MERS-CoV M^{pro} was inhibited with a Kd value of 54.91 μM by hypericin (Table 4).

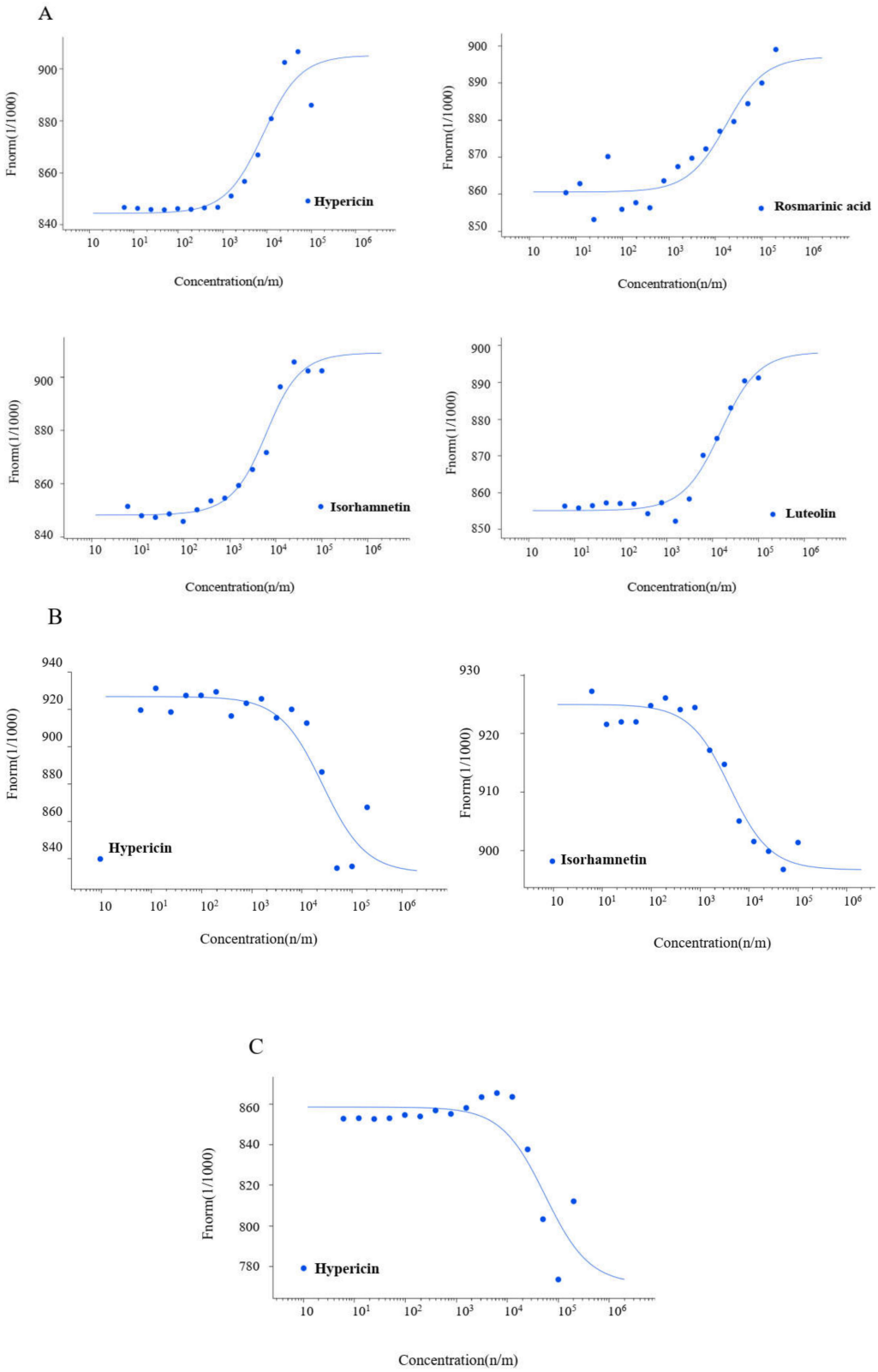

Figure 5. Binding of inhibitors to (**A**) SARS-CoV-2, (**B**) SARS-CoV-1, and (**C**) MERS-CoV main protease as measured by MST.

Table 4. K_d values of selected compounds inhibiting main proteases of SARS-CoV-2, SARS-CoV-1, and MERS-CoV.

Compound	Kd Value (μM)		
	SARS-CoV-2 M^{pro}	**SARS-CoV-1 M^{pro}**	**MERS-CoV M^{pro}**
Hypericin	7.73 ± 6.50	25.49 ± 13.61	54.91 ± 13.80
Rosmarinic acid	15.47 ± 4.77	n.a.	n.a.
Isorhamnetin	4.37 ± 3.90	3.60 ± 2.60	n.a.
Luteolin	13.41 ± 2.70	n.a.	n.a.

2.4. Binding of the Top Candidates

Molecular docking in silico revealed high binding affinities of the best candidate compounds and the control inhibitor, GC376, to M^{pro} of seven human coronaviruses (Table 5). Figure 6A–C shows the molecular interactions of potential inhibitors and GC376 with SARS-CoV-2, SARS-CoV-1, and MERS-CoV M^{pro}. The best candidate compounds shared the same binding site at M^{pro} as the control inhibitor, GC376. Hypericin, rosmarinic acid, isorhamnetin, luteolin, and the control inhibitor, GC376, formed hydrogen bonds or hydrophobic interactions with at least one of the catalytic residues (Cys^{145}, His^{41}) in the binding site of M^{pro} of SARS-CoV-2, SARS-CoV-1, and MERS-CoV (Figure 7A–C). Moreover, these compounds interacted with $Glu1^{166}$ of SARS-CoV-2 and SARS-CoV-1 and Glu^{169} of MERS-CoV, all of which play an important role in the dimerization of M^{pro} [28–31].

2.5. Cell Viability Assay

The inhibitory effects on the cell viability of the potential M^{pro} inhibitors toward human MRC-5 fibroblasts were assessed using the resazurin assay. As shown in Figure 8, luteolin and rosmarinic acid did not show significant inhibitory effects within the tested concentration range. Hypericin and isorhamnetin showed a slight inhibition of viability of MRC-5 cells with CC_{50} values of 55.46 ± 2.2 μM and 36.80 ± 3.4 μM, respectively (Table 6). The therapeutic indices of hypericin for SARS-CoV-2, SARS-CoV-1, and MERS-CoV M^{pro} were 2.38, 2.85, and 1.11, respectively. For isorhamnetin, the therapeutic index was 4.37 and 2.8 for SARS-CoV-2 and SARS-CoV-1, respectively (Table 7).

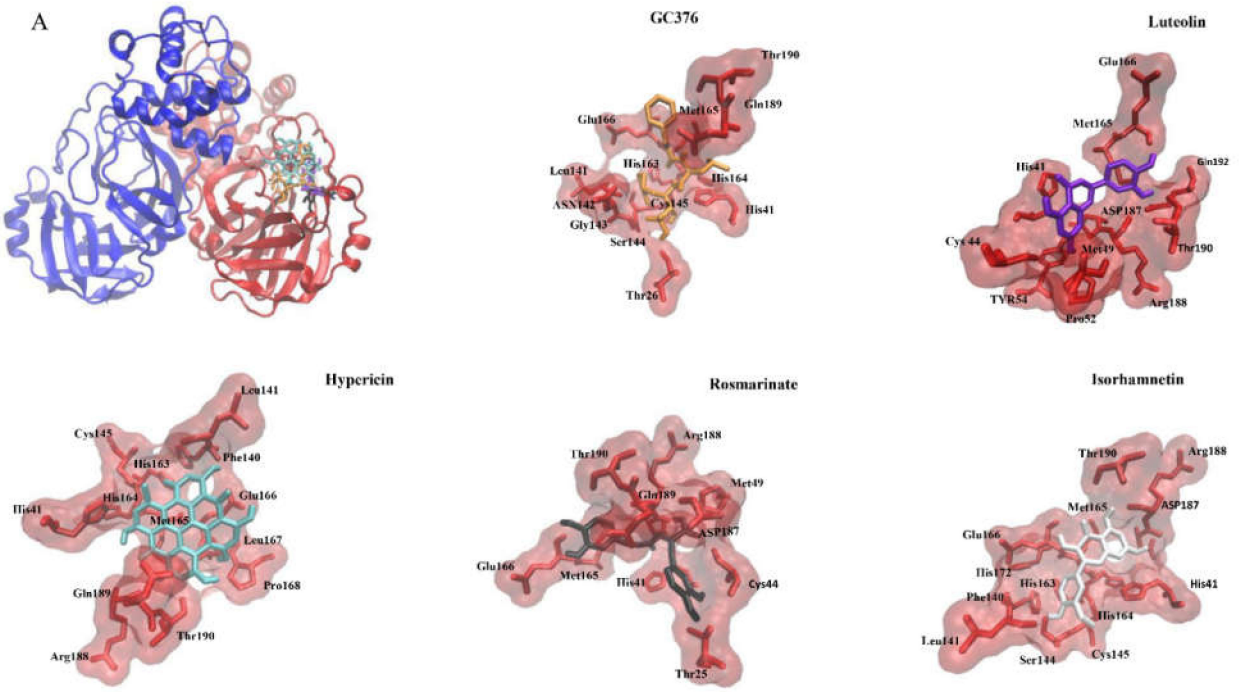

Figure 6. *Cont.*

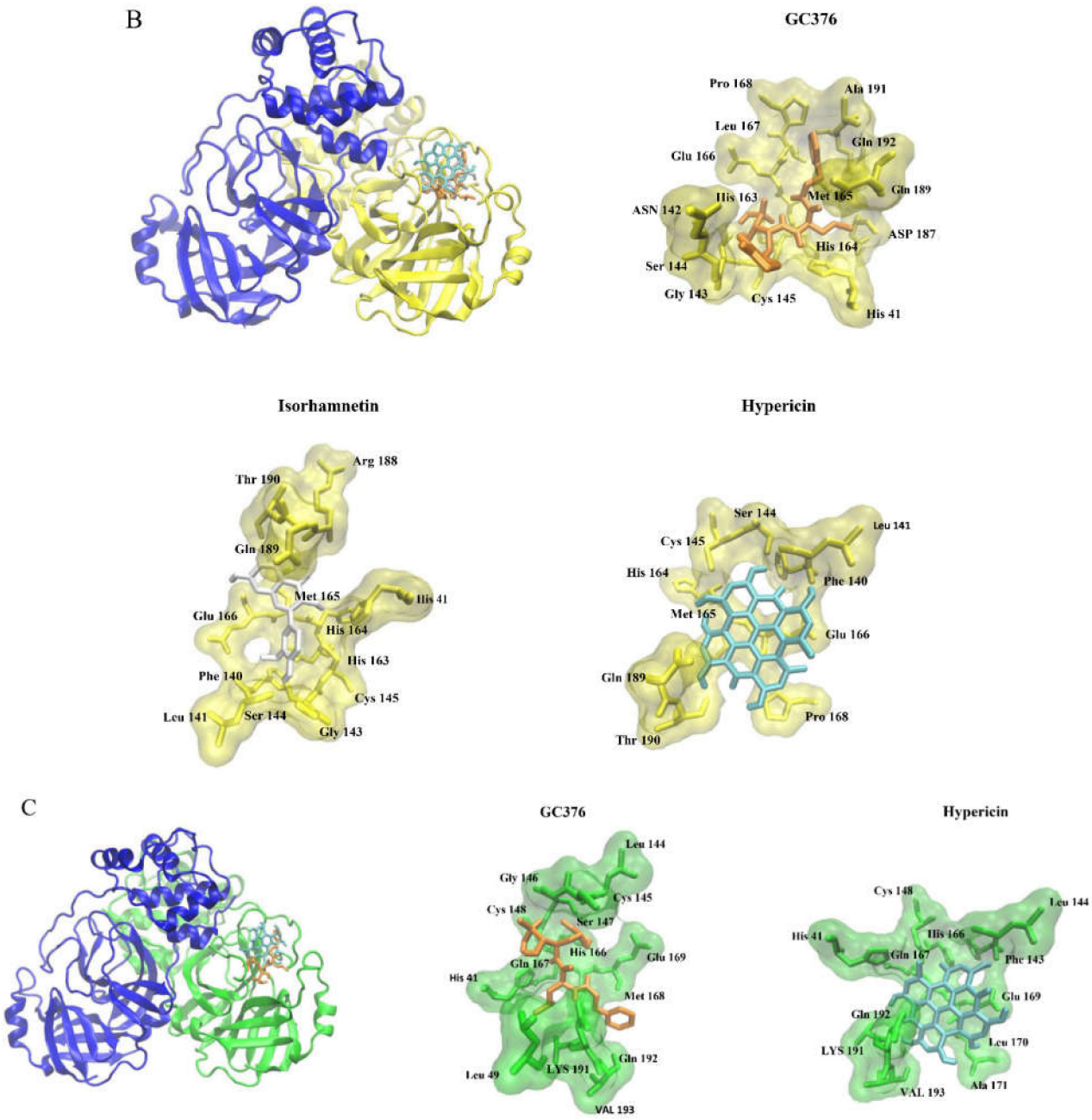

Figure 6. Molecular docking of potential inhibitors and GC376 (positive control) to the binding site of (**A**) SARS-CoV-2 M^{pro} (PDB ID: 6XMk), (**B**) SARS-CoV-1 M^{pro} (PDB ID:6xhl), and (**C**) MERS-CoV M^{pro} (PDB ID:6vh0).

Table 5. Molecular docking of potential inhibitors and GC376 (positive control) to the catalytic center of main proteases of human-pathogenic coronaviruses.

Compound	Lowest Binding Energy (kcal/mol)						
	SARS-CoV-2	**SARS-CoV-1**	**MERS-CoV**	**HCoV-HKU1**	**HCoV-NL63**	**HCoV-OC43**	**HCoV-229E**
Hypericin	−12.44 ± <0.01	−11.53 ± 0.005	−11.98 ± 1.77	−9.11 ± < 0.01	−9.77 ± 0.31	−12.99 ± <0.01	−10.65 ± <0.01
Rosmarinic acid	−9.90 ± 0.08	−9.80 ± 0.03	−10.12 ± 0.21	−10.48 ± 0.31	−10.18 ± 0.11	−10.06 ± 0.06	−10.61 ± 0.05
Isorhamnetin	−9.06 ± <0.01	−8.83 ± <0.01	−8.59 ± <0.01	−8.50 ± <0.01	−8.57 ± <0.01	−8.33 ± <0.01	−8.19 ± 0.01
Luteolin	−9.01 ± <0.01	−7.66 ± <0.01	−7.67 ± 0.06	−7.65 ± <0.01	−9.25 ± <0.01	−8.21 ± <0.01	−8.02 ± <0.01
GC376 (positive control)	−12.58 ± 0.29	−12.17 ± 0.27	−13.65 ± 0.44	−12.78 ± 0.5	−11.04 ± 0.09	−12.28 ± 0.05	−11.52 ± 0.09

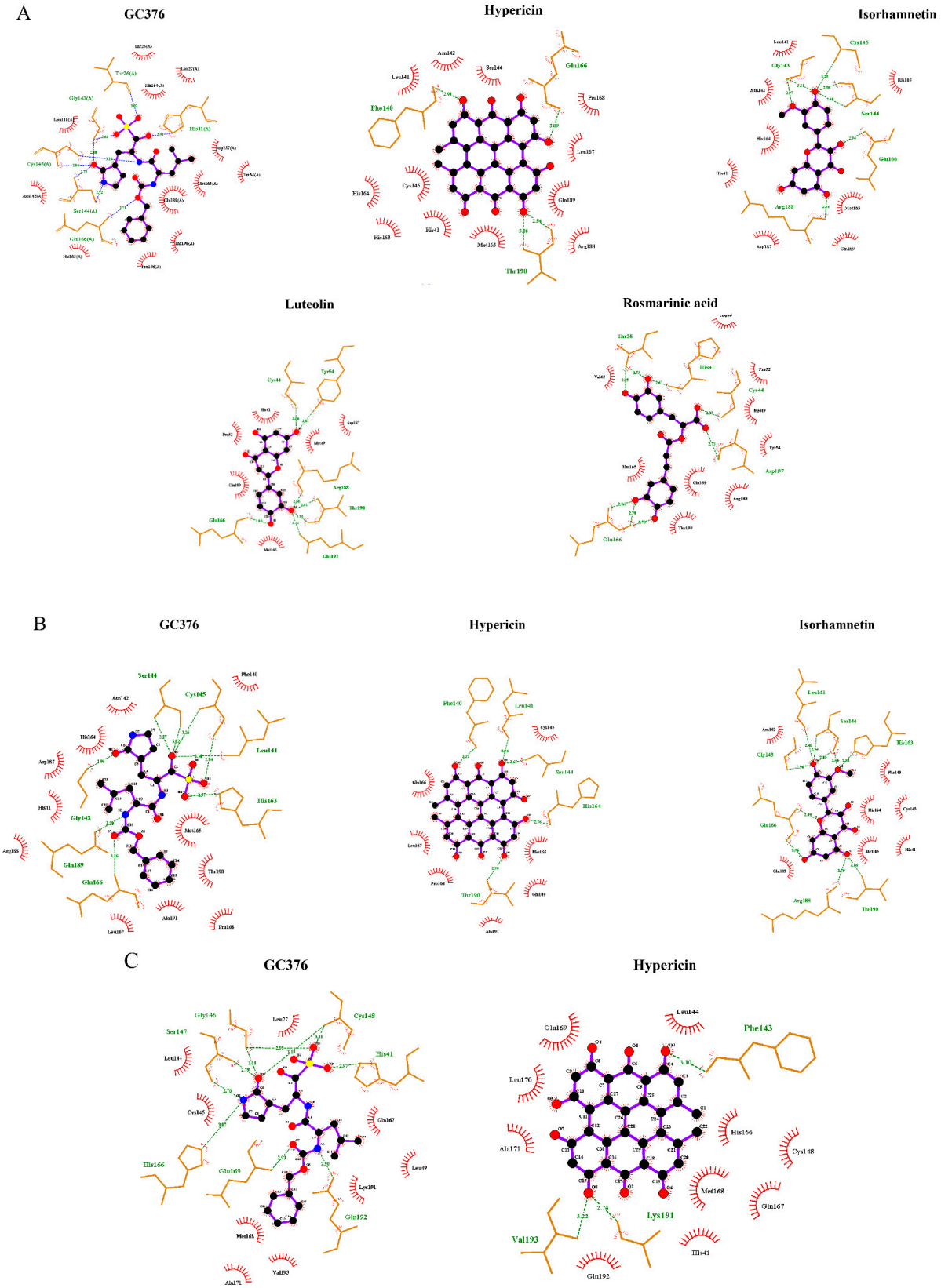

Figure 7. Two-dimensional representations of inhibitor interactions with (**A**) SARS-CoV-2 M^{pro}, (**B**) SARS-CoV-1 M^{pro}, and (**C**) MERS-CoV M^{pro} were analyzed using Ligplot. Hydrogen bonds are shown as green dotted lines, while the spoked arcs represent residues forming hydrophobic interactions with the ligands.

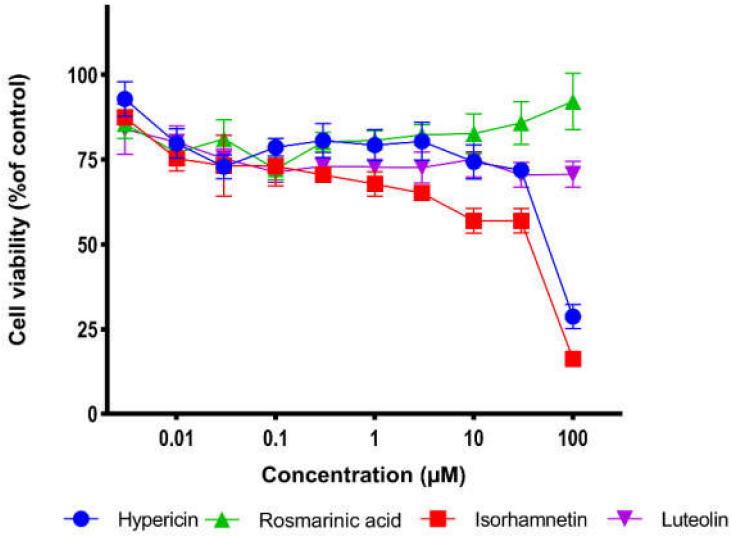

Figure 8. Dose-response curves of candidate compounds against MRC-5 cell line. Data are shown as mean values ± standard deviations of three independent experiments by the resazurin assay.

Table 6. Cytotoxicity of candidate compounds toward human fetal MRC-5 lung fibroblast cells as determined by the resazurin reduction assay.

Compound	CC_{50} Value (μM)
	(mean ± SD)
Hypericin	55.46 ± 2.2
Isorhamnetin	36.80 ± 3.4
Rosmarinic acid	n.a.
Luteolin	n.a.

Table 7. Therapeutic index values of hypericin and isorhamnetin.

Compound	Therapeutic Index		
	SARS-CoV-2 M^{pro}	SARS-CoV-1 M^{pro}	MERS-CoV M^{pro}
Hypericin	2.38	2.85	1.11
Isorhamnetin	4.37	2.80	n.a.

3. Discussion

During the past two decades, highly infectious pathogens rapidly emerged, such as SARS-CoV-1 in 2003, MERS-CoV in 2012, and SARS-CoV-2 at the end of 2019. Therefore, there is an urgent need to investigate new broad-spectrum anti-CoVs drugs. The main protease was proposed as a promising target for the development of pan-coronaviral drugs as it significantly differs from human proteases and is highly conserved between coronavirus family members [16].

In this study, we first performed a computer-based approach to screen 39,442 natural-product-like compounds from the ZINC database and 121 preselected natural products from medicinal plants with known antiviral activity to find candidate compounds with a high binding affinity to SARS-CoV-2 M^{pro}. As a result of PyRx-based virtual drug screening, assessment using the Lipinski rule of five, and molecular docking using AutoDock 4.2.6, 33 compounds were selected and subjected to AutoDock to validate the virtual screening results. Twelve compounds were selected for further in vitro experiments. To analyze whether these 12 compounds affect SARS-CoV-2 M^{pro} activity in vitro, we performed M^{pro} enzyme activity inhibition assays. Hypericin, rosmarinic acid, isorhamnetin, and luteolin inhibited SARS-CoV-2 M^{pro}. The binding site of SARS-CoV-2 includes a catalytic dyad (His41 and Cys145) and several subsites (S1–S5). The S1 subunit consists of His163, Glu166,

Cys145, Gly143, His172, and Phe140. The S2 subunit comprises Cys145, His41, and Thr25. S3–S5 consists of Met165, Met49, His41, Glu166, and Gln189. These subunits play a key role in substrate binding [32,33]. Molecular docking revealed that hypericin, rosmarinic acid, isorhamnetin, and luteolin not only bound to M^{pro} through these subunits but also interacted (hydrophobic or hydrogen binding) with at least one of the catalytic center residues (His41 and Cys145) (Figure 7A). Moreover, microscale thermophoresis confirmed the binding of these four natural compounds to SARS-CoV-2 M^{pro}. Although the K_d values were different, all compounds showed a high binding affinity to SARS-CoV-2 M^{pro}. Consequently, we concluded that the in silico data reflected the in vitro situation as there was a good correlation between the computationally predicted lowest binding energies (−12.44, −9.98, −9.06, and −9.01 kcal/mol) and the experimentally measured percentages of activity (4.95%, 8.28%, 8.56%, and 10.10%) of SARS-CoV-2 M^{pro} in the presence of hypericin, rosmarinic acid, isorhamnetin, and luteolin, respectively. To develop a potential pan-HCoV inhibitor, we also performed M^{pro} enzyme activity inhibition assays for SARS-CoV-1 and MERS-CoV. Hypericin and isorhamnetin inhibited SARS-CoV-1 M^{pro}, while only hypericin inhibited MERS-CoV M^{pro}. Microscale thermophoresis confirmed that these two compounds were bound to SARS-CoV-1 and MERS-CoV M^{pro} with high affinities.

Cell viability assays showed that luteolin and rosmarinic acid did not inhibit human fetal MRC-5 lung fibroblasts in the highest concentration tested (100 μM) while hypericin and isorhamnetin showed slight toxicity.

Hypericin is a natural polyquinone from *Hypericum perforatum* (St. John's wort) and is traditionally used as an anti-depressive and wound-healing drug [34]. Hypericin has antitumor, antivirus, and anti-depression activity. It exhibits in vitro activity against infectious bronchitis virus (IBV) by the inhibition of apoptosis in host cells and the production of reactive oxygen species [35]. Additionally, hypericin inhibits hepatitis C virus (HCV) replication via downregulation of heme oxygenase-1 expression and deacetylation in vitro [36]. However, hypericin caused phytotoxicity without detectable anti-HCV activity in patients with chronic HCV infection who were provided oral doses of 0.05 and 0.10 mg/kg/d [37]. Although hypericin inhibits human immunodeficiency virus (HIV) in vitro and in vivo [38,39], a clinical trial revealed phytotoxicity of orally administered hypericin (0.5 mg/kg daily) without antiretroviral activity in a limited number of patients [40]. Moreover, hypericin inhibits the replication of α-coronaviruses (PEDV and TGEV) through the inhibition of M^{pro} [41]. Hypericin inhibits M^{pro} of SARS-CoV-2 with a CC_{50} value of 63.6 μM [42]. Our in silico and in vitro results indicated that hypericin both binds and inhibits M^{pro} of β-coronaviruses. Previous in silico and in vitro studies showed that hypericin has anti-inflammatory activity [43–45] and is a potential treatment for rheumatoid arthritis [44]. Thus, hypericin is a promising pan-CoV inhibitor that, due to its anti-inflammatory effects, may be used in coronavirus-infected patients suffering from autoimmune reactions ("long COVID") who are prohibited from obtaining anti-coronavirus vaccinations. This is an advantageous feature that distinguishes this compound from other approved drugs.

Rosmarinic acid, an ester of caffeic acid and 3,4-dihydroxy phenyl lactic acid, is present in most Lamiaceae species [46]. It has a broad inhibitory effect on a variety of viruses, e.g., rosmarinic acid inhibits HBV replication in HBV-infected cells by specifically targeting DNA polymerase ε binding [47]. It also inhibits influenza viruses and enterovirus 71 [48,49]. Although previous studies suggested that rosmarinic acid inhibits SARS-CoV-2 replication with an IC_{50} value of 25.47 ng/μL, the mechanism of action is still unknown [50]. Our results indicated that rosmarinic acid binds to SARS-CoV-2 M^{pro} with an IC_{50} value of 9.43 μM. Additionally, several animal studies revealed that rosmarinic acid has anti-inflammatory activity through the inhibition of NF-κB and STAT3 signaling pathways [51,52] and may be applied against arthritis, inflammatory bowel disease, and asthma [53]. Hence, rosmarinic acid is a potential therapeutic against COVID-19, especially for fighting immunological overreactions (i.e., the cytokine storm) during severe courses of the disease.

Isorhamnetin is a flavonoid from *Hippophae rhamnoides* L. [54], *Artemisia absinthium* L. [55], and other plants. Isorhamnetin has a wide range of pharmacological effects on cardiovascular diseases, a variety of tumors, and neurodegenerative diseases [54]. Isorhamnetin exerts anti-influenza effects in vitro and in vivo by inhibition of hemagglutinin and neuraminidase [56]. Isorhamnetin also inhibits SARS-CoV-2 entry through inhibition of the Spike protein [57]. Our results showed that isorhamnetin binds and inhibits M^{pro} of SARS-CoV-2 and SARS-CoV-1 with IC_{50} values of 8.42 and 13.13 µM, respectively. Isorhamnetin has anti-inflammatory effects against different diseases, such as inflammatory bowel disease [58], osteoarthritis, and periodontitis, by suppressing the production of inflammatory mediators, cytokines, and reactive oxygen species [54]. Hence, targeting the Spike protein and M^{pro} makes isorhamnetin a promising drug candidate for the inhibition of coronavirus entry and replication.

Luteolin is a natural flavonoid that is extensively present in many plant species [59]. It has multiple biological effects such as anti-inflammation, antiallergy, and anticancer activities [60]. In vivo and in vitro studies demonstrated that luteolin inhibits HBV replication through ERK-mediated downregulation of HNF4α expression [61]. It also exhibits antiviral activity against influenza A virus, HIV-1, and JEV [62–64]. Our results demonstrated that luteolin binds to SARS-CoV-2 M^{pro} and inhibits its activity with an IC_{50} value of 11.81 µM. Several in vivo and in vitro studies revealed that luteolin has an anti-inflammatory effect by blocking the NF-κB and AP-1 activation pathways [65–68]. Luteolin was also suggested as a potential therapeutic strategy for various autoimmune diseases, such as Hashimoto's thyroiditis and multiple sclerosis [69,70]. Therefore, luteolin may be beneficial for COVID-19 patients with overshooting autoimmune reactions.

In conclusion, we demonstrated that it is possible to identify natural products that exert activity against several coronaviruses and may be useful for developing pan-coronaviral drugs. There was some selectivity between the inhibition of coronaviral M^{pro} and cytotoxic activity toward human lung cells. Though the cytotoxicity was very low, the inhibitory rates toward the tested coronaviral main proteases were in the micromolar but not nanomolar range. Hence, animal experimentation should clarify whether this in vitro activity is reflected in vivo. Furthermore, the chemical scaffolds of the identified natural products may serve as lead structures when generating (semi)synthetic derivatives with improved activity. The concept of developing pan-coronaviral drugs is attractive for being prepared for future outbreaks of epidemic or pandemics by known or novel coronaviruses.

4. Materials and Methods

4.1. Compounds

The chemical structures of natural products were downloaded from ZINC and PubChem databases in three-dimensional SDF format. Based on in silico studies, 12 selected compounds were provided by Fischer Analytics/Fischer Organics GmbH (Weiler, Germany). The compounds had a purity of >95%.

4.2. Virtual Screening

In this study, the PyRx software was used for the virtual screening of 39,442 natural-product-like compounds from the ZINC database and 121 natural compounds used in herbal medicines against viral diseases. As a target, the dimeric form of SARS-CoV-2 M^{pro} (PDB ID: 6XMk) was chosen to identify compounds with high binding affinity and low binding energy (kcal/mol). AutoDock version 1.5.6 was used to convert the Protein Data Bank files of target proteins (PDB) to PDBQT files. The energy of the compounds was minimized and converted from SDF format to PDBQT format using the PyRx software.

4.3. Sequence Alignment

The full-length amino acid sequences of M^{pro} of SARS-CoV-2, SARS-CoV-1, MERS-CoV, HCoV-HKU1, HCoV-NL63, HCoV-OC43, and HCoV-229E were accessed from the UniProt database and aligned by Clustal Omega; figures were prepared using Jalviwe 2.11.1.4.

4.4. Inhibition of M^{pro} Enzyme Activity

Enzymatic assays were performed using the SensoLyte SARS-CoV-2 3CL Protease Activity Assay Kit (AnaSpec, San Francisco, CA, USA), SARS-CoV-1 Assay Kit, and 3CL Protease MERS-CoV Assay Kit (BPS Bioscience, San Diego, CA, USA). Twelve selected compounds were diluted in assay buffer to a final concentration of 1 mM. Compound aliquots of 10 µL were added to black 96-well plates (Greiner, Frickenhausen, Germany), and 40 µL of 0.1 mg/mL M^{pro} was added to each well of the plates and incubated with the compounds at 37 °C for 30 min. The enzymatic reactions were initiated by adding a fluorescent substrate. The final concentration of the compound was 100 µM. Fluorescence was measured using an Infinite M2000 Pro plate reader (Tecan, Crailsheim, Germany). All values were subtracted from blank values. Then, compounds exhibiting more than 50% inhibitory activity at a fixed concentration of 100 µM were selected for dose-response studies in a concentration range from 0 to 100 µM for SARS-CoV-2, SARS-CoV-1, and MERS-CoV to calculate 50% inhibition concentrations (IC_{50}). The activity percentage of M^{pro} was calculated using the following equation: Activity % = $100 - [(RFU_{\text{Vehicle control}} - RFU_{\text{tested sample}})/RFU_{\text{Vehicle control}} \times 100]$.

4.5. Molecular Docking

The top compounds obtained from in vitro experiments were subjected to AutoDock 4.2.6 to identify their binding affinity to M^{pro} of SARS-CoV-2, SARS-CoV-1 (PDB ID: 6xhl), MERS-CoV (PDB ID: 6vh0), HCoV-HKU1 (PDB ID: 3d23), HCoV-NL63 (PDB ID: 3tlo), HCoV-OC43, and HCoV-229E (PDB ID: 2zu2). SWISS-MODEL was used to model the main protease structure. For this purpose, a Lamarckian algorithm was used with 250 runs and 2.5 million energy evaluations, as previously described in [71]. Docking was conducted using the high-performance supercomputer, MOGON II (Johannes Gutenberg University, Mainz, Germany). Three-dimensional illustrations of the compound–protein interactions were prepared using Molecular Dynamics (VMD) software.

4.6. Microscale Thermophoresis

We performed microscale thermophoresis (MST) to determine the dissociation constant (Kd) values for binding of hypericin, rosmarinic acid, isorhamnetin, and luteolin to recombinant M^{pro} proteins of SARS-CoV-2, SARS-CoV-1, and MERS-CoV (Bio-Techne, Wiesbaden, Germany). This method was performed as previously described in [71]. The three recombinant proteins were labeled with Monolith Protein Labeling Kit RED-NHS 2nd Generation (MO-L011, Nano Temper Technologies GmbH, Munich, Germany) according to the manufacturer's instructions. The final protein concentrations after labeling were 3530, 882, and 910 nM for recombinant M^{pro} of SARS-CoV-2, SARS-CoV-1, and MERS-CoV, respectively. Titration was performed using a wide concentration range of compounds (dilution steps 1:1). The incubation time of ligand and protein was 30 min at room temperature in assay buffer (50 mM Tris buffer (pH 7.4) containing 10 mM $MgCl_2$, 150 mM NaCl, and 0.05% Tween-20). Measurements were carried out in Monolith NT.115 standard capillaries (MO-K022, Nano Temper Technologies GmbH, Munich, Germany). Signals were measured using Monolith NT.115 instrument (Nano Temper Technologies) under the settings 40% LED power and 20, 10, and 40 MST power for recombinant M^{pro} proteins of SARS-CoV-2, SARS-CoV-1, and MERS-CoV, respectively. Fitting curves and Kd values were calculated by MO.Affinity Analysis software (Nano Temper Technologies).

4.7. Cell Viability Assay

Cell viability was measured using the resazurin assay as previously described in [72]. Human diploid MRC-5 lung fibroblasts was kindly provided by Dr. rer. nat. Sebastian Zahnreich (Department of Radiation Oncology and Radiation Therapy, University Medical Center of the Johannes Gutenberg University, Mainz, Germany) were seeded (5×10^5 cells per well) into 96-well culture plates and incubated overnight before treatment. On the second day, the cells were treated with 10 concentrations of the four compounds in a

range of 0.3–100 µM. After 72 h incubation, 20 µL 0.01% resazurin (Promega, Mannheim, Germany) was added to each well. Fluorescence was detected after 4 h incubation using an Infinite M2000 Pro plate reader (Tecan) at Ex/Em = 550 nm/590 nm wavelength. Cell viability was calculated in comparison to DMSO control. The DMSO final concentration was 0.5%. The 50% cytotoxicity concentration (CC_{50}) values were calculated in comparison to the DMSO-treated control. Each experiment was independently repeated three times with six wells for each concentration. Therapeutic indices were calculated using the following equation: Therapeutic index = TD_{50}/ED_{50}.

5. Conclusions

Overall, our in silico and in vitro results demonstrated that hypericin is a potential novel pan-anti-coronaviral agent as it binds to and inhibits M^{pro} of human-pathogenic coronaviruses. Moreover, isorhamnetin showed inhibitory effects toward SARS-CoV-2 and SARS-CoV-1 M^{pro}, while luteolin revealed inhibitory effects against SARS-CoV-2 M^{pro} (Figure 9). Our results need to be further validated in animal models and clinical trials. A typical feature of natural products is that they are frequently multi-specific, i.e., they exert specific activities against several targets [73]. Therefore, the anti-coronaviral activity of the compounds we investigated is complemented with known anti-inflammatory effects reported in the literature. This may qualify these compounds not only to inhibit coronavirus replication but also to improve inflammatory conditions in severe courses of COVID-19 and other coronavirus infections. Natural products are generally considered to be of low toxicity. This is another property that speaks in favor of the four compounds we investigated.

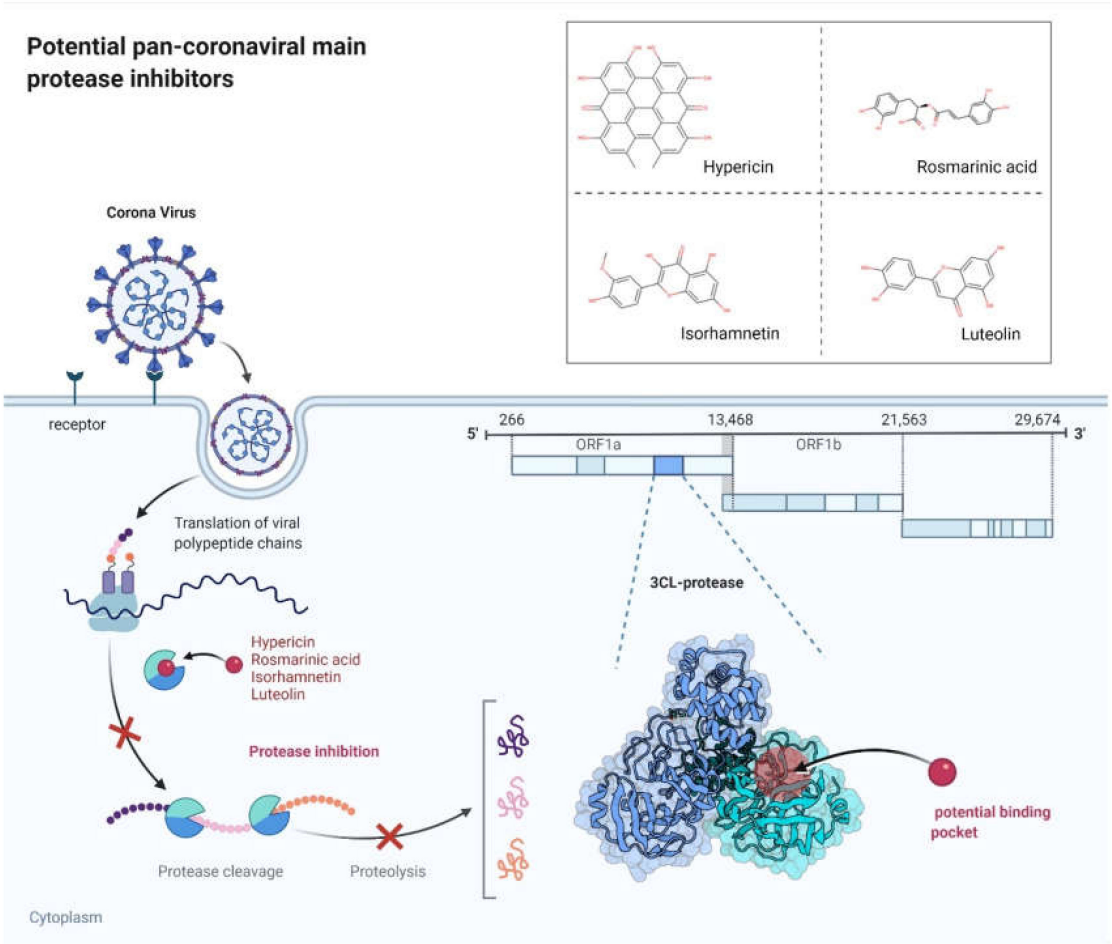

Figure 9. Potential pan-coronaviral M^{pro} inhibitors. Image adapted from BioRender.com (2022) with permission.

Author Contributions: Conceptualization, N.S., S.A., and T.E.; methodology, N.S. and SA.; formal analysis, N.S.; writing—original draft preparation, N.S.; writing—review and editing, N.S., S.A., and T.E.; supervision, T.E. All authors have read and agreed to the published version of the manuscript.

Funding: This research was funded by a donation from Marc Strobel, CVC Capital Partners, Frankfurt a. M., Germany.

Institutional Review Board Statement: Not applicable.

Informed Consent Statement: Not applicable.

Data Availability Statement: Data is contained within the article.

Acknowledgments: We are grateful for a stipend from the Georg Scheuing Foundation to N.S and Edmond Fischer (Fischer Analytics/Fischer Organics (Weiler, Germany) for the provision of compounds and Sebastian Zahnreich for donating the MRC-5 cells.

Conflicts of Interest: The authors declare that there is no conflict of interest. The stipend, donation, and provision of compounds had no influence on the design, performance, or evaluation of results.

References

1. V'Kovski, P.; Kratzel, A.; Steiner, S.; Stalder, H.; Thiel, V. Coronavirus biology and replication: Implications for SARS-CoV-2. *Nat. Rev. Microbiol.* **2021**, *19*, 155–170. [CrossRef]
2. Park, S.E. Epidemiology, virology, and clinical features of severe acute respiratory syndrome -coronavirus-2 (SARS-CoV-2; Coronavirus Disease-19). *Korean J. Pediatr.* **2020**, *63*, 119–124. [CrossRef]
3. Totura, A.L.; Bavari, S. Broad-spectrum coronavirus antiviral drug discovery. *Expert Opin. Drug Discov.* **2019**, *14*, 397–412. [CrossRef] [PubMed]
4. Xia, S.; Yan, L.; Xu, W.; Agrawal, A.S.; Algaissi, A.; Tseng, C.-T.K.; Wang, Q.; Du, L.; Tan, W.; Wilson, I.A.; et al. A pan-coronavirus fusion inhibitor targeting the HR1 domain of human coronavirus spike. *Sci. Adv.* **2019**, *5*, eaav4580. [CrossRef] [PubMed]
5. Menachery, V.D.; Yount, B.L., Jr.; Debbink, K.; Agnihothram, S.; Gralinski, L.E.; Plante, J.A.; Graham, R.L.; Scobey, T.; Ge, X.-Y.; Donaldson, E.F.; et al. A SARS-like Cluster of Circulating Bat Coronaviruses Shows Potential for Human Emergence. *Nat. Med.* **2015**, *21*, 1508–1513. [CrossRef]
6. Xiao, K.; Zhai, J.; Feng, Y.; Zhou, N.; Zhang, X.; Zou, J.-J.; Li, N.; Guo, Y.; Li, X.; Shen, X.; et al. Isolation of SARS-CoV-2-related coronavirus from Malayan pangolins. *Nature* **2020**, *583*, 286–289. [CrossRef]
7. Wacharapluesadee, S.; Tan, C.W.; Maneeorn, P.; Duengkae, P.; Zhu, F.; Joyjinda, Y.; Kaewpom, T.; Ni Chia, W.; Ampoot, W.; Lim, B.L.; et al. Evidence for SARS-CoV-2 related coronaviruses circulating in bats and pangolins in Southeast Asia. *Nat. Commun.* **2021**, *12*, 972. [CrossRef]
8. Grange, Z.L.; Goldstein, T.; Johnson, C.K.; Anthony, S.; Gilardi, K.; Daszak, P.; Olival, K.J.; O'Rourke, T.; Murray, S.; Olson, S.H.; et al. Ranking the risk of animal-to-human spillover for newly discovered viruses. *Proc. Natl. Acad. Sci. USA* **2021**, *118*, e2002324118. [CrossRef]
9. Johnson, C.K.; Hitchens, P.L.; Pandit, P.S.; Rushmore, J.; Evans, T.S.; Young, C.C.W.; Doyle, M.M. Global shifts in mammalian population trends reveal key predictors of virus spillover risk. *Proc. R. Soc. B Biol. Sci.* **2020**, *287*, 20192736. [CrossRef]
10. Lu, R.; Zhao, X.; Li, J.; Niu, P.; Yang, B.; Wu, H.; Wang, W.; Song, H.; Huang, B.; Zhu, N.; et al. Genomic characterisation and epidemiology of 2019 novel coronavirus: Implications for virus origins and receptor binding. *Lancet* **2020**, *395*, 565–574. [CrossRef]
11. Harrison, A.G.; Lin, T.; Wang, P. Mechanisms of SARS-CoV-2 Transmission and Pathogenesis. *Trends Immunol.* **2020**, *41*, 1100–1115. [CrossRef] [PubMed]
12. Hu, B.; Guo, H.; Zhou, P.; Shi, Z.-L. Characteristics of SARS-CoV-2 and COVID-19. *Nat. Rev. Microbiol.* **2021**, *19*, 141–154. [CrossRef] [PubMed]
13. Kneller, D.W.; Phillips, G.; O'Neill, H.M.; Jedrzejczak, R.; Stols, L.; Langan, P.; Joachimiak, A.; Coates, L.; Kovalevsky, A. Structural plasticity of SARS-CoV-2 3CL Mpro active site cavity revealed by room temperature X-ray crystallography. *Nat. Commun.* **2020**, *11*, 3202. [CrossRef]
14. Jin, Z.; Du, X.; Xu, Y.; Deng, Y.; Liu, M.; Zhao, Y.; Zhang, B.; Li, X.; Zhang, L.; Peng, C.; et al. Structure of Mpro from SARS-CoV-2 and discovery of its inhibitors. *Nature* **2020**, *582*, 289–293. [CrossRef] [PubMed]
15. Ma, C.; Sacco, M.D.; Hurst, B.; Townsend, J.A.; Hu, Y.; Szeto, T.; Zhang, X.; Tarbet, B.; Marty, M.; Chen, Y.; et al. Boceprevir, GC-376, and calpain inhibitors II, XII inhibit SARS-CoV-2 viral replication by targeting the viral main protease. *Cell Res.* **2020**, *30*, 678–692. [CrossRef] [PubMed]
16. Ullrich, S.; Nitsche, C. The SARS-CoV-2 main protease as drug target. *Bioorg. Med. Chem. Lett.* **2020**, *30*, 127377. [CrossRef]
17. Hilgenfeld, R. From SARS to MERS: Crystallographic studies on coronaviral proteases enable antiviral drug design. *FEBS J.* **2014**, *281*, 4085–4096. [CrossRef]
18. Lipinski, C.A.; Lombardo, F.; Dominy, B.W.; Feeney, P.J. Drug Delivery Reviews Experimental and computational approaches to estimate solubility and permeability in drug discovery and development settings. *Adv. Drug Deliv. Rev.* **2001**, *46*, 3–26. [CrossRef]

19. Musarra-Pizzo, M.; Pennisi, R.; Ben-Amor, I.; Mandalari, G.; Sciortino, M. Antiviral Activity Exerted by Natural Products against Human Viruses. *Viruses* **2021**, *13*, 828. [CrossRef]
20. Koehn, F.E.; Carter, G.T. The evolving role of natural products in drug discovery. *Nat. Rev. Drug Discov.* **2005**, *4*, 206–220. [CrossRef]
21. Kadioglu, O.; Saeed, M.; Greten, H.J.; Efferth, T. Identification of novel compounds against three targets of SARS CoV-2 coronavirus by combined virtual screening and supervised machine learning. *Comput. Biol. Med.* **2021**, *133*, 104359. [CrossRef] [PubMed]
22. Miskovsky, P. Hypericin—A New Antiviral and Antitumor Photosensitizer: Mechanism of Action and Interaction with Biological Macromolecules. *Curr. Drug Targets* **2002**, *3*, 55–84. [CrossRef]
23. Fukuchi, K.; Okudaira, N.; Adachi, K.; Odai-Ide, R.; Watanabe, S.; Ohno, H.; Yamamoto, M.; Kanamoto, T.; Terakubo, S.; Nakashima, H.; et al. Antiviral and Antitumor Activity of Licorice Root Extracts. *In Vivo* **2016**, *30*, 777–786. [CrossRef] [PubMed]
24. Jennings, M.; Parks, R. Curcumin as an Antiviral Agent. *Viruses* **2020**, *12*, 1242. [CrossRef] [PubMed]
25. Vázquez-Calvo, A.; de Oya, N.J.; Martin-Acebes, M.A.; Garcia-Moruno, E.; Saiz, J.-C. Antiviral Properties of the Natural Polyphenols Delphinidin and Epigallocatechin Gallate against the Flaviviruses West Nile Virus, Zika Virus, and Dengue Virus. *Front. Microbiol.* **2017**, *8*, 1314. [CrossRef]
26. Cataneo, A.H.D.; Kuczera, D.; Koishi, A.C.; Zanluca, C.; Silveira, G.F.; De Arruda, T.B.; Suzukawa, A.A.; Bortot, L.O.; Dias-Baruffi, M.; Verri, W.A., Jr.; et al. The citrus flavonoid naringenin impairs the in vitro infection of human cells by Zika virus. *Sci. Rep.* **2019**, *9*, 16348. [CrossRef]
27. Kai, H.; Obuchi, M.; Yoshida, H.; Watanabe, W.; Tsutsumi, S.; Park, Y.K.; Matsuno, K.; Yasukawa, K.; Kurokawa, M. In vitro and in vivo anti-influenza virus activities of flavonoids and related compounds as components of Brazilian propolis (AF-08). *J. Funct. Foods* **2014**, *8*, 214–223. [CrossRef]
28. Cheng, S.-C.; Chang, G.-G.; Chou, C.-Y. Mutation of Glu-166 Blocks the Substrate-Induced Dimerization of SARS Coronavirus Main Protease. *Biophys. J.* **2010**, *98*, 1327–1336. [CrossRef]
29. Zhang, L.; Lin, D.; Sun, X.; Curth, U.; Drosten, C.; Sauerhering, L.; Becker, S.; Rox, K.; Hilgenfeld, R. Crystal structure of SARS-CoV-2 main protease provides a basis for design of improved α-ketoamide inhibitors. *Science* **2020**, *368*, 409–412. [CrossRef]
30. Tomar, S.; Johnston, M.L.; John, S.E.S.; Osswald, H.L.; Nyalapatla, P.R.; Paul, L.N.; Ghosh, A.K.; Denison, M.R.; Mesecar, A.D. Ligand-induced Dimerization of Middle East Respiratory Syndrome (MERS) Coronavirus nsp5 Protease (3CLpro): Implications for Nsp5 Regulation and the Development of Antivirals. *J. Biol. Chem.* **2015**, *290*, 19403–19422. [CrossRef]
31. Ho, B.-L.; Cheng, S.-C.; Shi, L.; Wang, T.-Y.; Ho, K.-I.; Chou, C.-Y. Critical Assessment of the Important Residues Involved in the Dimerization and Catalysis of MERS Coronavirus Main Protease. *PLoS ONE* **2015**, *10*, e0144865. [CrossRef] [PubMed]
32. Khan, S.A.; Zia, K.; Ashraf, S.; Uddin, R.; Ul-Haq, Z. Identification of chymotrypsin-like protease inhibitors of SARS-CoV-2 via integrated computational approach. *J. Biomol. Struct. Dyn.* **2021**, *39*, 2607–2616. [CrossRef] [PubMed]
33. Lu, I.-L.; Mahindroo, N.; Liang, P.-H.; Peng, Y.-H.; Kuo, C.-J.; Tsai, K.-C.; Hsieh, H.-P.; Chao, Y.-S.; Wu, S.-Y. Structure-Based Drug Design and Structural Biology Study of Novel Nonpeptide Inhibitors of Severe Acute Respiratory Syndrome Coronavirus Main Protease. *J. Med. Chem.* **2006**, *49*, 5154–5161. [CrossRef] [PubMed]
34. Birt, D.F.; Widrlechner, M.P.; Hammer, K.D.P.; Hillwig, M.L.; Wei, J.; Kraus, G.A.; Murphy, P.A.; McCoy, J.A.; Wurtele, E.S.; Neighbors, J.D.; et al. Hypericum in Infection: Identification of Anti-Viral and Anti-Inflammatory Constituents. *Pharm. Biol.* **2009**, *47*, 774–782. [CrossRef] [PubMed]
35. Chen, H.; Feng, R.; Muhammad, I.; Abbas, G.; Zhang, Y.; Ren, Y.; Huang, X.; Zhang, R.; Diao, L.; Wang, X.; et al. Protective effects of hypericin against infectious bronchitis virus induced apoptosis and reactive oxygen species in chicken embryo kidney cells. *Poult. Sci.* **2019**, *98*, 6367–6377. [CrossRef]
36. Shih, C.-M.; Wu, C.-H.; Wu, W.-J.; Hsiao, Y.-M.; Ko, J.-L. Hypericin inhibits hepatitis C virus replication via deacetylation and down-regulation of heme oxygenase-1. *Phytomedicine* **2018**, *46*, 193–198. [CrossRef]
37. Jacobson, J.M.; Feinman, L.; Liebes, L.; Ostrow, N.; Koslowski, V.; Tobia, A.; Cabana, B.E.; Lee, D.-H.; Spritzler, J.; Prince, A.M. Pharmacokinetics, Safety, and Antiviral Effects of Hypericin, a Derivative of St. John's Wort Plant, in Patients with Chronic Hepatitis C Virus Infection. *Antimicrob. Agents Chemother.* **2001**, *45*, 517–524. [CrossRef]
38. Lavie, G.; Valentine, F.; Levin, B.; Mazur, Y.; Gallo, G.; Lavie, D.; Weiner, D.; Meruelo, D. Studies of the mechanisms of action of the antiretroviral agents hypericin and pseudohypericin. *Proc. Natl. Acad. Sci. USA* **1989**, *86*, 5963–5967. [CrossRef]
39. Xu, Y. Raman spectroscopic study on structure of human immu-nodeficiency virus (HIV) and hypericin-induced photosen-sitive damage of HIV. *Sci. China Ser. C Life Sci.* **2005**, *48*, 117. [CrossRef]
40. Gulick, R.M.; McAuliffe, V.; Holden-Wiltse, J.; Crumpacker, C.; Liebes, L.; Stein, D.S.; Meehan, P.; Hussey, S.; Forcht, J.; Valentine, F.T. Phase I Studies of Hypericin, the Active Compound in St. John's Wort, as an Antiretroviral Agent in HIV-Infected Adults: AIDS Clinical Trials Group Protocols 150 and 258. *Ann. Intern. Med.* **1999**, *130*, 510–514. [CrossRef]
41. Zhang, Y.; Chen, H.; Zou, M.; Oerlemans, R.; Shao, C.; Ren, Y.; Zhang, R.; Huang, X.; Li, G.; Cong, Y. Hypericin Inhibit Alpha-Coronavirus Replication by Targeting 3CL Protease. *Viruses* **2021**, *13*, 1825. [CrossRef] [PubMed]
42. Pitsillou, E.; Liang, J.; Karagiannis, C.; Ververis, K.; Darmawan, K.K.; Ng, K.; Hung, A.; Karagiannis, T.C. Interaction of small molecules with the SARS-CoV-2 main protease in silico and in vitro validation of potential lead compounds using an enzyme-linked immunosorbent assay. *Comput. Biol. Chem.* **2020**, *89*, 107408. [CrossRef] [PubMed]

43. Dellafiora, L.; Galaverna, G.; Cruciani, G.; Dall'Asta, C.; Bruni, R. On the Mechanism of Action of Anti-Inflammatory Activity of Hypericin: An In Silico Study Pointing to the Relevance of Janus Kinases Inhibition. *Molecules* **2018**, *23*, 3058. [CrossRef] [PubMed]
44. Zhang, K.; Gao, S.; Guo, J.; Ni, G.; Chen, Z.; Li, F.; Zhu, X.; Wen, Y.; Guo, Y. Hypericin-photodynamic therapy inhibits proliferation and induces apoptosis in human rheumatoid arthritis fibroblast-like synoviocytes cell line MH7A. *Iran. J. Basic Med. Sci.* **2018**, *21*, 130–137. [CrossRef] [PubMed]
45. Perinbam, K.; Mahendrakumar, M.; Seeni, S. Hypericin, an anthraquinone derivative of Hypericum hookerianum wight and Arn. (Hypericaceae) of Palni Hills, South India, exhibits anti-inflammatory property in lipopolysaccharide—stimulated raw 264.7 macrophages. *Pharmacogn. Mag.* **2018**, *14*, 378. [CrossRef]
46. Levsh, O.; Pluskal, T.; Carballo, V.; Mitchell, A.J.; Weng, J.-K. Independent evolution of rosmarinic acid biosynthesis in two sister families under the Lamiids clade of flowering plants. *J. Biol. Chem.* **2019**, *294*, 15193–15205. [CrossRef]
47. Tsukamoto, Y.; Ikeda, S.; Uwai, K.; Taguchi, R.; Chayama, K.; Sakaguchi, T.; Narita, R.; Yao, W.-L.; Takeuchi, F.; Otakaki, Y.; et al. Rosmarinic acid is a novel inhibitor for Hepatitis B virus replication targeting viral epsilon RNA-polymerase interaction. *PLoS ONE* **2018**, *13*, e0197664. [CrossRef]
48. Mahalapbutr, P.; Sangkhawasi, M.; Kammarabutr, J.; Chamni, S.; Rungrotmongkol, T. Rosmarinic Acid as a Potent Influenza Neuraminidase Inhibitor: In Vitro and In Silico Study. *Curr. Top. Med. Chem.* **2020**, *20*, 2046–2055. [CrossRef]
49. Hsieh, C.-F.; Jheng, J.-R.; Lin, G.-H.; Chen, Y.-L.; Ho, J.-Y.; Liu, C.-J.; Hsu, K.-Y.; Chen, Y.-S.; Chan, Y.F.; Yu, H.-M.; et al. Rosmarinic acid exhibits broad anti-enterovirus A71 activity by inhibiting the interaction between the five-fold axis of capsid VP1 and cognate sulfated receptors. *Emerg. Microbes Infect.* **2020**, *9*, 1194–1205. [CrossRef]
50. Elebeedy, D.; Elkhatib, W.F.; Kandeil, A.; Ghanem, A.; Kutkat, O.; Alnajjar, R.; Saleh, M.A.; El Maksoud, A.I.A.; Badawy, I.; Al-Karmalawy, A.A. Anti-SARS-CoV-2 activities of tanshinone IIA, carnosic acid, rosmarinic acid, salvianolic acid, baicalein, and glycyrrhetinic acid between computational and in vitro insights. *RSC Adv.* **2021**, *11*, 29267–29286. [CrossRef]
51. Jiang, K.; Ma, X.; Guo, S.; Zhang, T.; Zhao, G.; Wu, H.; Wang, X.; Deng, G. Anti-inflammatory Effects of Rosmarinic Acid in Lipopolysaccharide-Induced Mastitis in Mice. *Inflammation* **2017**, *41*, 437–448. [CrossRef]
52. Jin, B.-R.; Chung, K.-S.; Cheon, S.-Y.; Lee, M.; Hwang, S.; Hwang, S.N.; Rhee, K.-J.; An, H.-J. Rosmarinic acid suppresses colonic inflammation in dextran sulphate sodium (DSS)-induced mice via dual inhibition of NF-κB and STAT3 activation. *Sci. Rep.* **2017**, *7*, srep46252. [CrossRef]
53. Luo, C.; Zou, L.; Sun, H.; Peng, J.; Gao, C.; Bao, L.; Ji, R.; Jin, Y.; Sun, S. A Review of the Anti-Inflammatory Effects of Rosmarinic Acid on Inflammatory Diseases. *Front. Pharmacol.* **2020**, *11*, 153. [CrossRef]
54. Gong, G.; Guan, Y.-Y.; Zhang, Z.-L.; Rahman, K.; Wang, S.-J.; Zhou, S.; Luan, X.; Zhang, H. Isorhamnetin: A review of pharmacological effects. *Biomed. Pharmacother.* **2020**, *128*, 110301. [CrossRef]
55. Haghi, G.; Safaei, A.; Ghomi, J.S. Identification and determination of flavonoids in leaf, dried aqueous and dried hydroalcoholic extract of Artemisia absinthium by HPLC. *Iran. J. Basic Med. Sci.* **2004**, *3*, 89–90.
56. Dayem, A.A.; Choi, H.Y.; Kim, Y.B.; Cho, S.-G. Antiviral Effect of Methylated Flavonol Isorhamnetin against Influenza. *PLoS ONE* **2015**, *10*, e0121610. [CrossRef]
57. Zhan, Y.; Ta, W.; Tang, W.; Hua, R.; Wang, J.; Wang, C.; Lu, W. Potential antiviral activity of isorhamnetin against SARS-CoV-2 spike pseudotyped virus in vitro. *Drug Dev. Res.* **2021**, *82*, 1124–1130. [CrossRef]
58. Dou, W.; Zhang, J.; Li, H.; Kortagere, S.; Sun, K.; Ding, L.; Ren, G.; Wang, Z.; Mani, S. Plant flavonol isorhamnetin attenuates chemically induced inflammatory bowel disease via a PXR-dependent pathway. *J. Nutr. Biochem.* **2014**, *25*, 923–933. [CrossRef]
59. Imran, M.; Rauf, A.; Abu-Izneid, T.; Nadeem, M.; Shariati, M.A.; Khan, I.A.; Imran, A.; Orhan, I.E.; Rizwan, M.; Atif, M.; et al. Luteolin, a flavonoid, as an anticancer agent: A review. *Biomed. Pharmacother.* **2019**, *112*, 108612. [CrossRef]
60. Lin, Y.; Shi, R.; Wang, X.; Shen, H.-M. Luteolin, a Flavonoid with Potential for Cancer Prevention and Therapy. *Curr. Cancer Drug Targets* **2008**, *8*, 634–646. [CrossRef]
61. Bai, L.; Nong, Y.; Shi, Y.; Liu, M.; Yan, L.; Shang, J.; Huang, F.; Lin, Y.; Tang, H. Luteolin Inhibits Hepatitis B Virus Replication through Extracellular Signal-Regulated Kinase-Mediated Down-Regulation of Hepatocyte Nuclear Factor 4α Expression. *Mol. Pharm.* **2015**, *13*, 568–577. [CrossRef] [PubMed]
62. Fan, W.; Qian, S.; Qian, P.; Li, X. Antiviral activity of luteolin against Japanese encephalitis virus. *Virus Res.* **2016**, *220*, 112–116. [CrossRef] [PubMed]
63. Yan, H.; Ma, L.; Wang, H.; Wu, S.; Huang, H.; Gu, Z.; Jiang, J.; Li, Y. Luteolin decreases the yield of influenza A virus in vitro by interfering with the coat protein I complex expression. *J. Nat. Med.* **2019**, *73*, 487–496. [CrossRef] [PubMed]
64. Mehla, R.; Bivalkar-Mehla, S.; Chauhan, A. A Flavonoid, Luteolin, Cripples HIV-1 by Abrogation of Tat Function. *PLoS ONE* **2011**, *6*, e27915. [CrossRef] [PubMed]
65. Ueda, H.; Yamazaki, C.; Yamazaki, M. Luteolin as an Anti-Inflammatory and Anti-Allergic Constituent of Perilla. *Biol. Pharm. Bull.* **2002**, *25*, 1197–1202. [CrossRef]
66. Chen, C.-Y.; Peng, W.-H.; Tsai, K.-D.; Hsu, S.-L. Luteolin suppresses inflammation-associated gene expression by blocking NF-κB and AP-1 activation pathway in mouse alveolar macrophages. *Life Sci.* **2007**, *81*, 1602–1614. [CrossRef]
67. Franza, L.; Carusi, V.; Nucera, E.; Pandolfi, F. Luteolin, inflammation and cancer: Special emphasis on gut microbiota. *BioFactors* **2021**, *47*, 181–189. [CrossRef]
68. Theoharides, T.C. Luteolin as a therapeutic option for multiple sclerosis. *J. Neuroinflamm.* **2009**, *6*, 29. [CrossRef]

69. Xia, N.; Chen, G.; Liu, M.; Ye, X.; Pan, Y.; Ge, J.; Mao, Y.; Wang, H.; Wang, J.; Xie, S. Anti-inflammatory effects of luteolin on experimental autoimmune thyroiditis in mice. *Exp. Ther. Med.* **2016**, *12*, 4049–4054. [CrossRef]
70. Zeino, M.; Saeed, M.E.M.; Kadioglu, O.; Efferth, T. The ability of molecular docking to unravel the controversy and challenges related to P-glycoprotein—a well-known, yet poorly understood drug transporter. *Investig. New Drugs* **2014**, *32*, 618–625. [CrossRef]
71. Abdelfatah, S.; Berg, A.; Böckers, M.; Efferth, T. A selective inhibitor of the Polo-box domain of Polo-like kinase 1 identified by virtual screening. *J. Adv. Res.* **2019**, *16*, 145–156. [CrossRef]
72. Abdelfatah, S.; Fleischer, E.; Klinger, A.; Wong, V.K.W.; Efferth, T. Identification of inhibitors of the polo-box domain of polo-like kinase 1 from natural and semisynthetic compounds. *Investig. New Drugs* **2019**, *38*, 1–9. [CrossRef]
73. Efferth, T. Complex Interactions between Phytochemicals. The Multi-Target Therapeutic Concept of Phytotherapy. *Curr. Drug Targets* **2011**, *12*, 122–132. [CrossRef]

Biomedicine & Pharmacotherapy 183 (2025) 117841

Contents lists available at ScienceDirect

Biomedicine & Pharmacotherapy

journal homepage: www.elsevier.com/locate/biopha

Diketopiperazine/piperidine alkaloid as a potential broad-spectrum coronaviral entry inhibitor identified by supercomputer-based virtual screening from a large natural product-based library

Nasim Shahhamzehei [a], Sara Abdelfatah [a], Ejlal A. Omer [a], Max Riedl [b,c], Christian Meesters [b], Hannah S. Schwarzer-Sperber [d], Kathrin Sutter [d,e], Gerhard Bringmann [f], Roland Schwarzer [e,*], Thomas Efferth [a,*]

[a] Department of Pharmaceutical Biology, Institute of Pharmaceutical and Biomedical Sciences, Johannes Gutenberg University, Staudinger Weg 5, Mainz 55128, Germany
[b] HPC-Group, NHR-Southwest, Johannes Gutenberg University, Mainz, Germany
[c] Institute for Medical Informatics, Statistics and Epidemiology, University of Leipzig, Germany
[d] Institute for the Research on HIV and AIDS-associated Diseases (HIV-AAD), University Hospital Essen, University Duisburg-Essen, Essen, Germany
[e] Institute for Virology, University Hospital Essen, University Duisburg-Essen, Essen, Germany
[f] Institute of Organic Chemistry, University of Würzburg, Am Hubland, Würzburg 97074, Germany

ARTICLE INFO

Keywords:
Alkaloids
COVID-19
Natural products
SARS-CoV-2 spike protein
Virtual drug screening

ABSTRACT

The COVID-19 pandemic has underscored the urgent need for antiviral agents capable of targeting a broad range of coronaviruses, including emerging variants of SARS-CoV-2. While vaccines have been pivotal, the search for drugs that can prevent viral entry into host cells remains crucial, especially against evolving viral forms and other coronaviruses. In this study, we investigated natural products as a source of antiviral agents, focusing on their potential to block the spike protein's receptor-binding domain (RBD). Utilizing a library of over 210,000 natural product-based compounds from the ZINC database, we employed a Snakemake workflow to screen for inhibitors against RBDs of SARS-CoV-2, its variants, SARS-CoV, and MERS-CoV. Among top N-heterocyclic candidates from virtual screening we found that one compound, *i.e.*, ((2 *R*,8*S*)-6-(1-benzylpiperidin-4-yl)-2-naphthalen-1-yl-3,6,17-triazatetracyclo[8.7.0.03,8.011,16]heptadeca-1(10),11,13,15 tetraene-4,7-dione), inhibited SARS-CoV-2 pseudovirus and live virus entry in HEK-ACE2 and Vero E6 host cells at low micromolar IC_{50} values. Cell viability assays showed that this compound exerted low cytotoxicity towards HEK-ACE2 while it was not toxic against Vero E6 and MRC5 cell lines. Microscale thermophoresis revealed that this compound strongly bound to the RBDs of SARS-CoV-2, SARS-CoV-2 XBB, SARS-CoV, MERS-CoV, and HCoV-HKU1, with their K_d values increasing as sequence similarity decreased. Molecular docking studies indicated this active compound binds to the SARS-CoV-2 spike protein RBD and interacts with hotspot amino acid residues required for the RBD-ACE2 interaction and cellular infection. These findings show that this diketopiperazine/piperidine-type alkaloid can be considered for further development as a potential pan-coronavirus entry inhibitor.

1. Introduction

The COVID-19 pandemic caused by severe acute respiratory syndrome coronavirus 2 (SARS-CoV-2) had a profound impact on global health, marking the fifth viral pandemic since the 1918 influenza outbreak [1]. Following its first report in Wuhan, China in 2019, it quickly spread around the world with more than 7 million fatalities and close to 776 million reported cases as of September 2024 [2]. While vaccines, monoclonal antibodies, and antiviral drugs have been developed and deployed to curb the spread of SARS-CoV-2, the continuous emergence of new mutant strains, particularly the Omicron subvariants, poses a significant challenge. These variants have demonstrated an increased ability to evade immune detection, reducing the efficacy of existing vaccines and antibody therapies [3,4]. Furthermore, re-infections have a cumulative impact, emphasizing the need for robust and enduring antiviral interventions [5,6]. Current antiviral therapies

* Corresponding authors.
E-mail addresses: Roland.Schwarzer@uk-essen.de (R. Schwarzer), efferth@uni-mainz.de (T. Efferth).

https://doi.org/10.1016/j.biopha.2025.117841
Received 1 October 2024; Received in revised form 3 January 2025; Accepted 10 January 2025
Available online 13 January 2025

for SARS-CoV-2, such as molnupiravir and remdesivir, target the RNA-dependent RNA polymerase (RdRp), while Paxlovid® inhibits the main protease (Mpro). However, these treatments are not without limitations. Concerns about the mutagenic potential of molnupiravir, resistance development to remdesivir, and significant drug-drug interactions with Paxlovid® highlight the need for novel antiviral agents [7]. To date, no small molecule has been approved to target the spike protein, a trimeric structure on the viral surface that plays a vital role in the attachment of the virus and its entry into host cells. Notably, no approved small molecule currently targets the spike protein, a key component responsible for viral attachment and entry into host cells. The spike protein, a trimeric structure, consists of two subunits S1 and S2, each with distinct domains crucial for its function [8]. The receptor-binding domain (RBD) within the S1 subunit plays a pivotal role in binding to the angiotensin-converting enzyme 2 (ACE2) receptor on host cells, facilitating viral entry [9]. Given the central role of the spike protein RBD in the viral infection process, it represents a promising target for therapeutic intervention.

Natural products have demonstrated substantial potential as antiviral agents against SARS-CoV-2 and related respiratory viruses. Several bioactive compounds, including flavonoids, terpenoids, alkaloids, and phenolics, have shown inhibitory effects on key viral targets such as the main protease (Mpro), papain-like protease (PLpro), and the receptor-binding domain (RBD) of the spike protein. For instance, hypericin has demonstrated broad-spectrum inhibitory activity against the main protease (Mpro) of coronaviruses[10]. EGCG, the most active compound extracted from green tea and betulinic acid, is reported to blocks the binding and attachment of the RBD to the ACE2 receptor, reducing the infection rate, inhibiting virus infections[11]. Drug discovery and development remain costly and time-intensive endeavors [12]. Recent advances in computer-aided drug discovery (CADD) offer a solution to expedite this process, particularly through *in silico* screening methods that have proven invaluable during the COVID-19 pandemic [13]. These approaches allow for the rapid identification and optimization of potential drug candidates, significantly reducing the time and costs associated with traditional drug discovery methods. In this study, we employed a high-throughput *in silico* screening approach using a Snakemake workflow on the high-performance computing cluster "Mogon II" [14,15]. This automated, reproducible workflow enabled the efficient screening of over 210,000 natural product-based small molecules from the ZINC database against the RBD of the SARS-CoV-2 spike protein, its variants, SARS-CoV, and MERS-CoV. Following virtual screening, we conducted *in vitro* experiments to evaluate the top candidates' efficacy, aiming to develop a broad-spectrum entry inhibitor against the coronavirus family. This approach ensured automated, highly reproducible execution, facilitating the efficient screening of 210,541 natural-based small molecules from the ZINC database against the receptor-binding domain (RBD) of the spike protein of SARS-CoV2, its variants, SARS-CoV1, and MERS-CoV. Subsequently, we tested the top candidates through various *in vitro* experiments to develop a pan-entry inhibitor against the coronavirus family.

2. Materials and methods

2.1. Cell lines

Human embryonic kidney cells (HEK-ACE2) were purchased from ATCC (American Type Culture Collection, Virginia, USA). The HEK 293 T cell line was generously provided by Dr. Helen May-Simera (Institute of Molecular Physiology, Johannes Gutenberg University, Mainz, Germany). They were cultured in Dulbecco's Modified Eagle Medium (DMEM) (Gibco, Eggenstein, Germany) supplemented with 10 % fetal bovine serum (FBS) and 1 % penicillin/streptomycin (P/S) (Invitrogen, Darmstadt, Germany). Human fetal lung fibroblast cells (MRC-5) were acquired from Dr. Sebastian Zahnreich (Department of Radiation Oncology and Radiation Therapy, University Medical Center of the Johannes Gutenberg University, Mainz, Germany) and cultured in DMEM, low glucose, pyruvate medium with 15 % FBS, 1 % P/S, and 1 % MEM. Non-essential amino acids (Thermo Fisher, Dreieich, Germany) were used for cultivation. Vero E6 cells were obtained from ATCC and cultured in DMEM supplemented with 10 % FBS, 1 % L-glutamine (Capricorn Scientific, Epsdorfergrund, Germany), and 1 % P/S. All cell lines were incubated in a humidified atmosphere at 37 °C and 5 % CO_2.

2.2. Compounds

The top 30 compounds selected from virtual screening were purchased from Vitas M Chemical (Hong Kong SAR, China). The compounds had a purity of $>$ 90 %. All compounds were dissolved in DMSO at a concentration of 20 mM and stored at −20 °C.

2.3. Virtual drug screening

Virtual screening and estimation of binding affinities were performed using a Snakemake workflow that implemented automated steps of structural-based screening. The workflow uses Snakemake (version 6.0.5) for the workflow orchestration, Vina LC (version 1.3.0) for structure-based ligand screening, Open Babel (version 3.0.0) to convert chemical data formats, build indices of datasets, search for substructures, and minimize energy, and Biopython (version 1.75) for the preparation of the target structure. Three major steps constituted the presented workflow: First, preprocessing including, downloading library of 210,541 natural product-based compounds, downloading the target structures (SARS-CoV-2 PDB ID: 7CWM) and preparing ligands by removing error causing structures and energy minimization, removing unwanted structures from the target files and converting those to pdbqt file format and providing the grid box file for the target structures, screening and postprocessing. Second, screening: After preparing the protein structures and compounds using the programs implemented in the workflow, the actual screening takes place. First, only the spike protein of SARS-CoV2 (PDB ID: 7CWM) is screened. The top 30 % of the results, based on their lowest binding energy (cutoff value −8 kcal/mol), are then re-screened with the spike protein of the variants of concern for SARS-CoV-2 (D614G) PDB ID: 7bnn, Epsilon variant PDB ID: 7n8h, Gamma variant PDB ID: 7m8k, Beta variant (B.1.351) PDB ID: 7lyn, Alpha variant (B.1.1.7) PDB ID:7edf, the Swiss model was used to model the spike protein of Delta and Mu variants, as well as SARS-CoV1 (PDB ID:6acd) and MERS-CoV (PDB ID:6nb03).

2.4. Plasmids

To produce pseudoviruses, the following plasmids were obtained from BEI Resources (Littleton, CO, USA): pHAGE-CMV-Luc2-IRES-ZsGreen-W (Cat. # NR-52516), HDM-Hgpm2 (Cat. # NR-52517), HDM-tat1b (Cat. # NR-52518), pRC-CMV-Rev1b (Cat. # NR-52519), pHAGE2-CMV-ZsGreen-W (Cat. # NR-52520), and HDM-IDTSpike-fixK-HA-tail (Cat. # NR-53765). The plasmids were amplified using One Shot™ TOP10 chemically competent *E. coli* (Invitrogen, Thermo Fisher,) and subsequently extracted and purified using the Plasmid Plus Maxi Kit (QIAGEN, Hilden, Germany) to generate a working stock.

2.5. Production of SARS-CoV-2 pseudoviruses and titration

HEK 293 T cells were cultured in DMEM medium supplemented with 10 % FBS to reach 70–80 % confluency the following day. The cells were transfected 24 h post-seeding using Lipofectamine™ 2000 transfection reagent (Invitrogen, Thermo Fisher) with 1 μg of the Luciferase IRES ZsGreen (NR-52516) backbone, along with 0.22 μg each of the plasmids HDM-Hgpm2 (NR-52517), pRC-CMV-Rev1b (NR-52519), and HDM-tat1b (NR-52518), and with or without 0.34 μg of SARS-CoV-2 spike (NR-53765) as a negative control. At 18 h post-transfection, the medium was replaced with fresh DMEM. Supernatants were collected at 48 and

72 h post-transfection, centrifuged at 1250 rpm for 3 min, and stored at −80 °C. For pseudovirus titration, HEK-ACE2 cells were seeded at a density of 12,500 cells per well in white 96-well plates (Cat. # 655074; Greiner, Frickenhausen, Germany). A serial dilution of spike-pseudotyped Luciferase IRES ZsGreen virus was prepared 24 h later, starting from undiluted virus and making six 1:2 dilutions. Then, 24 h after infection, the cell supernatants were replaced with 50 µl of fresh medium per well, followed by the addition of 50 µl of Bright-Glo Luciferase Assay reagent (E2610; Promega, Walldorf, Germany). The cells were incubated for 2 min at room temperature. The luciferase activity was then measured using an Infinite M2000™ Pro plate reader (Tecan, Crailsheim, Germany). The luciferase activity, expressed as relative light units (RLU) *versus* virus dilution, was plotted. The amount of pseudovirus selected for further assays exhibited a signal intensity over 10,000-fold above the cell-only background and was within the linear range of the curve [16,17]. Bald virus expressing no viral spike protein were used as a negative control.

2.6. Pseudovirus inhibition assay

HEK-ACE2 cells (12,500 cells/well) were seeded in white 96-well plates (Greiner, Cat. #655074) 1 d prior to infection. The next day, pseudoviruses were incubated at 37 °C for 1.5 h with either 30 µM of the test compounds or DMSO before being added to the cells. At 24 h post-infection, the medium was replaced with 50 µl of fresh medium per well, followed by the addition of 50 µl of Bright-Glo Luciferase reagent (E2610, Promega). The plates were incubated in the dark at room temperature for 2 min, and luminescence was measured using an Infinite M2000 Pro™ plate reader (Tecan) with a luminescence integration time of 1 sec. Compounds that exhibited more than 50 % inhibitory activity at 30 µM were selected for subsequent dose-response studies, ranging from 0 to 30 µM. Etravirine was used as a positive control [18]. The percentage of infection was calculated using the formula: % infection = [(mean RLU from each sample (virus + compound) - mean RLU from negative cell control) / (mean RLU from virus control - mean RLU from negative cell control)] × 100. The percentage of infection *versus* the log concentration of the inhibitors was used to calculate IC_{50} values [16,17]. For a confirmatory assay, fluorescence microscopy was performed using EVOS digital inverted microscope (Life Technologies GmbH, Darmstadt, Germany). HEK-ACE2 cells (10,000 cells/well) were plated in black 96-well plates (Greiner, Cat. #655936) 1 d before infection. On the day of infection, pseudoviruses were incubated at 37 °C for 1.5 h with 5 µM test compounds or DMSO. At 72 h post-infection, GFP fluorescence was quantified EVOS digital inverted microscope (Life Technologies GmbH, Darmstadt, Germany) and the results were analyzed using ImageJ.

2.7. SARS-CoV-2 propagation and quantification

A SARS-CoV-2 isolate (referred to as the "Essen isolate") derived from patient material, was utilized for infection experiments following the protocol described previously [19]. Vero E6 cells were seeded at a concentration of 2×10^6 cells in a T75 flask and incubated for 24 h at 37 °C with 5 % CO_2 in DMEM supplemented with 10 % FBS, 1 % L-glutamine, 1 % penicillin, and 1 % streptomycin. Subsequently, the cells were infected with the isolated virus and maintained for an additional 72 h under the same conditions. The culture supernatant was then clarified by centrifugation and stored at −80 °C. Viral concentrations were determined using an endpoint dilution assay to quantify the 50 % tissue culture infective dose ($TCID_{50}$). All experiments with infectious SARS-CoV-2 isolates were conducted under BSL3 conditions at the Institute of Virology of the University Hospital Essen, Germany.

2.8. SARS-CoV-2 in-cell ELISA procedure

Virus infections were quantified using an in-cell ELISA method based on a recently published protocol [20]. Cells were seeded at a density of 2×10^4 per well in a flat-bottom 96-well plate 1 d prior to infection. Then, inhibitory compounds were added for at least 30 minutes, prior to infection with SARS-CoV-2 for 24 h. Subsequently, cells were fixed with 4 % paraformaldehyde in phosphate-buffered saline (PBS). Permeabilization was achieved using a 1 % Triton-X-100 solution in PBS, followed by blocking with 3 % fetal calf serum (FCS) in PBS. The primary antibody (Anti-SARS-CoV-2 Nucleocapsid monoclonal antibody ABIN6952435, Antibodies Online, Aachen, Germany) was then added and incubated for 2 h at room temperature. Subsequently, a peroxidase-labeled secondary antibody (Cat. # 115–035–003, Jackson ImmunoResearch, Cambridge, UK) was applied for an additional hour, followed by washing with a 0.05 % Tween-20 solution in PBS. Finally, tetramethylbenzidine (TMB) substrate was added, and the enzymatic reaction was halted using 0.5 M HCl. The absorbance of the resulting dye was measured at 450 nm using a Spark® 10 M multimode microplate reader (Tecan).

2.9. Cell viability assay

Cell viability was evaluated using the resazurin assay, following the protocol previously described [21]. MRC-5 and HEK-ACE2 were seeded in 96-well plates at densities of 2×10^4 cells/well and 1×10^4 cells/well, respectively, and incubated overnight prior to treatment. The following day, cells were exposed to ten different concentrations of compounds ranging from 0.3 to 100 µM. After a 24-h incubation period, 20 µl of 0.01 % resazurin solution (Promega) was added to each well. Fluorescence intensity was measured following a 4-h incubation using an Infinite M2000™ Pro plate reader (Tecan) at an excitation/emission wavelength of 550 nm/590 nm. Cell viability was assessed relative to the DMSO control, with a final concentration of 0.5 % DMSO in the solution. The CC_{50} values, indicating the concentration causing 50 % cytotoxicity, were determined relative to the DMSO-treated control. Each experiment was repeated three times, with six wells per concentration per repetition. Vero E6 cells were seeded at a density of 20,000 cells per well in 96-well plates and incubated overnight. The next day, the cells were exposed to varying concentrations of chemicals. After a 24-h incubation period, the media were replaced with 100 µl of fresh medium. Subsequently, 20 µl of CellTiter-Blue™ reagent (Promega) were added to each well, and the plates were incubated at 37 °C with 5 % CO_2 for 4 h. A Spark® 10 M multimode microplate reader (Tecan) was used to measure fluorescence, exciting the cells at 560 nm and detecting emitted light at 590 nm, to assess cell viability after treatment.

2.10. Sequence alignment

The complete amino acid sequences of the receptor-binding domain (RBD) from the spike proteins of SARS-CoV-2 (P0DTC2), SARS-CoV (P59594), MERS-CoV (K9N5Q8), and HCoV-HKU1 (Q0ZME7) were retrieved from the UniProt database. For the SARS-CoV-2 variant XBB.1, sequences were obtained from the Protein Data Bank (PDB ID: 8iou). Sequence alignment was conducted using Clustal Omega (EMBL-EBI, Wellcome Genome Campus, Hinxton, Cambridgeshire, UK), and graphical representations were generated using Jalview 2.11.3.2 (University of Dundee, Scotland, UK).

2.11. Microscale thermophoresis

The recombinant RBD of spike proteins of SARS-CoV-2, SARS-CoV-2 XBB.1, SARS-CoV, MERS-CoV, and HCoV-HKU1 were obtained from Bio-Techne (Wiesbaden, Germany) to conduct microscale thermophoresis (MST), following established protocols [22,23]. Briefly, these recombinant proteins were labeled using the Monolith Protein Labeling Kit RED-NHS 2nd Generation (MO-L011, Nano Temper Technologies GmbH, Munich, Germany) according to the manufacturer's guidelines. The final protein concentrations post-labeling were 1500 nM for SARS-CoV-2, SARS-CoV-2 XBB.1, and HCoV-HKU1, 1000 nM for

Table 1
Virtual screening results of top 30 natural-derived selected compounds binding to the RBD of spike protein of different coronaviruses.

Compound number	ZINC-ID	Compound-IUPAC name	7CWM SARS-CoV2	7BNN D614G SARS-CoV2	7EDF Alpha Variant	7LYN Beta Variant	7M8K Gamma Variant	Delta Variant	7N8H Epsilon Variant	Mu Variant	6ACD SARS-CoV	6NB3 MERS-CoV
Compound 1	ZINC263586489	(2*Z*,9S)−2-(2,3-dihydro−1,4-benzodioxin−6-ylmethylidene)−9-(7-methyl−2-oxo-1H-quinolin−3-yl)−8,9-dihydrofuro[2,3-*f*]chromene−3,7-dione	−10.8	−11.3	−11.3	−10.5	−11.6	−9.2	−10.5	−9.4	−12.4	−10.3
Compound 2	ZINC253623674	(10 R)−3-(4-chlorophenyl)−5-hydroxy−10-(2-oxo-1H-quinolin−3-yl)−9,10-dihydropyrano[2,3-*h*]chromene−4,8-dione	−10.6	−10.2	−10.3	−9.4	−11.2	−10.8	−10.8	−10.7	−10.2	−11.0
Compound 3	ZINC85876788	(1S,9 R)−11-[[6-[[4-(4-fluorophenyl)−3,6-dihydro-2H-pyridin−1-yl]methyl]−5-hydroxy−1-methyl−4-oxopyridin−2-yl]methyl]−7,11-diazatricyclo [7.3.1.02,7]trideca−2,4-dien−6-one	−10.4	−10.5	−10.6	−9.8	−10.7	−9.4	−10.0	−8.8	−11.0	−10.3
Compound 4	ZINC2104424	(2S,8S)−6-[(2-fluorophenyl)methyl]−2-naphthalen−1-yl−3,6,17-triazatetracyclo[8.7.0.03,8.011,16]heptadeca−1(10),11,13,15-tetraene−4,7-dione	−10.4	−12.0	−9.9	−9.7	−10.7	−9.4	−9.9	−10.0	−10.5	−10.5
Compound 5	ZINC70687282	6-[2-[(4aR,8aS)−4a-hydroxy−1,3,4,5,6,7,8,8a-octahydroisoquinolin−2-yl]−2-oxoethyl]−5,9-dimethyl−3-naphthalen−2-ylfuro[3,2-*g*]chromen−7-one	−10.4	−11.1	−11.2	−9.4	−11.2	−8.7	−11.1	−9.2	−10.9	−11.3
Compound 6	ZINC108450839	(10 R)−5-hydroxy−3-(4-methoxyphenyl)−10-(6-oxo-5H-[1,3]dioxolo[4,5-*g*]quinolin−7-yl)−9,10-dihydropyrano[2,3-*h*]chromene−4,8-dione	−10.3	−10.4	−10.0	−9.9	−11.0	−10.4	−11.9	−10.7	−11.0	−10.6
Compound 7	ZINC15956900	(1S,3 R,3aR,6aS)−1-(1H-indol−3-ylmethyl)−5-naphthalen−2-ylspiro [1,2,3a,6a-tetrahydropyrrolo[3,4-*c*]pyrrole−3,3′-1H-indole]−2′,4,6-trione	−10.3	−11.5	−10.6	−11.7	−11.7	−10.4	−11.1	−9.0	−13.8	−11.8
Compound 8	ZINC85878578	10 R)−5-hydroxy−3-(4-methoxyphenyl)−10-(7-methyl−2-oxo-1H-quinolin−3-yl)−9,10 dihydropyrano[2,3-*h*]chromene−4,8-dione	−10.3	−10.5	−10.4	−9.9	−11.1	−10.2	−11.1	−10.4	−11.0	−10.4
Compound 9	ZINC108447506	(10 R)−5-hydroxy−3-(4-methoxyphenyl)−10-(7-oxo−3,6-dihydro-2H-[1,4]dioxino[2,3-*g*]quinolin−8-yl)−9,10-dihydropyrano[2,3-*h*]chromene−4,8-dione	−10.3	−10.7	−10.4	−9.5	−11.2	−10.5	−11.9	−9.7	−11.3	−11.7
Compound 10	ZINC96114211	(10 R)−5-hydroxy−3-(4-hydroxyphenyl)−10-(7-methyl−2-oxo-1H-quinolin−3-yl)−9,10-dihydropyrano[2,3-*h*]chromene−4,8-dione	−10.2	−10.2	−10.6	−9.6	−11.1	−10.6	−11.4	−10.6	−11.3	−11.6
Compound 11	ZINC883189	(6S,9S)−6-(6-methyl−4-oxochromen−3-yl)−9-phenyl−5,6,8,9,10,11-hexahydrobenzo[*b*][1,4]benzodiazepin−7-one	−10.1	−10.3	−10.5	−10.0	−10.4	−9.3	−9.9	−9.1	−10.3	−11.3
Compound 12	ZINC70706632	(1 R,3 R,3aR,6aS)−5-(4-acetylphenyl)−5′-chloro−1-(1H-indol−3-ylmethyl)−7′-methylspiro[1,2,3a,6a-tetrahydropyrrolo[3,4-*c*]pyrrole−3,3′-1H-indole]−2′,4,6-trione	−10.1	−11.0	−10.5	−9.6	−11.2	−9.1	−10.5	−8.6	−11.8	−11.1
Compound 13	ZINC253401787	(2 R)−10-hydroxy−2-(2-oxo−2-piperidin−1-ylethyl)−6-phenyl−5,13-dioxa−15-azapentacyclo[12.8.0.03,12.04,9.016,21]docosa1(22),3(12),4(9),6,10,14,16,18,20-nonaen−8-one	−10.1	−10.5	−11.5	−10.8	−12.3	−10.1	−11.4	−8.9	−10.8	−12.4
Compound 14	ZINC85876098	(10 R)−5-hydroxy−3-(4-methoxyphenyl)−10-(2-oxo-1H-quinolin−3-yl)−9,10-dihydropyrano[2,3-*h*]chromene−4,8-dione	−10.1	−10.8	−10.0	−9.7	−11.1	−10.3	−11.1	−10.2	−10.9	−10.3
Compound 15	ZINC253623643	(2*Z*,9S)−2-(2,3-dihydro−1,4-benzodioxin−6-ylmethylidene)−9-(7-methoxy−2-oxo-1H-quinolin−3-yl)−8,9-dihydrofuro[2,3-*f*]chromene−3,7-dione	−10.1	−10.5	−10.3	−9.3	−10.9	−8.8	−10.4	−8.8	−11.9	−10.3
Compound 16	ZINC70706585	(1 R,3 R,3aR,6aS)−5-(1,3-benzodioxol−5-ylmethyl)−7'-chloro−1-(1H-indol−3-ylmethyl)spiro[1,2,3a,6a-tetrahydropyrrolo[3,4-*c*]pyrrole−3,3'-1H-indole]−2',4,6-trione	−10.0	−10.9	−11.0	−10.7	−11.1	−9.7	−11.4	−9.7	−13.1	−10.9
Compound 17	ZINC253399830	(10 R)−3-(4-chlorophenyl)−10-[2-(dimethylamino)quinolin−3-yl]−5-hydroxy−9,10-dihydropyrano[2,3-*h*]chromene−4,8-dione	−10.0	−11.3	−9.8	−11.0	−11.1	−9.1	−10.4	−9.2	−12.0	−11.4
Compound 18	ZINC11867127	6-[2-[(4aR,8aS)−4a-hydroxy−1,3,4,5,6,7,8,8a-octahydroisoquinolin−2-yl]−2-oxoethyl]−5-methyl−3-naphthalen−2-ylfuro[3,2-*g*]chromen−7-one	−10.0	−10.6	12.0	−10.8	−11.6	−10.7	−11.1	−9.3	−11.4	−12.0
Compound 19	ZINC253623842	(10 R)−3-(4-chlorophenyl)−5-hydroxy−10-(7-methoxy−2-oxo-1H-quinolin−3-yl)−9,10-dihydropyrano[2,3-*h*]chromene−4,8-dione	−10.0	−10.1	−9.6	−10.0	−11.4	−10.2	−11.3	−10.5	−10.6	−10.5
Compound 20	ZINC70705159	(1S,3S,3aR,6aS)−5′-chloro−5-(2,3-dihydro−1,4-benzodioxin−6-yl)−1-(1H-indol−3 ylmethyl)spiro[1,2,3a,6a-tetrahydropyrrolo[3,4-*c*]pyrrole−3,3′-1H-indole]−2′,4,6-trione	−10.0	−11.1	−11.1	−9.2	−10.7	−9.0	−10.3	−8.6	−11.4	−10.9
Compound 21	ZINC8792352	10-[4-(3chlorophenyl)piperazine−1-carbonyl]−1,11 diazapentacyclo [10.7.1.02,7.08,20.013,18]icosa−2,4,6,8,10,12(20),13,15,17-nonaen−19-one	−10.0	−10.4	−10.6	−10.1	−11.2	−9.5	−11.1	−9.2	−12.2	−11.3

(*continued on next page*)

Table 1 (*continued*)

Compound number	ZINC-ID	Compound-IUPAC name	7CWM SARS-CoV2	7BNN D614G SARS-CoV2	7EDF Alpha Variant	7LYN Beta Variant	7M8K Gamma Variant	Delta Variant	7N8H Epsilon Variant	Mu Variant	6ACD SARS-CoV	6NB3 MERS-CoV
Compound 22	ZINC253401049	2-[5-[(10 R)−3-(4-chlorophenyl)−5-hydroxy−4,8-dioxo−9,10-dihydropyrano[2,3-*h*]chromen−10-yl]furan−2-yl]benzoic acid	−9.9	−10.9	−11.0	−10.5	−11.4	−9.9	−11.6	−10.1	−11.0	−10.8
Compound 23	ZINC70701640	(2 R,11S)-N-[(2S)−1-[(2-chloro−6-fluorophenyl)methylamino]−3-methyl−1-oxobutan−2-yl]−9-oxo−10,20diazapentacyclo[11.7.0.02,10.03,8.014,19]icosa−1(13),3,5,7,14,16,18-heptaene−11-carboxamide	−9.9	−10.2	−10.8	−10.7	−11.5	−8.9	−9.9	−8.5	−10.5	−10.6
Compound 24	ZINC19782240	2-[[(6S)−10,10-dimethyl−9-oxa−2-azaspiro[5.5]undecan−2-yl]methyl]spiro[3,6-dihydrobenzo[*h*]quinazoline−5,1′-cyclohexane]−4-one	−9.9	−10.7	−10.7	−10.1	−11.2	−9.9	−10.9	−8.8	−11.0	−13.0
Compound 25	ZINC104739723	6-[3-[(4aR,8aS)−4a-hydroxy−1,3,4,5,6,7,8,8a-octahydroisoquinolin−2-yl]−3-oxopropyl]−5-methyl−3-naphthalen−2-ylfuro[3,2-*g*]chromen−7-one	−9.9	−10.5	−10.7	−9.8	−10.8	−9.8	−10.7	−9.1	−11.6	−10.7
Compound 26	ZINC70670218	(5 R)−1-benzyl−5-(naphthalen−1-ylmethyl)−5-[[(1S,9 R)−6-oxo−7,11diazatricyclo[7.3.1.02,7]trideca−2,4-dien−11-yl]methyl]−1,3-diazinane−2,4,6-trione	−9.9	−11.1	−10.9	−10.7	−11.7	−9.6	−10.3	−8.5	−12.4	−11.3
Compound 27	ZINC85878218	3-[3-(4-benzo[*b*][1,4]benzoxazepin−6-yl)piperazin−1-yl)−3-oxopropyl]−3,13,21triazapentacyclo[11.8.0.02,10.04,9.015,20]henicosa−1(21),2(10),4,6,8,15,17,19-octaen−14-one	−9.9	−11.6	−11.4	−11.8	−12.9	−9.5	−11.8	−10.3	−11.7	−11.4
Compound 28	ZINC70686498	(2 R,8S)−6-(1-benzylpiperidin−4-yl)−2-naphthalen−1-yl−3,6,17-triazatetracyclo[8.7.0.03,8.011,16]heptadeca−1(10),11,13,15-tetraene−4,7-dione	−9.9	−11.7	−11.0	−11.6	−11.8	−10.6	−10.9	−8.9	−11.3	−10.7
Compound 29	ZINC70699829	(1S,3 R,3aR,6aS)−5-(2,3-dihydro−1,4-benzodioxin−6-yl)−1-(1H-indol−3-ylmethyl)−6′,7′-dimethylspiro[1,2,3a,6a-tetrahydropyrrolo[3,4-*c*]pyrrole−3,3′-1H-indole]−2′,4,6-trione	−9.9	−10.3	−10.3	−9.7	−11.3	−8.7	−10.9	−8.3	−10.5	−10.3
Compound 30	ZINC11867100	3-[2-[(4aS,8aR)−4a-hydroxy−1,3,4,5,6,7,8,8aoctahydroisoquinolin−2-yl]−2-oxoethyl]−4,8-dimethyl−7-[(2-methylnaphthalen−1-yl)methoxy]chromen−2-one	−9.9	−10.4	−10.0	−10.2	−10.8	−8.9	−11.2	−9.1	−10.2	−10.4

SARS-CoV, and 750 nM for MERS-CoV (Nanodrop, Thermo Fisher Scientific). Titration was performed using 16 serial dilutions, ranging from 200 to 0.006 M concentration (dilution steps 1:1). Titration involved 16 serial dilutions ranging from 200 to 0.006 M (1:1 dilution steps). The ligand and protein were incubated for 30 min at room temperature in an assay buffer containing 50 mM Tris (pH 7.4), 10 mM $MgCl_2$, 150 mM NaCl, and 0.05 % Tween-20. Measurements were performed using Monolith NT.115 standard capillaries (MO-K022, Nano Temper Technologies GmbH, Munich, Germany) with laser power settings of 10 %, 20 %, 40 %, and 60 %, and an LED power at 20 % for MERS-CoV, HCoV-HKU1, and 30 % for SARS-CoV-2, SARS-CoV-2 XBB.1, and SARS-CoV. Signals were measured with the Monolith NT.115 instrument (Nano Temper Technologies). Fitting curves and Kd values were determined using NT Analysis 1.5.41 software (Nano Temper Technologies).

2.12. Molecular docking

The most promising compound identified from initial *in vitro* experiments (compound 28) was subjected to the molecular docking studies against the receptor-binding domains (RBDs) of several coronaviruses: SARS-CoV-2 (PDB ID: 7bnn), SARS-CoV-2 XBB.1 (PDB ID: 8iou), SARS-CoV (PDB ID: 6acd), MERS-CoV (PDB ID: 6nb03), and HCoV-HKU1 (PDB ID: 8opo). AutoDock 4.2.6 was employed in a defined docking mode using the Lamarckian algorithm. The protein was kept rigid, while the ligand moved during the docking simulation. The parameters were set to 250 runs and 2,500,000 energy evaluations for each cycle, while the other docking parameters were kept at default values as described by our group [24] to assess the binding affinities and elucidate the amino acid residues critical for interaction within these RBDs. Computational docking simulations were executed on the high-performance supercomputer MOGON at Johannes Gutenberg University (Mainz, Germany). Visualization and interpretation of the docking outcomes were facilitated using Discovery Studio Visualizer V 21.1.0.20298 (San Diego, CA, USA).

2.13. Statistics and data fitting

All inhibition assays were performed at least as duplicates per plate, and all results shown are the average of at least three independent experiments. The binding data were converted to percent infection and fitted with standard log inhibitor *versus* normalized response models (four parameters) using nonlinear regression in GraphPad Prism 8 (GraphPad, La Jolla, CA, USA) to establish half-maximal toxicity or inhibitory concentrations (CC_{50}, IC_{50}). The selectivity index (SI) of an active compound was calculated using: $SI = CC_{50}/EC_{50}$ equation for live and pseudo-typed viruses. The correlation between the Kd values and the percentage of identity of RBDs was determined using Pearson's correlation test.

3. Results

3.1. Virtual screening

Vina LC software was used to run a Snakemake workflow which combined all major aspects of structure-based ligand screening: Automated execution of intricate preparation and screening steps, including retrieval of ligands libraries from databases, optional decompression and energy minimization, protein download from the Protein Data Bank (RCBS) database and protein preparation followed by selection of screening parameters. Screening was performed on a high-performance computer (Mogon II) to screen a ZINC library of 210,541 natural product-based compounds towards the RBD of spike protein of different coronaviruses. The protein binding pocket was identified based on amino acids known to be involved in spike RBD-receptor interactions. For all coronavirus spike proteins under investigation, 626 different compounds had binding energy less than −8 kcal/mol. The top 30

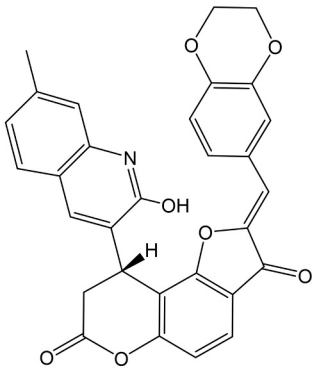

Compound **1**

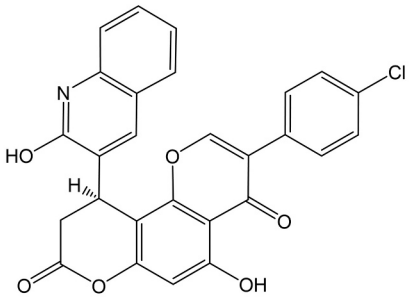

Compound **2**

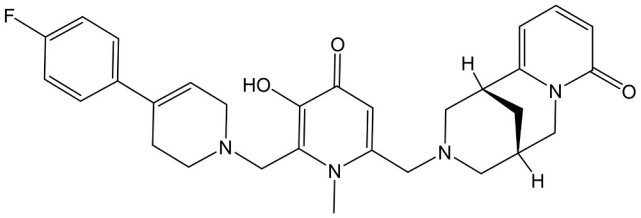

Compound **3**

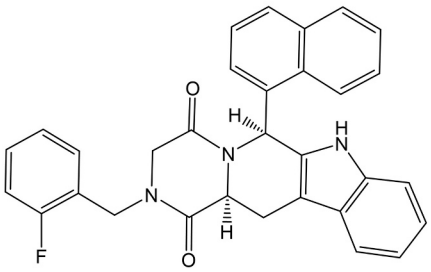

Compound **4**

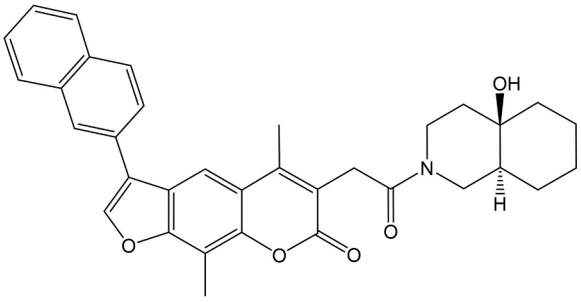

Compound **5**

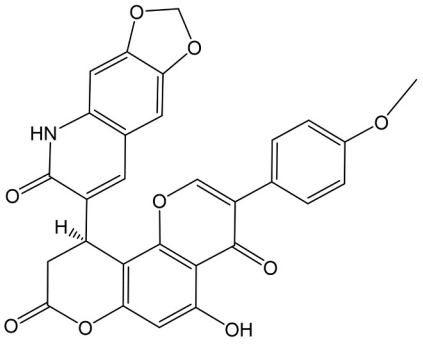

Compound **6**

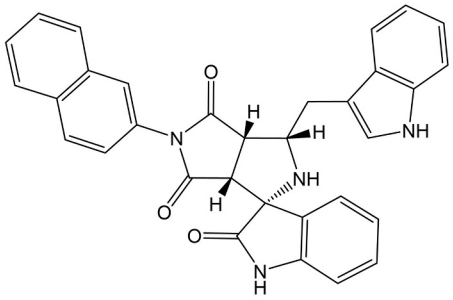

Compound **7**

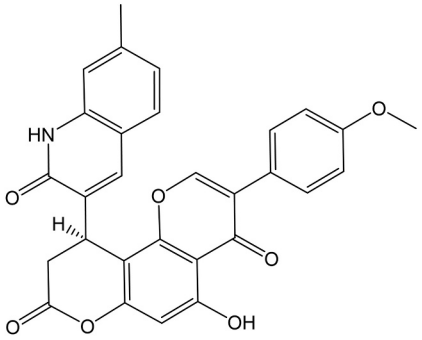

Compound **8**

Fig. 1. Chemical structures of the top 30 natural-derived compounds exhibiting highest binding affinity to the RBD of the SARS-CoV-2 spike protein. The binding affinities are expressed as lowest binding energies (LBE) in kcal/mol obtained.

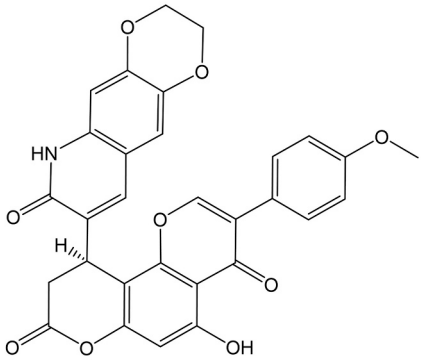

Compound **9**

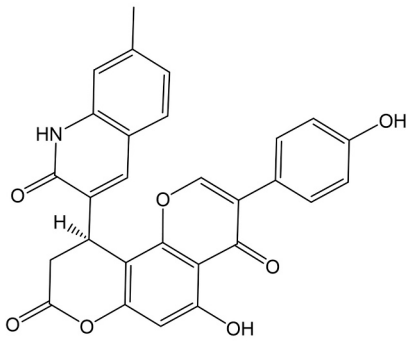

Compound **10**

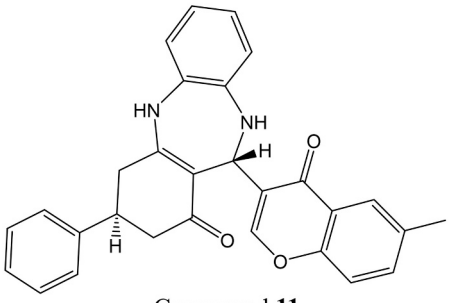

Compound **11**

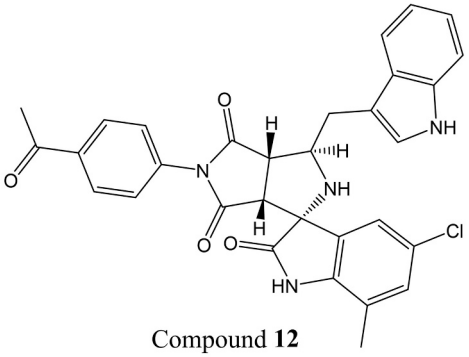

Compound **12**

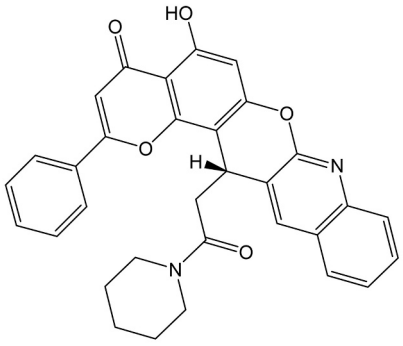

Compound **13**

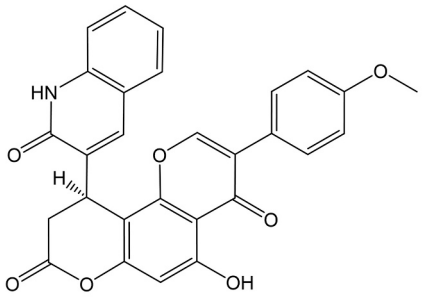

Compound **14**

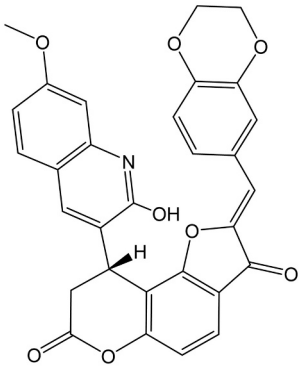

Compound **15**

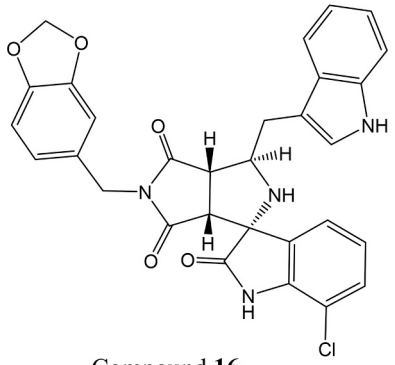

Compound **16**

Fig. 1. (*continued*).

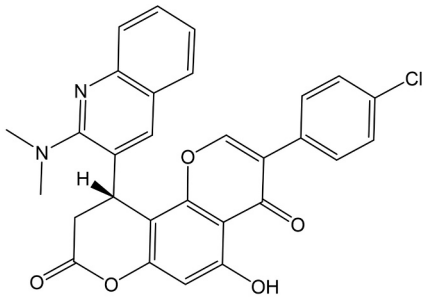

Compound **17**

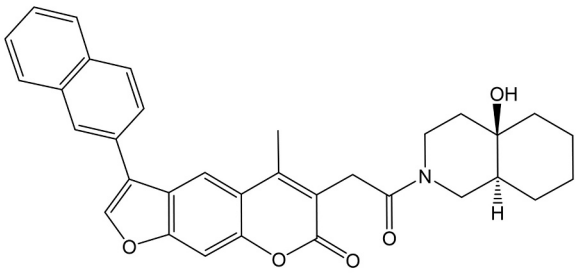

Compound **18**

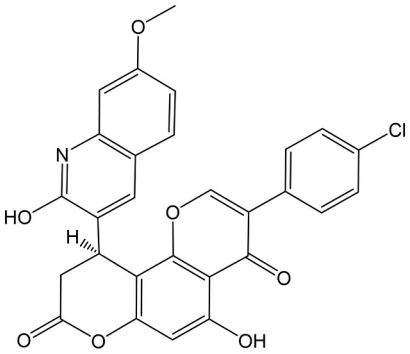

Compound **19**

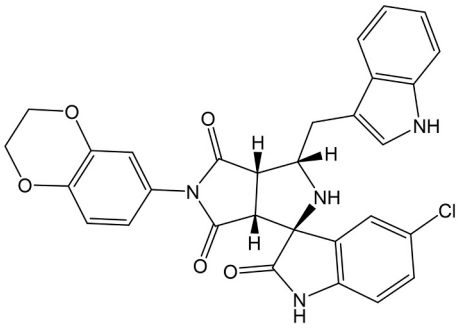

Compound **20**

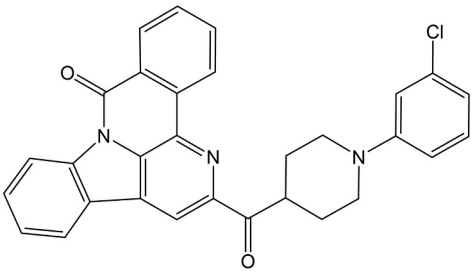

Compound **21**

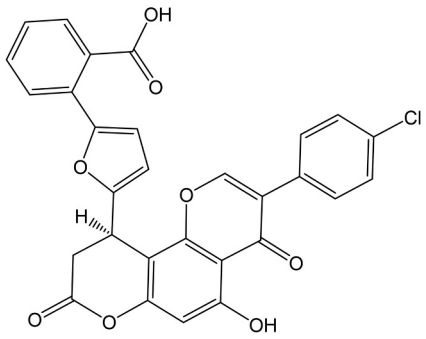

Compound **22**

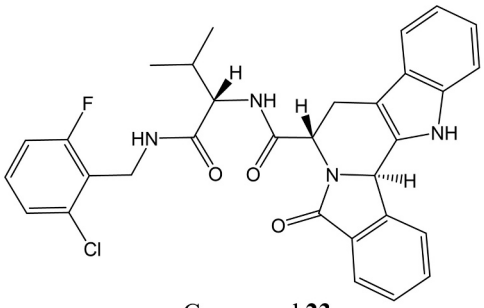

Compound **23**

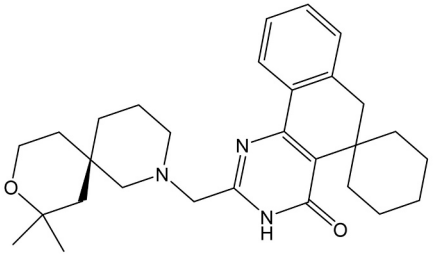

Compound **24**

Fig. 1. (*continued*).

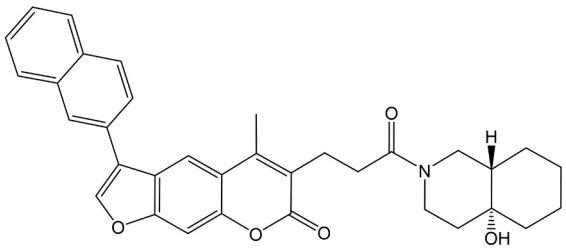

Compound **25**

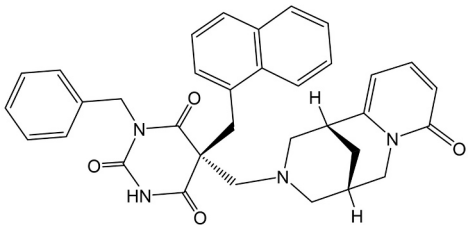

Compound **26**

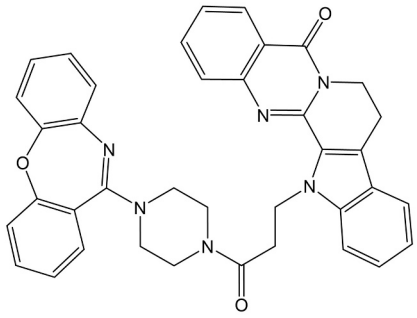

Compound **27**

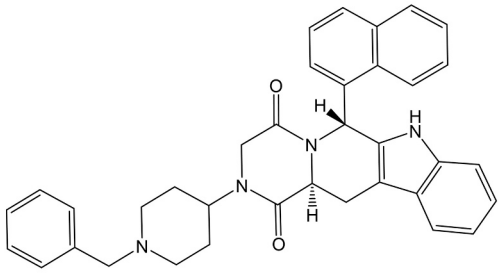

Compound **28**

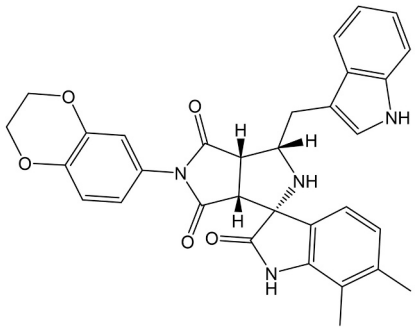

Compound **29**

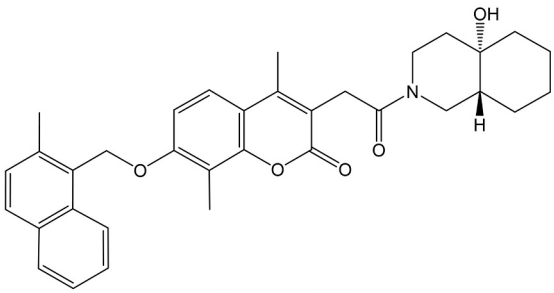

Compound **30**

Fig. 1. (*continued*).

candidates were selected for the *in vitro* experiments (Table 1). The candidates were selected based on their binding affinity to SARS-CoV-2 RBD, prioritizing those with the lowest binding energies. Additionally, the commercial availability of the compounds was a crucial factor in the selection process. The chemical structures of the top 30 compounds are shown in Fig. 1.

3.2. Inhibition of pseudotyped and live SARS-CoV-2 infection

Luciferase assays were conducted in HEK-ACE2 cells to screen the top 30 candidates identified from in silico studies, aiming to discover novel anti-SARS-CoV-2 entry inhibitors. While following the initial screening (Fig. 2A), six compounds (**2**, **6**, **14**, **17**, **19**, and **28**) demonstrated more than 50 % inhibition of pseudovirus entry at the concentration of 30 μM, only compound 28 was subjected to dose-response experiments to determine the concentration required to inhibit pseudovirus entry by 50 % (IC_{50}), since the other compounds showed high toxicity against HEK-ACE2 cells ($CC_{50} \leq 30$) (Table 2). The IC_{50} values for compound **28** was 1.96 ± 0.14 μM (Fig. 2B). GFP fluorescence measured via live fluorescence microscopy revealed that compound **28** provided strong protection against pseudovirus, 72 h after infection, which was consistent with the results from the luciferase inhibition assay (Fig. 2C-D).

The inhibitory efficacy of compound **28** against live SARS-CoV-2 viruses was evaluated through titration assays to determine its IC_{50} value. The result demonstrated that compound **28** inhibited SARS-CoV-2 infection at the cellular level with an IC_{50} value of 5.024 ± 0.53 μM (Fig. 2E).

3.3. Cell viability

The cytotoxicity of compound **28** was tested on MRC-5, HEK-ACE2, and Vero E6 cell lines, using the resazurin assay. The cell viability assay showed that compound **28** was cytotoxic against HEK-ACE2, with a CC_{50} value of 43.4 ± 7.4 while it did not show toxicity towards MRC-5 and Vero E6 cells even in the high concentration (Fig. 3).

3.4. Sequence alignment

To evaluate whether our leading compound can bind to the spike protein of various coronavirus family members, sequence alignments were conducted to assess the similarity between the receptor-binding domains (RBD) of the spike proteins from different coronaviruses. The alignments revealed sequence identities of 89.91 % with SARS-CoV-2

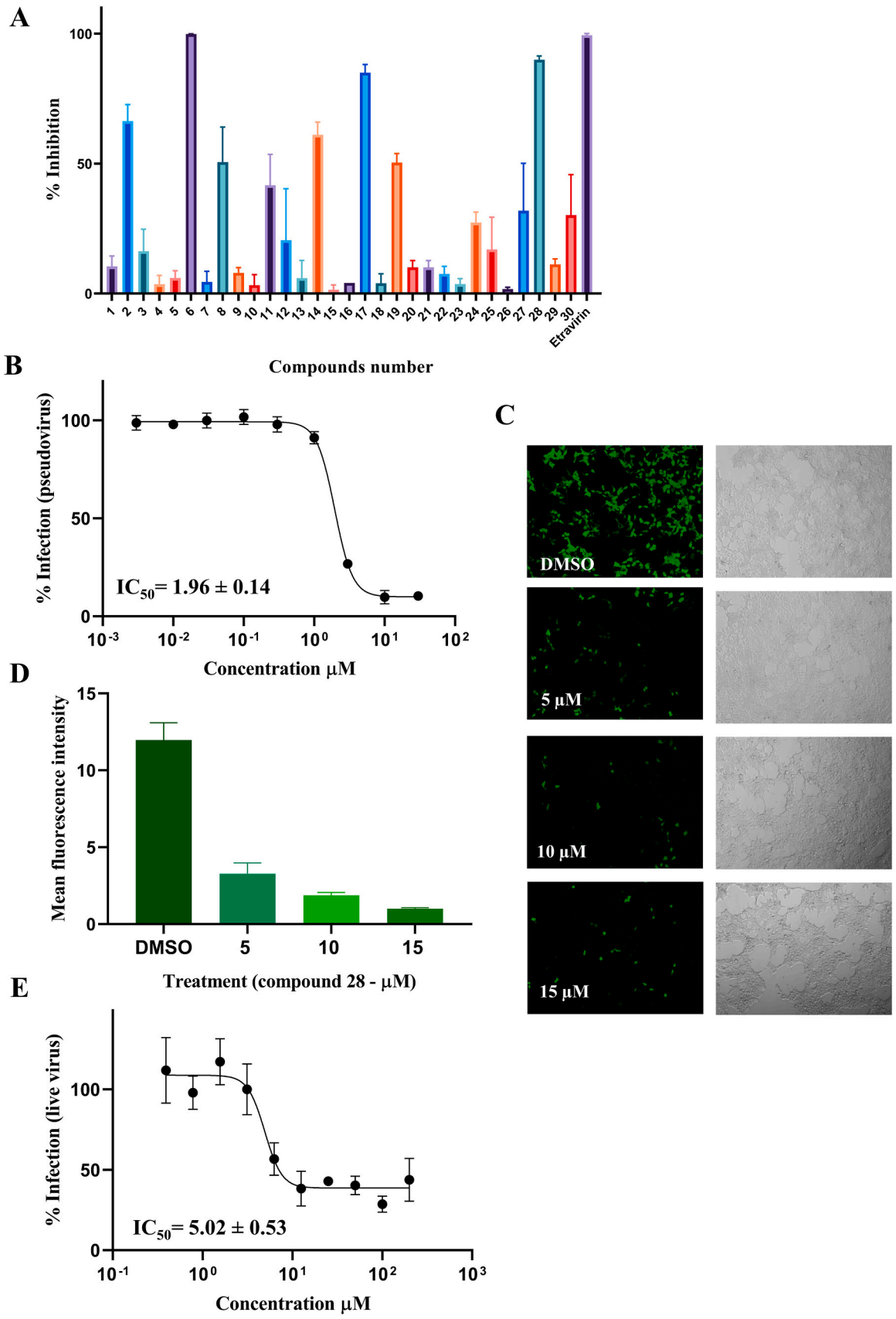

(caption on next page)

Fig. 2. Identification of entry inhibitors against pseudotyped SARS-CoV-2 lentivirus in HEK-ACE2 cells: (A) Percentage of inhibition of the SARS-CoV-2 pseudovirus in the presence of 30 selected natural-derived compounds and etravirine as a positive control (30 μM). (B) Dose-response curves of compound **28** on the SARS-CoV-2 pseudovirus, IC_{50} values and data points are shown as mean ± SD for three independent replicates. (C) Fluorescence microscopic images of HEK-ACE2 treated with pseudotyped SARS-CoV-2 lentivirus in the presence of 0, 5, 10, and 15 μM of compound **28**. (D) Quantification of GFP fluoresces standardized to the mean of fluorescence intensity using Image J, at 0, 5, 10, and 15 μM concentration of compound **28** and presented as mean ± S.D of three replicates. (E) Inhibition of fully replication-competent SARS-CoV-2. Vero E6 cells were infected with a clinical SARS-CoV-2 isolate for 24 h in the presence of compound **28** at the indicated concentrations. Infection levels were quantified by in-cell ELISA and normalized to mock-treated control wells (infected, but non-treated). Infection data were fitted with a four parameters inhibitor vs. response function (Y = Bottom + (Top - Bottom)/(1 + (IC_{50} / X) ^ HillSlope) using the statistics software GraphPad prism. Data points show mean ± standard error of the mean, calculated from at least three independent titrations of each compound.

Table 2
CC_{50} values of seven active compounds from pseudovirus inhibition assay screening, towards HEK-ACE2. The data are plotted as mean values ± SD of three independent experiments.

Compounds ZINC-ID	Compounds number	CC_{50} (μM)
ZINC253623674	**2**	10.86 ± 0.95
ZINC108450839	**6**	2.53 ± 0.44
ZINC85878578	**8**	14.45 ± 2.007
ZINC85876098	**14**	15.16 ± 0.36
ZINC253399830	**17**	18.96 ± 2.83
ZINC253623842	**19**	11.57 ± 1.58
ZINC70686498	**28**	43.40 ± 7.40

XBB.1 (Omicron variant), 73.42 % with SARS-CoV, 18.75 % with MERS-CoV, and 19.81 % with HCoV-HKU1, compared to the SARS-CoV-2 spike RBD. The multiple sequence alignment of the RBD domain of these coronaviruses is shown in Fig. 4, which is colored with the Taylor color scheme. Here, the colors are set by the variation in polarity and size of different amino acid chains. Hydrophobic amino acids are colored green, aromatic amino acids are green-blue, large polar/basic amino acids are purple and blue, amino acids found in loops are orange and red.

3.5. Microscale thermophoresis

As a sensitive technology, microscale thermophoresis was utilized to determine the binding affinity between the compound **28** and the labeled RBD of spike proteins from various coronavirus species, including different SARS-CoV-2 variants, SARS-CoV, MERS-CoV, and the endemic strain HCoV-HKU1. For this purpose, the labeled recombinant RBDs of spike proteins from SARS-CoV-2, SARS-CoV-2 XBB.1, SARS-CoV, MERS-CoV, and HCoV-HKU1 were titrated against varying concentrations of selected compound. Compound 28 bound to the RBD of spike proteins of SARS-CoV-2, SARS-CoV-2XBB.1, SARS-CoV, HCoV-HKU1, and MERS-CoV, with K_d values of 2.96, 4.2, 7.02, 20.08, and 23.06 μM, respectively (Fig. 5).

3.6. Binding mode of the top candidate

Molecular docking studies using AutoDock 4.2.6 revealed that compounds **28** exhibited high binding affinities to the RBD of spike proteins of SARS-CoV-2, SARS-CoV-2 XBB.1, SARS-CoV, MERS-CoV, and HCoV-HKU1, which have the potential to block the binding of RBD to ACE2, thereby protecting healthy cells and preventing further degeneration in the early stages of infection. Compound **28** had low binding energy (LBE) values ranging from −9.66 to −11.09 kcal/mol and predicted inhibition constants (pKi) between 7.36 and 83.56 nM. The amino acid interactions between the candidate compounds and the target proteins are illustrated in Fig. 6.

4. Discussion

During the past two decades, the world has experienced major outbreaks of coronavirus infection that threatened the global health, in 2002–2003 by SARS-CoV and in 2011 by MERS-CoV. The most recent coronavirus outbreak, known as COVID-19, happened in 2019 [25]. Despite the rapid development and deployment of vaccines and FDA-approved small-molecule antivirals, effective prophylactic and treatment options for COVID-19 are still needed to supplement vaccination efforts and ensure preparedness for future coronavirus outbreaks, including future variants against which current vaccines may be less effective.

As such, with the aim of finding novel pan-coronaviral substances, we screened 210,541 natural products using a Snakemake workflow. The 30 compounds identified according to their lowest binding energies (kcal/mol) from the virtual screening are structurally most divergent, but have, all of them, in common the presence of nitrogen atoms (even up to six in the case of compound **27**), all containing *N*-heterocycles, mono- or bicyclic, or even having more complex polycyclic ring systems. In addition, most of the compounds (no less than 21 out of 30) also possess oxygen-containing heterocycles. In 16 cases, there are even several oxygen-heterocycles and/or heterocycles with more than one oxygen atom. But apart from these similarities, the 30 preselected structures are rather characterized by a large structural diversity,

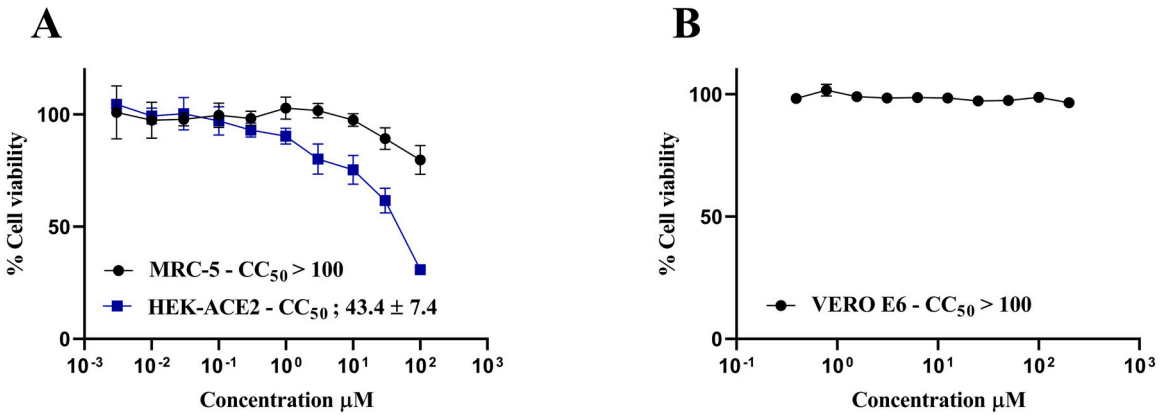

Fig. 3. Cytotoxic effects of compound **28** against (A) HEK-ACE2 and MRC-5 and (B) Vero E6 cell lines. The cytotoxicity was assessed using the resazurin method. Each data point represents the mean value ± SD of three independent experiments with six replicates each.

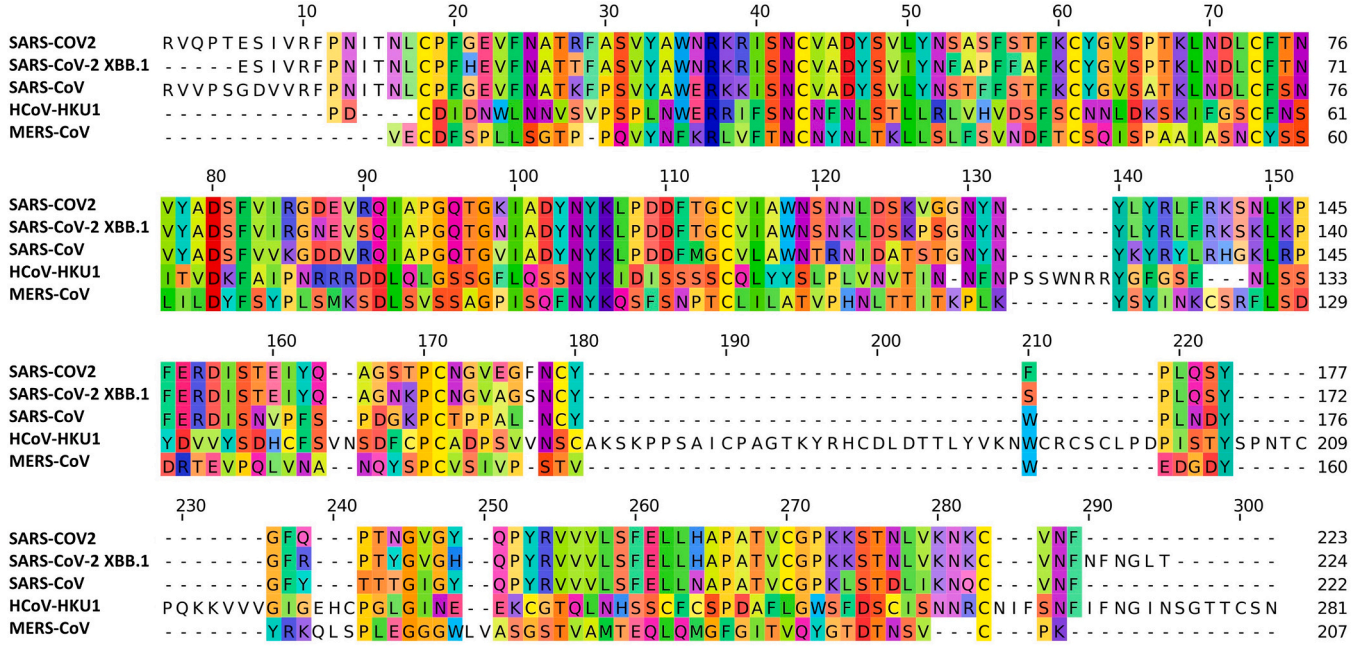

Fig. 4. Multiple sequence alignments of the RBD of spike proteins of SARS-CoV-2, SARS-CoV-2 XBB.1, SARS-CoV, MERS-CoV, and HCoV-HKU1.

making it difficult to find significant structure-activity relationships.

More interesting is a closer look at compound **28**, which is the only one that is active *in vitro* and possesses several types of heterocyclic rings-diketopiperazine, piperidine, and indole units. Compound **28** has its nitrogen in several mono- and bicyclic rings, even forming in a tetracyclic ring system, consisting of a tetrahydroharman (1,2,3,4-tetrahydro-β-carboline) system, fused to the mentioned diketopiperazine. Here, in **28**, the natural amino acid L-tryptophan, as part of an *N*-benzylpiperidine-substituted 2,5-diketopiperazine, has undergone a further Pictet-Spengler-type cyclization with (non-natural) naphthalene-1-carbaldehyde to form a remarkable tetracyclic ring system. In contrast to the other investigated molecules, **28** does not contain any oxygen-heterocycles.

Nitrogen-containing heterocyclic compounds are abundant in nature and serve as the basis for a diverse range of molecules, including alkaloids, vitamins, hormones, dyes, antibiotics, herbicides, and medicines. Notable examples of nitrogen-containing molecules that occur naturally include morphine, caffeine, nicotine, thiamine, and atropine. These compounds are categorized as alkaloids. In addition, *N*-heterocyclic compounds have several biological actions, including antifungal, anti-inflammatory, antibacterial, antioxidant, anticonvulsant, antiallergic, enzyme inhibitory, herbicidal, anti-HIV, antidiabetic, anticancer, and insecticidal properties. Nitrogen-containing heterocycles have long been a central focus of scientific investigation because of their varied structures and biological importance [26].

A recent analysis has shown that 82 % (262 out of 321) of the small-molecule medications that received approval from the FDA between 2013 and 2023 have a nitrogen heterocycle. Out of all the new small-molecule medications, a majority of 89 (28 %) are specifically authorized for cancer therapies. Among them, 55 compounds are classified as kinase inhibitors. The category of anti-infective pharmaceuticals is the second most common in terms of diseases, with 56 (17 %) new drugs. Out of these, ten have been licensed for treating hepatitis C, a remarkable achievement in the field of antiviral drug research [27,28].

Piperidine, a six-membered ring with one nitrogen atom, and piperazine, a six-membered ring with two nitrogen atoms, are prime examples of nitrogen-containing heterocycles [28]. Piperidine itself exhibits tremendous utility in the field of therapeutics [29]. This motif occurs abundantly in nature among alkaloids and exists in many genera including *Nicotiana, Conium, Lobelia, Pinus, Punica, Duboisia, Sedum, Withania, Carica, Hydrangea, Dichroa, Cassia, Prosopis, Genista, Ammodendron, Lupinus, Liparia*, *Ancistrocladus,* and *Collidium*. During the past years, alkaloid-based antiviral therapies have garnered significant attention. Numerous studies have demonstrated that alkaloids can effectively prevent and treat viral infections [30]. Thus, Dongwei et al. developed a series of piperidine derivatives as inhibitors of HIV-1 and influenza A virus replication in cell culture, showing that nearly half of the tested compounds exhibited potent activity against WT HIV-1 in MT-4 cells, with EC_{50} values ranging from 3.93 to 27.33 μM [31]. Similarly, piperidine alkaloids from *Senna spectabilis* flowers have potential for repurposing as anti-Chikungunya virus drugs, with EC_{50} values between 8.3 and 14.9 μM in BHK-21 cells [32].

The *N*-benzyl substitution on piperidine within drug molecules has demonstrated a strong affinity for molecular targets, resulting in its widespread presence as the *N*-benzyl piperidine (NBP) fragment in bioactive compounds. This *N*-benzyl substitution enhances solubility by forming a salt at the tertiary nitrogen and facilitates essential cation-π and π-π interactions with active sites of various targets [33].

Indole diketopiperazine alkaloids are metabolites produced by microbes, predominantly isolated from fungi such as *Aspergillus, Penicillium, Pestalotiopsis*, and *Chromocleista* [34]. These substances are defined by their unique condensation products, which typically involve a complete tryptophan molecule and a second amino acid, such as L-tryptophan, L-proline, L-phenylalanine, L-histidine, or L-leucine, resulting in the formation of an indole diketopiperazine unit [35,36]. The interest in indole diketopiperazines stems from their notable biological activities, including antimicrobial, antiviral, anticancer, immunomodulatory, antioxidant, and insecticidal properties. Consequently, these compounds hold promise for potential drug applications and may serve as valuable lead structures in drug development [36]. During the past decade many studies have highlighted their potential antiviral applications for instance, neoechinulin B, an indole diketopiperazine alkaloid, isolated from *Eurotium rubrum* Hiji025, and its derivatives exhibited antiviral effects against hepatitis C virus (HCV) and SARS-CoV-2 in Huh 7 cell line with the IC_{50} values of 4.9–0.0059 μM and 32.9–6.0 μM, respectively [37]. Additionally, 2,5-diketopiperazine derivatives exhibited negative results in influenza virus propagation at a concentration of 25 μg/ml in embryonated chicken eggs [38]. We first used a

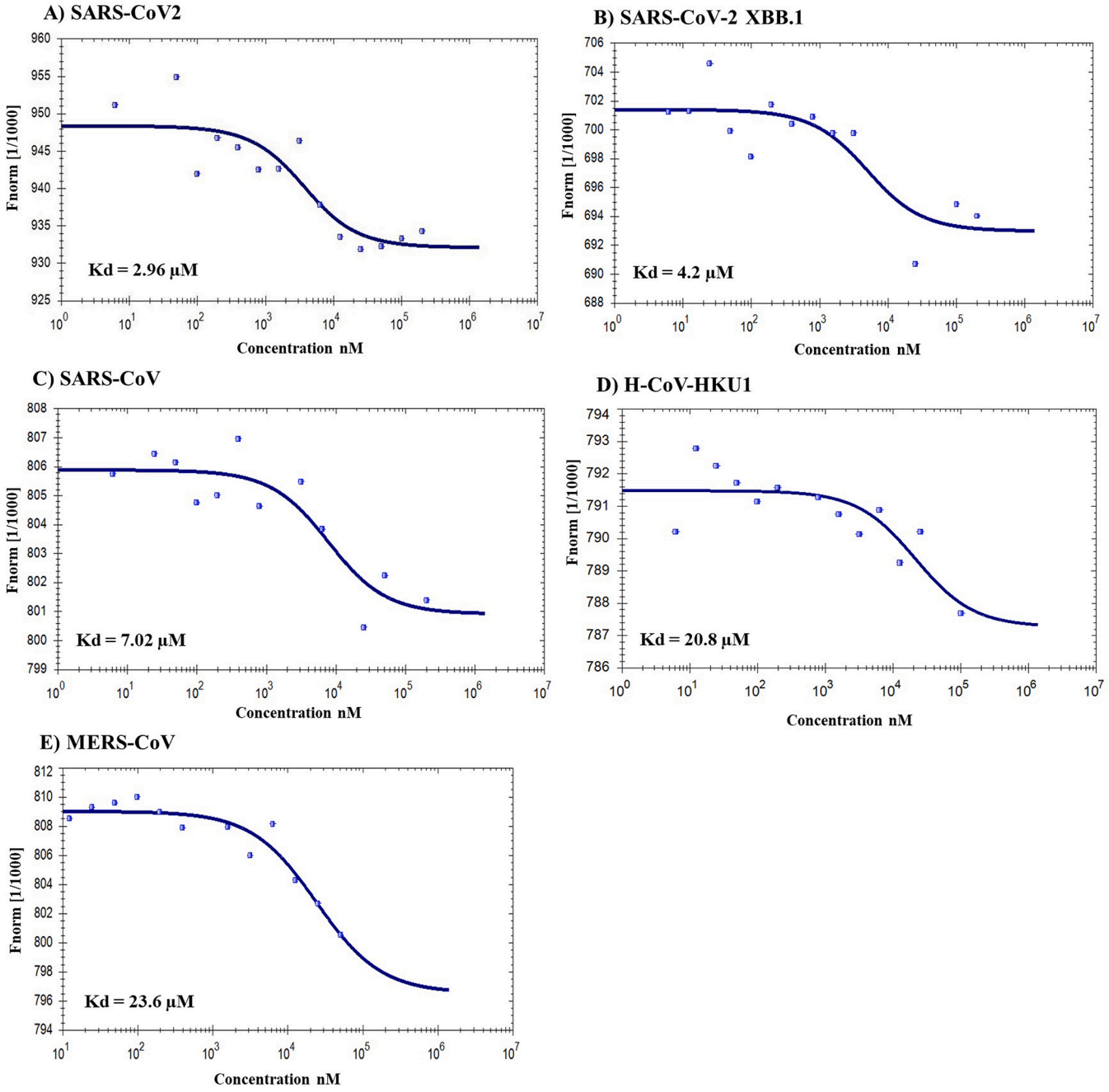

Fig. 5. Microscale thermophoresis analysis of compound **28** with the RBD of spike protein of (A) SARS-CoV-2, (B) SARS-CoV-2 XBB.1, (C) SARS-CoV, (D) H-CoV-HKU1, and /E) MERS-CoV.

pseudovirus technology to screen preselected compounds from virtual screening against the viral entry process in a biosafety level 2 laboratory. The pseudovirus inhibition assays showed that compound **28** strongly inhibits the cellular pseudovirus entry, with a IC_{50} value of 1.96 ± 0.14 µM and a selectivity index of 21.75 in HEK-ACE2. To validate the results of the pseudovirus inhibition assays, the active compound was subjected to the inhibition of live SARS-CoV2 replication assays in a biosafety level 2 laboratory. The results revealed that compound **28** has inhibitory effects against SARS-CoV2 with IC_{50} values of 5.024 ± 0.53 µM. The IC_{50} values from the pseudovirus inhibition assay were lower related to the low titer of pseudovirus compared to the live viruses. Remarkably, the cell viability assays showed that compounds **28** has a very low cytotoxicity against HEK-ACE2, while it is not toxic towards MRC-5 and Vero E6 cell lines.

Up to now, there has been a significant number of studies dedicated to identifying natural chemicals that can bind to the spike protein of SARS-CoV2 and inhibit viral infection. For instance, epigallocatechin gallate (EGCG) had an inhibitory effect, with an IC_{50} value of 0.32 µM against pseudovirus and an EC_{50} value of 24.08 against plaque formation of the live virus [39]. A total of 24 flavonoids exhibited antiviral entry activity with IC_{50} values ranging from 172.63 to 10.27 µM [40] which were higher than the IC_{50} values of compound **28**.

Despite the development of various peptides and small molecules as pan-coronavirus inhibitors targeting the spike protein in the past, these compounds specifically aimed at the fusion peptide of the spike protein, thereby blocking the cellular entry of coronaviruses by inhibiting membrane fusion, with low micromolar IC_{50} values [41–43].

With the objective of developing pan-coronaviral inhibitors that

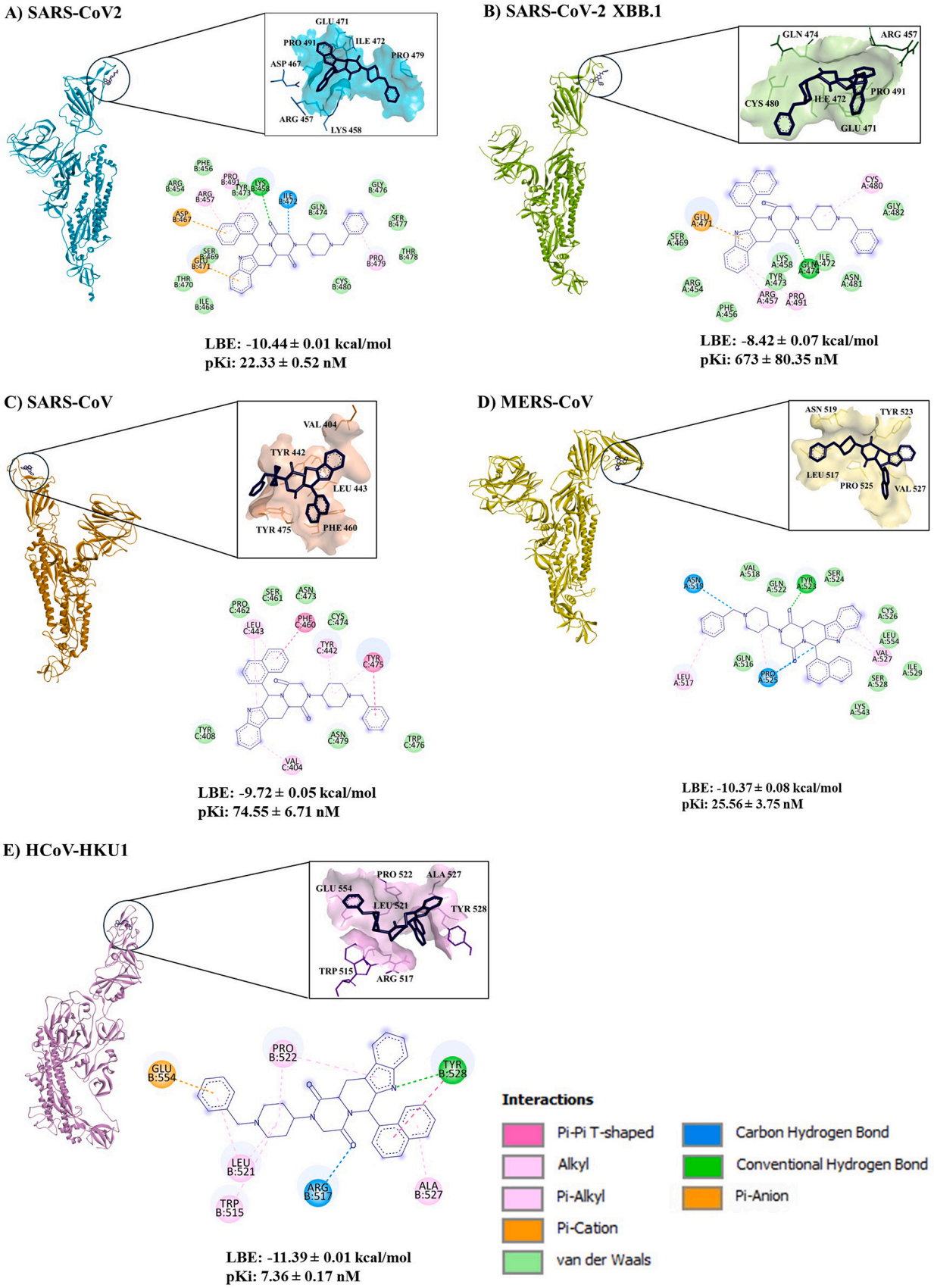

Fig. 6. The binding mode and 2D representation of compound **28** with the RBD of spike protein of (A) SARS-CoV-2 (PDB ID: 7bnn), (B) SARS-CoV-2 XBB.1 (PDB ID: 8iou), (C) SARS-CoV1 (PDB ID: 6acd), (D) MERS-CoV (PDB ID: 6nb3), and (E) HCoV-HKU1 (PDB ID: 8opo). These visualizations were generated using Discovery Studio Visualizer software (version v.24.1.0.23298). The lowest binding energies (LBE) and the predicted inhibition constant (pKi) of each compound were calculated using AutoDock 4.2.6.

specifically target the receptor-binding domain (RBD) of the spike protein, we initially conducted a sequence alignment for the RBD of SARS-CoV-2, SARS-CoV-2 XBB.1 (Omicron variant), SARS-CoV, MERS-CoV, and HCoV-HKU1. The Omicron variant exhibited the highest homology to wild-type SARS-CoV-2, while MERS-CoV showed the lowest. Subsequently, we employed microscale thermophoresis to examine the binding affinity of compound **28** to the RBD of the spike protein of these coronaviruses. The analysis confirmed that compound **28** successfully bound to the RBD of SARS-CoV-2, SARS-CoV-2 XBB.1, SARS-CoV, MERS-CoV, and HCoV-HKU1, with binding affinities correlating inversely with sequence homology identified in the alignment as indicated by an R value of −0.99 and a *p*-value of 0.001.

Previous studies have identified several hotspot residues on the RBD of SARS-CoV-2 critical for protein-protein or protein-ligand interactions, including R402, N439, N440, L441, K433, V444, G446, Y449, Y453, L452, L455, F456, T470, E471, I472, N481, E484, F486, N487, Y489, F490, Q493, Q498, P499, T500, N501, and Y505 [44–46]. A pharmacophore analysis based on the docking simulation revealed that compound **28** interacts with some of these hotspot residues, including F456, T470, and E471. Thus, the compound may interfere with the interaction between these residues and ACE2. The Omicron and wild-type RBDs shared similar overall structures, while the RBD of Omicron showed higher binding affinity for the ACE2 compared to the wild-type RBD [45]. Our molecular docking analysis revealed that compound **28** interacts with some of the hotspot residues in the RBDs of SARS-CoV-2 XBB.1, *i.e.*, F456, E471, I472 and N481, that may interfere with the interaction between RBD and ACE2. Moreover, molecular docking revealed that compound **28** may inhibit the HCoV-HKU1 virus entry through the interaction with the R517, L521, W515, Y528, and D529 hotspot residues [46,47] and SARS-CoV entry via the interaction with N473 and Y475 hotspot residues [46]. Although compound **28** does not interact with the hotspot residues of MERS-CoV [48], it still exert high affinities to the RBD based on their LBE of molecular docking and K_d values of microscale thermophoresis studies. Thus, the inhibitory effects of this compound towards MERS-CoV could take place by conformational changes of the RBD [49].

In summary, we present an *N*-heterocyclic natural product-derived compound as a broad-spectrum coronaviral entry inhibitor with low toxicity. By initially screening a large library of natural products, our strategy identified a highly promising agent. The presence of an *N*-heterocyclic structure in the active compound, despite the wide variety of other ZINC-derived starting structures, highlights the efficiency and specificity of our selection pathway, which effectively pinpointed this promising class of heterocycles from numerous candidates. This compound demonstrate the ability to protect cells from infection by both SARS-CoV-2 pseudoviruses and live viruses. Furthermore, *in silico* and *in vitro* studies revealed that they bind with high affinity to the RBD of SARS-CoV-2 XBB.1, SARS-CoV, MERS-CoV, and HCoV-HKU1. Thus, we conclude that compound **28** ((2 R,8S)-6-(1-benzylpiperidin-4-yl)-2-naphthalen-1-yl-3,6,17-triazatetracyclo[8.7.0.03,8.011,16]heptadeca-1(10),11,13,15-tetraene-4,7-dione) is a potential candidate for developing novel, potent pan-coronavirus entry inhibitors. Further investigations, including *in vivo* studies, will be necessary to validate these findings.

CRediT authorship contribution statement

Roland Schwarzer: Writing – review & editing, Methodology. **Hannah S. Schwarzer-Sperber:** Investigation. **Christian Meesters:** Writing – review & editing, Methodology. **Gerhard Bringmann:** Writing – review & editing, Writing – original draft, Conceptualization. **Kathrin Sutter:** Investigation. **Sara Abdelfatah:** Methodology, Conceptualization. **Nasim Shahhamzehei:** Writing – review & editing, Writing – original draft, Methodology, Investigation, Conceptualization. **Max Riedl:** Methodology, Investigation. **Ejlal A. Omar:** Investigation. **Thomas Efferth:** Writing – review & editing, Conceptualization.

Declaration of Competing Interest

The authors declare that they have no known competing financial interests or personal relationships that could have appeared to influence the work reported in this paper.

Acknowledgment

We are grateful to the financial support of Marc Strobel, Frankfurt a. M., Germany and CVC Philanthropy, Jersey.

References

[1] Y.C. Liu, R.L. Kuo, S.R. Shih, COVID-19: The first documented coronavirus pandemic in history, Biomed. J. 43 (2020) 328–333, https://doi.org/10.1016/j.bj.2020.04.007.
[2] WHO, Number of COVID-19 Cases Reported to WHO (Cumulative total) World, World Health Organization, 2024. ⟨https://data.who.int/dashboards/covid19/cases?n=o⟩.
[3] Y. Panahi, A.M. Gorabi, S. Talaei, F. Beiraghdar, A. Akbarzadeh, V. Tarhriz, et al., An overview on the treatments and prevention against COVID-19, Virol. J. 20 (2023) 1–29, https://doi.org/10.1186/s12985-023-01973-9.
[4] A. Yisimayi, W. Song, J. Wang, F. Jian, Y. Yu, X. Chen, et al., Repeated Omicron exposures override ancestral SARS-CoV-2 immune imprinting, Nature 625 (2024) 148–156, https://doi.org/10.1038/s41586-023-06753-7.
[5] C. Perrone, E. Fiabane, M. Maffoni, A. Pierobon, I. Setti, V. Sommovigo, et al., Vaccination hesitancy: to be vaccinated, or not to be vaccinated, that is the question in the era of COVID-19, Public Health Nurs. 40 (2023) 90–96, https://doi.org/10.1111/phn.13134.
[6] Z. Al-Aly, B. Bowe, Outcomes of SARS-CoV-2 reinfection, Res. Sq. (2022) 1–17.
[7] W.S. Ho, R. Zhang, Y.L. Tan, C.L.L. Chai, COVID-19 and the promise of small molecule therapeutics: are there lessons to be learnt? Pharmacol. Res. 179 (2022) 106201 https://doi.org/10.1016/j.phrs.2022.106201.
[8] J. Zhang, T. Xiao, Y. Cai, B. Chen, Structure of SARS-CoV-2 spike protein, Curr. Opin. Virol. 50 (2021) 173–182, https://doi.org/10.1016/j.coviro.2021.08.010.
[9] Y. Chen, Y. Guo, Y. Pan, Z.J. Zhao, Structure analysis of the receptor binding of 2019-nCoV, Biochem. Biophys. Res. Commun. 525 (2020) 135–140, https://doi.org/10.1016/j.bbrc.2020.02.071.
[10] N. Shahhamzehei, S. Abdelfatah, T. Efferth, In silico and in vitro identification of pan-coronaviral main protease inhibitors from a large natural product library, Pharmaceuticals 15 (2022) 1–19, https://doi.org/10.3390/ph15030308.
[11] S. Mhatre, S. Naik, V. Patravale, A molecular docking study of EGCG and theaflavin digallate with the druggable targets of SARS-CoV-2, Comput. Biol. Med. 129 (2021) 104137, https://doi.org/10.1016/j.compbiomed.2020.104137.
[12] A.V. Sadybekov, V. Katritch, Computational approaches streamlining drug discovery, Nature 616 (2023) 673–685, https://doi.org/10.1038/s41586-023-05905-z.
[13] X. Lin, X. Li, X. Lin, A review on applications of computational methods in drug screening and design, Molecules 25 (2020) 1–17, https://doi.org/10.3390/molecules25061375.
[14] F. Mölder, K.P. Jablonski, B. Letcher, M.B. Hall, C.H. Tomkins-Tinch, V. Sochat, et al., Sustainable data analysis with Snakemake, F1000Research 10 (2021) 33, https://doi.org/10.12688/f1000research.29032.1.
[15] E. Deelman, D. Gannon, M. Shields, I. Taylor, Workflows and e-science: an overview of workflow system features and capabilities, Future Gener. Comput. Syst. 25 (2009) 528–540, https://doi.org/10.1016/j.future.2008.06.012.
[16] K.H.D. Crawford, R. Eguia, A.S. Dingens, A.N. Loes, J.D. Bloom, K. Crawford, 2021, Pseudotyping lentiviral particles with SARS-CoV-2 Spike protein for neutralization assays V.2 Coronavirus Method Development Community 2021. https://doi.org/10.17504/protocols.io.br44m8yw..
[17] S.A. Almahboub, A. Algaissi, M.A. Alfaleh, M.Z. ElAssouli, A.M. Hashem, Evaluation of neutralizing antibodies against highly pathogenic coronaviruses: a detailed protocol for a rapid evaluation of neutralizing antibodies using vesicular stomatitis virus pseudovirus-based assay, Front. Microbiol. 11 (2020), https://doi.org/10.3389/fmicb.2020.02020.
[18] R.K.L. Lee, T.N. Li, S.Y. Chang, T.L. Chao, C.H. Kuo, M.Y.C. Pan, et al., Identification of entry inhibitors against delta and omicron variants of SARS-CoV-2, Int. J. Mol. Sci. 23 (2022), https://doi.org/10.3390/ijms23074050.
[19] C.S. Heilingloh, U.W. Aufderhorst, L. Schipper, U. Dittmer, O. Witzke, D. Yang, et al., Susceptibility of SARS-CoV-2 to UV irradiation, Am. J. Infect. Control 48 (2020) 1273–1275, https://doi.org/10.1016/j.ajic.2020.07.031.
[20] L. Schöler, V.T.K. Le-Trilling, M. Eilbrecht, D. Mennerich, O.E. Anastasiou, A. Krawczyk, et al., A novel In-Cell ELISA assay allows rapid and automated quantification of SARS-CoV-2 to analyze neutralizing antibodies and antiviral compounds, Front. Immunol. 11 (2020) 1–11, https://doi.org/10.3389/fimmu.2020.573526.
[21] V. Kuete, A.T. Mbaveng, E.C.N. Nono, C.C. Simo, M. Zeino, A.E. Nkengfack, et al., Cytotoxicity of seven naturally occurring phenolic compounds towards multifactorial drug-resistant cancer cells, Phytomedicine 23 (2016) 856–863, https://doi.org/10.1016/j.phymed.2016.04.007.

[22] E.-J. Seo, T. Efferth, Interaction of antihistaminic drugs with human translationally controlled tumor protein (TCTP) as novel approach for differentiation therapy, Oncotarget 7 (2016).
[23] M. Jerabek-Willemsen, C.J. Wienken, D. Braun, P. Baaske, S. Duhr, Molecular interaction studies using microscale thermophoresis, Assay. Drug Dev. Technol. 9 (2011) 342–353, https://doi.org/10.1089/adt.2011.0380.
[24] M. Zeino, M.E.M. Saeed, O. Kadioglu, T. Efferth, The ability of molecular docking to unravel the controversy and challenges related to P-glycoprotein - a well-known, yet poorly understood drug transporter, Investig. N. Drugs 32 (2014) 618–625, https://doi.org/10.1007/s10637-014-0098-1.
[25] Y. Yang, F. Peng, R. Wang, K. Guan, T. Jiang, G. Xu, et al., The deadly coronaviruses: The 2003 SARS pandemic and the 2020 novel coronavirus epidemic in China, J. Autoimmun. 109 (2020) 102434, https://doi.org/10.1016/j.jaut.2020.102434.
[26] A. Mermer, T. Keles, Y. Sirin, Recent studies of nitrogen containing heterocyclic compounds as novel antiviral agents: a review, Bioorg. Chem. 114 (2021) 105076, https://doi.org/10.1016/j.bioorg.2021.105076.
[27] C.M. Marshall, J.G. Federice, C.N. Bell, P.B. Cox, J.T. Njardarson, An update on the nitrogen heterocycle compositions and properties of U.S. FDA-approved pharmaceuticals (2013-2023), J. Med. Chem. (2024), https://doi.org/10.1021/acs.jmedchem.4c01122.
[28] E. Vitaku, D.T. Smith, J.T. Njardarson, Analysis of the structural diversity, substitution patterns, and frequency of nitrogen heterocycles among U.S. FDA approved pharmaceuticals, J. Med. Chem. 57 (2014) 10257–10274, https://doi.org/10.1021/jm501100b.
[29] M.M. Abdelshaheed, I.M. Fawzy, H.I. El-Subbagh, K.M. Youssef, Piperidine nucleus in the field of drug discovery, Futur J. Pharm. Sci. 7 (2021), https://doi.org/10.1186/s43094-021-00335-y.
[30] H. Ti, Z. Zhuang, Q. Yu, S. Wang, Progress of plant medicine derived extracts and alkaloids on modulating viral infections and inflammation, Drug Des. Dev. Ther. 15 (2021) 1385–1408, https://doi.org/10.2147/DDDT.S299120.
[31] D. Kang, Z. Fang, B. Huang, L. Zhang, H. Liu, C. Pannecouque, et al., Synthesis and preliminary antiviral activities of piperidine-substituted purines against HIV and influenza A/H1N1 infections, Chem. Biol. Drug Des. 86 (2015) 568–577, https://doi.org/10.1111/cbdd.12520.
[32] T.R. Freitas, R.M. Novais, I.A. Santos, D.O.S. Martins, A. Danuello, V. da Silva Bolzani, et al., In vitro antiviral activity of piperidine alkaloids from Senna spectabilis flowers on Chikungunya virus infection, Pharmacol. Rep. 74 (2022) 752–758, https://doi.org/10.1007/s43440-022-00381-0.
[33] M. Sharma, S.B. Bharate, N-benzyl piperidine fragment in drug discovery, ChemMedChem (2024), https://doi.org/10.1002/cmdc.202400384.
[34] Y.M. Ma, X.A. Liang, Y. Kong, B. Jia, Structural diversity and biological activities of indole diketopiperazine alkaloids from fungi, J. Agric. Food Chem. 64 (2016) 6659–6671, https://doi.org/10.1021/acs.jafc.6b01772.
[35] H. Gao, T. Zhu, D. Li, Q. Gu, W. Liu, Prenylated indole diketopiperazine alkaloids from a mangrove rhizosphere soil derived fungus Aspergillus effuses H1-1, Arch. Pharm. Res. 36 (2013) 952–956, https://doi.org/10.1007/s12272-013-0107-5.
[36] Y.H. Zhang, H.F. Du, Y.F. Liu, F. Cao, D.Q. Luo, C.Y. Wang, Novel anti-inflammatory diketopiperazine alkaloids from the marine-derived fungus Penicillium brasilianum, Appl. Microbiol. Biotechnol. 108 (2024), https://doi.org/10.1007/s00253-024-13026-4.
[37] K. Nishiuchi, H. Ohashi, K. Nishioka, M. Yamasaki, M. Furuta, T. Mashiko, et al., Synthesis and antiviral activities of neoechinulin B and its derivatives, J. Nat. Prod. 85 (2022) 284–291, https://doi.org/10.1021/acs.jnatprod.1c01120.
[38] W.S. Phutdhawong, 2,5-diketopiperazine derivatives as potential anti-influenza (H5N2) agents: synthesis, biological evaluation, and , and molecular docking study, Molecules (2022).
[39] D. Zhang, S. Hamdoun, R. Chen, L. Yang, C.K. Ip, Y. Qu, et al., Identification of natural compounds as SARS-CoV-2 entry inhibitors by molecular docking-based virtual screening with bio-layer interferometry, Pharmacol. Res. 172 (2021) 105820, https://doi.org/10.1016/j.phrs.2021.105820.
[40] J.R. Meng, J. Liu, L. Fu, T. Shu, L. Yang, X. Zhang, et al., Anti-entry activity of natural flavonoids against SARS-CoV-2 by targeting spike RBD, Viruses 14 (2022), https://doi.org/10.3390/v15010160.
[41] L. Guo, S. Lin, Z. Chen, Y. Cao, B. He, G. Lu, Targetable elements in SARS-CoV-2 S2 subunit for the design of pan-coronavirus fusion inhibitors and vaccines, Signal. Transduct. Target Ther. 8 (2023), https://doi.org/10.1038/s41392-023-01472-x.
[42] Q. Lan, L. Wang, F. Jiao, L. Lu, S. Xia, S. Jiang, Pan-coronavirus fusion inhibitors to combat COVID-19 and other emerging coronavirus infectious diseases, J. Med. Virol. 95 (2023), https://doi.org/10.1002/jmv.28143.
[43] S. Xia, L. Yan, W. Xu, A.S. Agrawal, A. Algaissi, C.T.K. Tseng, et al., A pan-coronavirus fusion inhibitor targeting the HR1 domain of human coronavirus spike, Sci. Adv. 5 (2019), https://doi.org/10.1126/sciadv.aav4580.
[44] L. Wang, Y. Wu, S. Yao, H. Ge, Y. Zhu, K. Chen, et al., Discovery of potential small molecular SARS-CoV-2 entry blockers targeting the spike protein, Acta Pharm. Sin. 43 (2022) 788–796, https://doi.org/10.1038/s41401-021-00735-z.
[45] J. Lan, X. He, Y. Ren, Z. Wang, H. Zhou, S. Fan, et al., Structural insights into the SARS-CoV-2 Omicron RBD-ACE2 interaction, Cell Res. 32 (2022) 593–595, https://doi.org/10.1038/s41422-022-00644-8.
[46] J. Lan, J. Ge, J. Yu, S. Shan, H. Zhou, S. Fan, et al., Structure of the SARS-CoV-2 spike receptor-binding domain bound to the ACE2 receptor, Nature 581 (2020) 215–220, https://doi.org/10.1038/s41586-020-2180-5.
[47] L. Xia, Y. Zhang, Q. Zhou, Structural basis for the recognition of HCoV-HKU1 by human TMPRSS2, Cell Res. (2024), https://doi.org/10.1038/s41422-024-00958-9.
[48] N. Wang, X. Shi, L. Jiang, S. Zhang, D. Wang, P. Tong, et al., Structure of MERS-CoV spike receptor-binding domain complexed with human receptor DPP4, Cell Res. 23 (2013) 986–993, https://doi.org/10.1038/cr.2013.92.
[49] S.R. Tzeng, C.G. Kalodimos, Protein activity regulation by conformational entropy, Nature 488 (2012) 236–240, https://doi.org/10.1038/nature11271.

Biomedicine & Pharmacotherapy 180 (2024) 117517

Contents lists available at ScienceDirect

Biomedicine & Pharmacotherapy

journal homepage: www.elsevier.com/locate/biopha

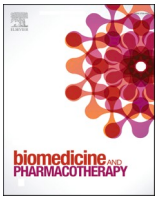

Identification of nitrile-containing isoquinoline-related natural product derivatives as coronavirus entry inhibitors *in silico* and *in vitro*

Nasim Shahhamzehei [a], Sara Abdelfatah [a], Hannah S. Schwarzer-Sperber [b], Kathrin Sutter [b,c], Rümeysa Yücer [a], Gerhard Bringmann [d], Roland Schwarzer [c,*], Thomas Efferth [a,*]

[a] Department of Pharmaceutical Biology, Institute of Pharmaceutical and Biomedical Sciences, Johannes Gutenberg University, Staudinger Weg 5, Mainz 55128, Germany
[b] Institute for the Research on HIV and AIDS-Associated Diseases (HIV-AAD), University Hospital Essen, University Duisburg-Essen, Essen, Germany
[c] Institute for Virology, University Hospital Essen, University Duisburg-Essen, Essen, Germany
[d] Institute of Organic Chemistry, University of Würzburg, Am Hubland, Würzburg 97074, Germany

ARTICLE INFO

Keywords:
ACE2
SARS-CoV-2
Nitrile-containing natural product derivatives
Isoquinoline
Pan-entry inhibitor
Virtual drug screening

ABSTRACT

Severe acute respiratory syndrome coronavirus 2 (SARS-CoV-2) has caused millions of infections and deaths worldwide since its emergence in Wuhan, China, in late 2019. Natural product inhibitors targeting the interaction between the receptor-binding domain (RBD) of the SARS-CoV-2 spike protein and human angiotensin-converting enzyme 2 (ACE2), crucial for viral attachment and cellular entry, are of significant interest as potential antiviral agents. In this study a library of nitrile- and sulfur-containing natural product derived compounds were used for virtual drug screening against the RBD of the SARS-CoV-2 spike protein. The top 18 compounds from docking were tested for their efficacy to inhibit virus entry. In vitro experiments revealed that compounds **9**, **14**, and **15** inhibited SARS-CoV-2 pseudovirus and live virus entry in HEK-ACE2 and Vero E6 host cells at low micromolar IC_{50} values. Cell viability assays showed these compounds exerted low cytotoxicity towards MRC5, Vero E6, and HEK-ACE2 cell lines. Microscale thermophoresis revealed all three compounds strongly bound to the RBDs of SARS-CoV-2, SARS-CoV-2 XBB, SARS-CoV-1, MERS-CoV, and HCoV-HKU1, with their K_d values increasing as RBD sequence similarity decreased. Molecular docking studies indicated compounds **9**, **14**, and **15** bound to the SARS-CoV-2 spike protein RBD and interacted with hotspot amino acid residues required for the RBD-ACE2 interaction and cellular infection. These three nitrile-containing candidates, particularly compound **15**, should be considered for further development as potential pan-coronavirus entry inhibitors.

1. Introduction

The COVID-19 (coronavirus disease 2019) pandemic caused by the severe acute respiratory syndrome coronavirus 2 (SARS-CoV-2) has infected more than 774 million individuals with more than 7 million deaths by the end of June 2024 (https://covid19.who.int/). In addition, this pandemic provoked an impending economic crisis and recession on a global scale [1]. Despite the development of successful vaccinations, antigenic mutations can result in immune evasion in convalescent COVID-19 patients and vaccines, which can cause infection, hospitalization, and even death [2]. Today, remdesivir [3] and molnupiravir, targeting RNA-dependent RNA polymerase, and nirmatrelvir/ritonavir, targeting the main protease (M^{pro}) are approved by the United States Food and Drug Administration (US FDA) for the treatment of COVID-19 in certain adults [4], but no small molecule has so far been approved to target the spike protein, which is a trimeric protein located on the surface of the viruses. The spike protein is one of the most important targets, since its inhibition prevents the entry of the virus into the host cells and thereby inhibits virus replication. Although the use of monoclonal antibodies (mAb), that target the spike protein, can be an alternative strategy to disrupt early events in the SARS-CoV-2 life cycle, there are novel SARS-CoV-2 variants evading mAb-induced protection [5]. Furthermore, issues with the solubility, immunogenicity, and appropriateness of the antibodies for oral or inhaled delivery pose challenges [6]. The spike protein has a full length of 1273 amino acids, including the N-terminus signal peptide, the S1 subunit, and the S2 subunit. S1 includes the N-terminal domain (NTD), the receptor-binding domain (RBD), and two C-terminal domains (CTD1 and CTD2), while S2

* Corresponding authors.
E-mail addresses: Roland.Schwarzer@uk-essen.de (R. Schwarzer), efferth@uni-mainz.de (T. Efferth).

https://doi.org/10.1016/j.biopha.2024.117517
Received 11 July 2024; Received in revised form 25 September 2024; Accepted 26 September 2024
Available online 1 October 2024

includes fusion peptide (FP), fusion-peptide proximal region (FPPR), heptad repeat 1 (HR1), central helix (CH), connector domain (CD), heptad repeat 2 (HR2), transmembrane segment (TM), and the cytoplasmic tail (CT). The receptor binding domain (RBD) contains two subdomains: a five-stranded antiparallel β-sheet connected by short helices and loops, and an extended loop, named receptor binding motif (RBM). The spike protein can bind to two or three host ACE2 molecules through the RBD [7], which makes it a promising target for drug development. Molecules containing sulfur are frequently found in nature. They are active both pharmacologically and physiologically and show vast anticancer, antiviral, antibacterial, and antifungal activities [8–10]. Nitrile-containing compounds can be found in a variety of organisms, including bacteria, fungi, plants, insects, sponges, and other aquatic creatures, and have a wide range of pharmacological activities, including anti-microbial, anti-cancer, anti-inflammatory, and antioxidant properties [11–13]. During the past decades, both nitrile- and sulfur-containing compounds have reached increasing importance in medicinal chemistry, thus attracting our attention to the development of pan-coronaviral inhibitors.

In this study, our aim was to explore natural pan-coronaviral inhibitors, focusing on sulfur- and nitrile-containing compounds, against different spike proteins of the coronavirus family. For this purpose, we studied 143 sulfur- and nitrile-containing compounds from the ZINC database and from the literature.

2. Materials and methods

2.1. Cell lines

HEK-ACE2 cells were obtained from ATCC (American Type Culture Collection, Virginia, USA). The 293T cell line was kindly provided by Dr. Helen May-Simera (Institute of Molecular Physiology, Johannes Gutenberg University, Mainz, Germany). They were grown in Dulbecco's Modified Eagle Medium (DMEM; Thermo Fisher) supplemented with 10 % fetal bovine serum (FBS) and 1 % penicillin/streptomycin (P/S). MRC-5 lung fibroblasts were obtained from Dr. Sebastian Zahnreich (Department of Radiation Oncology and Radiation Therapy, University Medical Centre of the Johannes Gutenberg University, Mainz, Germany) and grown in DMEM, low glucose, pyruvate medium with 15 % FBS, 1 % P/S, and 1 % MEM. Non-essential amino acids (Thermo Fisher) were used for cultivation. Vero E6 cells were obtained from ATCC and cultured in DMEM supplemented with 10 % FBS, 1 % L-glutamine (Capricorn Scientific, Germany), and 1 % P/S. All cell lines were incubated in a humidified atmosphere at 37 °C and 5 % CO_2.

2.2. Compounds

The chemical structures of 143 natural-derived nitrile- and sulfur-containing compounds were downloaded from the ZINC and PubChem databases in the three-dimensional SDF format. Based on *in silico* studies, 18 selected compounds were provided by Vitas-M Laboratory (Hong Kong, China). The compounds had a guaranteed purity of > 90 %. Based on the ^{1}H NMR spectra given by the provider, the purity of most of the compounds was higher, usually > 95 %. All compounds were dissolved in DMSO at a concentration of 20 mM and stored at − 20 °C.

2.3. Virtual screening

In this study, AutoDock Vina in PyRx 0.8 software was used for the virtual screening of 143 natural-derived compounds from the ZINC database and from the literature (blind docking mode). As a target, the RBD domain of the spike protein of SARS-CoV-2 (PDB ID: 7bnn) was chosen to identify compounds with high a affinity and low a binding energy (kcal/mol). For validation and verification of PyRx results, the top 84 compounds, with a cut-off value of − 6 kcal/mol, were subjected to AutoDock 4.2.6 (defined docking mode) to identify their binding affinity for the RBD domain of the spike protein of SARS-CoV-2 (PDB ID: 7bnn) using the Lamarckian algorithm. The protein was kept rigid, while the ligand moved during the docking simulation. The parameters were set to 250 runs and 2,500,000 energy evaluations for each cycle, while the other docking parameters were kept at default values as described by our group [14]. Docking was conducted using the high-performance supercomputer MOGON (Johannes Gutenberg University, Mainz, Germany). The AutoDock version 1.5.6 was used to convert the Protein Data Bank file of target proteins (PDB) to PDBQT files and create a grid box. The energy of the compounds was minimized and converted from SDF format to PDBQT format using the PyRx software.

2.4. Plasmids

For production of pseudovirus plasmids: pHAGE-CMV-Luc2-IRES-ZsGreen-W (BEI Cat. # NR-52516), HDM-Hgpm2 (BEI Cat. # NR-52517), HDM-tat1b (BEI Cat. # NR-52518), pRC-CMV-Rev1b (BEI Cat. # NR-52519), and HDM-IDTSpike-fixK-HA-tail (BEI Cat. # NR-53765) were obtained from BEI Resources (US). In order to generate a working stock, all plasmids were amplified in *Escherichia coli* using One Shot™ TOP10 chemically competent *E. coli* (Invitrogen, Thermo Fisher). They were extracted and purified using the Plasmid Plus Maxi Kit (QIAGEN).

2.5. Production of SARS-CoV-2 pseudoviruses and titration

293T cells were seeded in DMEM medium containing 10 % FBS so that they were 70–80 % confluent the next day. Twenty-four hours after seeding, the cells were transfected with 1 μg of the Luciferase IRES ZsGreen (NR-52516) backbone, 0.22 μg each of the plasmids HDM-Hgpm2 (NR-52517), pRC-CMV-Rev1b (NR-52519), and HDM-tat1b (NR-52518) with or without 0.34 μg SARS-CoV-2 spike (NR-53765) as a negative control using Lipofectamine™ 2000 transfection reagent (Invitrogen, Thermo Fisher). Eighteen hours after transfection, the medium was changed with fresh medium, 48 and 72 h after transfection, the supernatant was collected, centrifuged for 3 min at 1250 rpm, and stored at − 80 °C. For the titration of pseudoviruses, HEK-ACE2 was seeded (12.5×10^3 cells/well) in white 96-well plates (Greiner, Cat. # 655074). Twenty-four hours after seeding, a serial dilution of spike-pseudotyped Luciferase IRES ZsGreen virus was prepared. Starting with an undiluted virus, six 1:2 dilutions were made. Twenty-four hours after infection, cell supernatants were replaced with 50 μl fresh medium for each sample. Then, 50 μl Bright-Glo Luciferase Assay reagent (Promega, E2610) were added per well, and cells were incubated for 2 min at room temperature. Luciferase activities were measured using an Infinite M2000™ Pro plate reader (Tecan, Crailsheim, Germany). The measured luciferase activity, defined as relative light unit (RLU) *vs.* virus dilution, were plotted, and the amount of pseudovirus was selected for further assays, which has sufficient (> 1000-fold) signal intensity above the virus-only background and in the linear part of the curve [15,16].

2.6. Pseudovirus inhibition assay

HEK-ACE2 (12.5×10^3cells/well) were seeded in the white 96-well plate (Greiner, Cat. # 655074) 1 d before infection. The next day, the pseudoviruses were incubated at 37 °C for 1.5 h with either 30 μM of the compounds or DMSO, before being added to the cells. Twenty-four hours after infection, the medium was discarded, and 50 μl of fresh medium were added to each well, followed by 50 μl of Bright-Glo Luciferase reagent (Promega, E2610) and incubated for 2 min in the dark at room temperature. The luminescence was measured using an Infinite M2000 Pro™ plate reader (Tecan) without attenuation and a luminescence integration time of 1 s. As a next step, compounds exhibiting more than 50 % inhibitory activity at a fixed concentration of 30 μM were selected for dose-response studies in a concentration range from 0 to 30 μM in all experiments. Etravirine was used as a positive control [17]. To calculate

the percentage of infection, the following equation was used: % infection = [(mean RLU from each sample (virus + compound) - mean RLU from negative cell control/(mean RLU from virus control – mean RLU from negative cell control) × 100]. The percentage of infection vs. the log concentration of the inhibitors was used to calculate the IC_{50} values [15,16]. As a confirmatory assay, fluorescence microscopy was performed. HEK-ACE2 (10×10^3 cells/well) were seeded in black 96-well plates (Greiner, Cat.# 655936) 1 d before infection. The next day, before the infection pseudoviruses were incubated for 1.5 h at 37 °C in the presence of 5 μM test compounds or DMSO. Seventy-two hours after infection, GFP fluorescence quantified using live imaging system, results were analyzed using ImageJ.

2.7. SARS-CoV-2 propagation and quantification

A SARS-CoV-2 isolate (referred to as the Essen isolate) derived from patient material was used for infection experiments as previously described [18]. The virus was produced in Vero E6 cells, plated at a concentration of 2×10^6 Vero E6 cells in a T75 flask, and incubated for 24 h at 37 °C with 5 % CO_2 in DMEM supplemented with 10 % FBS, 1 % L-glutamine, 1 % penicillin, and 1 % streptomycin. The cells were then exposed to the isolated virus and incubated for an additional 72 h. The culture supernatant was then clarified by centrifugation and stored at − 80 °C. Viral concentrations were assessed using an endpoint dilution assay to determine the 50 % tissue culture infective dose ($TCID_{50}$).

2.8. SARS-CoV-2 in-cell ELISA procedure

Virus infections were quantified by in-cell ELISA following a recently published protocol [19]: A total of 2×10^4 cells/well were seeded in a flat-bottom 96-well plate 1 d prior to infection. The cells were then infected with SARS-CoV-2 for 24 h and subsequently fixed using 4 % paraformaldehyde in phosphate buffered saline (PBS). Permeabilization was conducted using a 1 % Triton-X-100 solution in PBS, followed by blocking with 3 % fetal calf serum (FCS) in PBS. Next, the primary antibody (anti-N mAb1 ABIN6952435, Antibodies Online, Aachen, Germany) was added and incubated for 2 h at room temperature. Subsequently, a peroxidase-labeled secondary antibody (Cat. # 115-035-003, Jackson Immuno Research, Cambridge, UK) was applied for an additional hour, followed by washing steps with a solution of 0.05 % Tween-20 in PBS. Finally, tetramethylbenzidine (TMB) substrate was added, and the enzymatic reaction was terminated using 0.5 M HCl. The absorbance of the dye was then measured at 450 nm using a Spark® 10 M multimode microplate reader (Tecan).

2.9. Cell viability assay

Cell viability was measured using the resazurin assay as previously described [20]. Human diploid MRC-5 lung fibroblasts and human embryonic kidney HEK-ACE2 cells were seeded (2×10^4 cells/well and 1×10^4, respectively) into 96-well culture plates and incubated overnight before treatment. On the second day, the cells were treated with ten concentrations of compounds in a range of 0.3–100 μM. After 24 h of incubation, 20 μl of 0.01 % resazurin (Promega, Mannheim, Germany) were added to each well. The fluorescence was detected after 4 h of incubation using an Infinite M2000™ Pro plate reader (Tecan) at Ex/Em = 550 nm/590 nm wavelength. The cell viability was calculated in comparison to the DMSO control. The DMSO final concentration was 0.5 %. The 50 % cytotoxicity concentration (CC_{50}) values were calculated in comparison to the DMSO-treated control. Each experiment was independently repeated three times, with six wells for each concentration. For the Vero E6 cell line, a total of 20×10^3 cells per well were seeded into 96-well culture plates and incubated overnight. On the second day, the cells were treated with a wide range of concentrations of compounds. After 24 h, the supernatants were replaced with 100 μl of fresh medium for each sample. Then, 20 μl of CellTiter-Blue™ reagent (Promega, Madison, USA) were added per well, and cells were incubated for 4 h at 37 °C with 5 % CO_2. Colorimetric analysis of treated cells was done with a Spark® 10 M multimode microplate reader (Tecan) detecting fluorescence with an excitation of 560 nm and an emission at 590 nm.

2.10. Sequence alignment

The full length of amino acid sequences of the RBD domain of the spike protein of SARS-CoV-2 (P0DTC2), SARS-CoV-1 (P59594), MERS-CoV (K9N5Q8), and HCoV-HKU1 (Q0ZME7) were accessed from the UniProt database, and for SARS-CoV-2 XBB.1. The sequences were downloaded from the Protein Data Bank (PDB ID: 8iou), and then the sequence alignment was performed using Clustal Omega (EMBL-EBI, Wellcome Genome Campus, Hinxton, Cambridgeshire, UK), and the figures were prepared using Jalviwe 2.11.3.2 (University of Dundee, Scotland, UK).

2.11. Microscale thermophoresis

The recombinant RBD of spike proteins of SARS-CoV-2, SARS-CoV-2 XBB.1, SARS-CoV-1, MERS-CoV, and HCoV-HKU1 were purchased from Bio-Techne (Wiesbaden, Germany) to perform microscale thermophoresis (MST), following previously established protocols [21,22]. Briefly, the recombinant proteins were labeled with the Monolith Protein Labeling Kit RED-NNHS 2nd Generation (MO-L011, Nano Temper Technologies GmbH, Munich, Germany) according to the manufacturer's instructions. The final protein concentrations after labeling were 1500 nM, 1500 nM, 1000 nM, 750 nM, and 1500 nM (Nanodrop, Thermo Fisher Scientific) for recombinant RBD of SARS-CoV-2, SARS-CoV-2 XBB.1, SARS-CoV-1, MERS-CoV, and HCoV-HKU1, respectively. Titration was performed using 16 serial dilutions, ranging from 200 to 0.006 M concentration (dilution steps 1:1). Ligand and protein were incubated for 30 min at room temperature in assay buffer (50 mM Tris buffer (pH 7.4) containing 10 mM $MgCl_2$, 150 mM NaCl, and 0.05 % Tween-20). Measurements were carried out in Monolith NT.115 standard capillaries (MO-K022, Nano Temper Technologies GmbH, Munich, Germany). The laser power was adjusted to 10 %, 20 %, 40 %, and 60 %, and the LED (light-emitting diodes) power was 20 % for SARS-CoV-2, SARS-CoV-1, MERS-CoV, HCoV-HKU1, and 30 % for SARS-CoV-2 XBB.1. Signals were measured using the Monolith NT.115 instrument (Nano Temper Technologies). Fitting curves and K_d values were calculated using NT Analysis 1.5.41. software (Nano Temper Technologies).

2.12. Molecular docking

The top compounds obtained from *in vitro* experiments were rescreened against RBD of the spike protein of SARS-CoV-2 (PDB ID: 7bnn), SARS-CoV-2 XBB.1(PDB ID: 8iou), SARS-CoV-1 (PDB ID: 6acd), MERS-CoV (PDB ID: 6nb03), and HCoV-HKU1 (PDB ID: 8opo) using AutoDock 4.2.6 (defined docking mode) in order to identify not only their binding affinity for different coronavirus RBD, but also the amino acid residues involved in the binding site. Docking was conducted using the high-performance supercomputer MOGON (Johannes Gutenberg University, Mainz, Germany). The visualization and imaging were created by Discovery Studio Visualizer V 21.1.0.20298 (San Diego, California, United States).

2.13. Statistics and data fitting

All inhibition assays were performed at least as duplicates per plate, and all results shown are the average of at least three independent experiments. The binding data were converted to percent infection and fitted with standard log inhibitor *vs.* normalized response models (four parameters) using nonlinear regression in GraphPad Prism 8 (GraphPad, La Jolla, CA, USA) to establish half-maximal toxicity or inhibitory

concentrations (CC_{50}, IC_{50}). The selectivity index (SI) of active compounds was calculated using the $SI = CC_{50} / EC_{50}$ equation for live and pseudo-typed viruses. The correlation between the K_d values and pecentage of identity of RBDs was calculated using the Pearson correlation tes.

3. Results

3.1. Virtual screening

Starting from a ZINC library of 97 natural-derived compounds and a library of 46 natural compounds preselected from the literature, virtual screening was performed with PyRx. A total of 84 compounds were selected based on their lowest PyRx-based binding energies (cut-off value: − 6 kcal/mol) to the RBD of the SARS-CoV-2 spike protein. For further evaluation and validation, they were subjected to AutoDock 4.2.6. Based on the lowest binding energy (cut-off value: − 7 kcal/mol), 18 candidates were selected for the *in vitro* experiments, and etravirine was used as a positive control, see Table 1. The structures of top 18 compounds are shown in Fig. 1.

3.2. Development of a SARS-CoV-2 pseudovirus assay

Our goal was to develop a sensitive SARS-CoV-2 neutralization assay by introducing SARS-CoV-2 spike protein into lentiviruses to evaluate inhibition of viral entry. The 293 T cell line was co-transfected with the plasmids and the supernatant was harvested 72 h later, which was then used to infect the HEK-ACE2 cells. Measuring the titers of the produced pseudoviruses was based on luminescence signal reads obtained from the activity of the expressed luciferase. The right titer of the generated pseudoviruses was selected as the dilution that results in an RLU above bald pseudovirus as a negative control and in the linear part of the curve (10^4–5×10^5) (Fig. 2A). In our case, 5×10^5 RLU/well were used to maximize the use of each lot of the produced pseudoviruses, and it worked very well in neutralization assays.

3.3. Inhibition of pseudotyped SARS-CoV-2 infection

Luciferase assays were performed in HEK-ACE2 cells to screen the 18 top candidates selected from the in silico studies to find novel anti-SARS-COV-2 entry inhibitors. After the preliminary screening (Fig. 2B), three compounds inhibited pseudovirus entry, substances **9**, **14**, and **15**. Notably, all three compounds contained a nitrile group. These three compounds were then subjected to dose-response experiments in order to calculate the concentration of each compound required to inhibit pseudovirus entry by half (IC_{50}). The IC_{50} values for compounds **9**, **14**, and **15** were 1.061 ± 0.08, 3.87 ± 0.28, and 1.85 ± 0.37 μM, respectively (Fig. 2C). GFP fluorescence measured from live fluorescence microscopy demonstrated that compound **9** strongly protected the cells from pseudovirus infection, while compound **15** had moderate and

Table 1
PyRx and molecular docking results of 18 natural-derived selected compounds and etravirine as a positive control binding to the RBD of spike protein of SARS-CoV-2 (PDB ID: 7bnn).

Compound number	ZINC-ID	Compound-IUPAC name	PyRx binding energy (kcal/mol)	AutoDock binding energy (kcal/mol)	Ki (μM)
Compound **1**	ZINC000002092410	Ethyl 2-{[(6-bromo-2-oxo-2H-chromen-3-yl)carbonyl]amino}-4,5,6,7,8,9,10,11,12,13-decahydrocyclododeca[*b*]thiophene-3-carboxylate	− 7.80	− 9.16 ± 0.03	0.193 ± 0.01
Compound **2**	ZINC000247984074	Ethyl (1R,2R,9R,12S)-6-(furan-2-carbonylamino)-16-methoxy-9-methyl-5-thiapentacyclo[10.8.0.02,9.04,8.013,18]icosa-4(8),6,13(18),14,16-pentaene-7-carboxylate	− 6.90	− 8.88 ± 0.16	0.32 ± 0.08
Compound **3**	ZINC000002060195	N-(3-cyano-4,5-diphenylfuran-2-yl)-2-(4-methoxyphenyl)acetamide325739–78–4	− 7.90	− 8.65 ± 0.004	0.45 ± 0.005
Compound **4**	ZINC000000568457	Methyl 5-[(1,3-benzodioxol-5-ylcarbonyl)amino]-4-cyano-3 methylthiophene-2-carboxylate	− 6.30	− 8.33 ± 0.009	0.77 ± 0.01
Compound **5**	ZINC000000846863	Ethyl 5-acetyl-4-methyl-2-({[(4-methyl-2-oxo-2H-chromen-7-yl)oxy]acetyl}amino)thiophene-3-carboxylate	− 7.20	− 8.27 ± 0.20	0.91 ± 0.27
Compound **6**	ZINC000001061006	N-(3-cyano-4,5-dimethylthiophen-2-yl)-2-((4-methyl-2-oxo-2H-chromen-7-yl)oxy) acetamide	− 6.40	− 7.87 ± 0.15	1.75 ± 0.39
Compound **7**	ZINC000000846827	Diethyl 3-methyl-5-{[(2*E*)-3-phenylprop-2-enoyl]amino}thiophene-2,4-dicarboxylate	− 6.30	− 7.84 ± 0.07	1.81 ± 0.23
Compound **8**	ZINC000100778515	4-imino-2-(6-methoxy-4-oxo-4H-chromen-3-yl)−6,7-dihydro-4H-[1,3]dioxolo[4,5-*g*]pyrido[2,1-*a*]isoquinoline-3-carbonitrile	− 8.30	− 7.82 ± 0.004	1.86 ± 0.008
Compound **9**	ZINC000101140820	4-imino-2-[3-methoxy-4-(propan-2-yloxy)phenyl]-6,7,11,12-tetrahydro-4H,10H-[1,4]dioxepino[2,3-*g*]pyrido[2,1-*a*]isoquinoline-3-carbonitrile	− 8.00	− 7.80 ± 0.01	1.91 ± 0.04
Compound **10**	ZINC000000037324	N-[4-(cyanomethyl)phenyl]-2-(4-methoxyphenyl)acetamide	− 6.30	− 7.68 ± 0.009	2.35 ± 0.02
Compound **11**	ZINC000101374185	2-(4-hydroxy-3-methoxyphenyl)-4-imino-9,10-dimethoxy-6,7-dihydro-4H-pyrido[2,1-*a*]isoquinoline-3-carbonitrile	− 6.50	− 7.67 ± 0.02	2.82 ± 0.08
Compound **12**	ZINC000001965160	Ethyl 4-cyano-5-(3,5-dimethoxybenzamido)-3-methylthiophene-2-carboxylate	− 6.00	− 7.52 ± 0.23	3.3 ± 1.09
Compound **13**	ZINC000000626395	2,4-diethyl 3-methyl-5-{2-[(4-methyl-2-oxo-2H-chromen-7-yl)oxy]acetamido}thiophene-2,4-dicarboxylate	− 7.00	− 7.48 ± 0.02	3.31 ± 0.14
Compound **14**	ZINC000100778854	4-imino-2-(3-methoxyphenyl)-6,7-dihydro-4H-[1,3]dioxolo[4,5-*g*]pyrido[2,1-*a*]isoquinoline-3-carbonitrile	− 8.00	− 7.34 ± 0.004	4.17 ± 0.01
Compound **15**	ZINC000101345860	2-(1,3-benzodioxol-5-yl)-4-imino-9,10-dimethoxy-6,7-dihydro-4H-pyrido[2,1-*a*]isoquinoline-3-carbonitrile	− 7.20	− 7.33 ± 0.10	4.33 ± 0.80
Compound **16**	ZINC000100779013	Methyl 4-(3-cyano-4-imino-6,7-dihydro-4H-[1,3]dioxolo[4,5-*g*]pyrido[2,1-*a*]isoquinolin-2-yl)benzoate	− 8.30	− 7.23 ± 0.02	4.9 ± 0.24
Compound **17**	ZINC000253412567	N~2~-[(7*S*)-7-(acetylamino)-1,2,3-trimethoxy-9-oxo-5,6,7,9-tetrahydrobenzo[*a*]heptalen-10-yl]-N-(2-hydroxyethyl)-L-methioninamide	− 6.40	− 7.05 ± 0.38	5.42 ± 1.53
Compound **18**	ZINC000005225262	Ethyl 2-[[2-[(2S)-2-benzamido-4-methylpentanoyl]oxyacetyl]amino]-5,6-dihydro-4H-cyclopenta[*b*]thiophene-3-carboxylate	− 6.3	− 7.01 ± 0.50	4.96 ± 1.45
Etravirine (positive control)	ZINC000000602632	4-[6-amino-5-bromo-2-(4-cyanoanilino)pyrimidin-4-yl]oxy-3,5-dimethylbenzonitrile	− 6.70	− 7.34 ± 0.02	4.15 ± 0.16

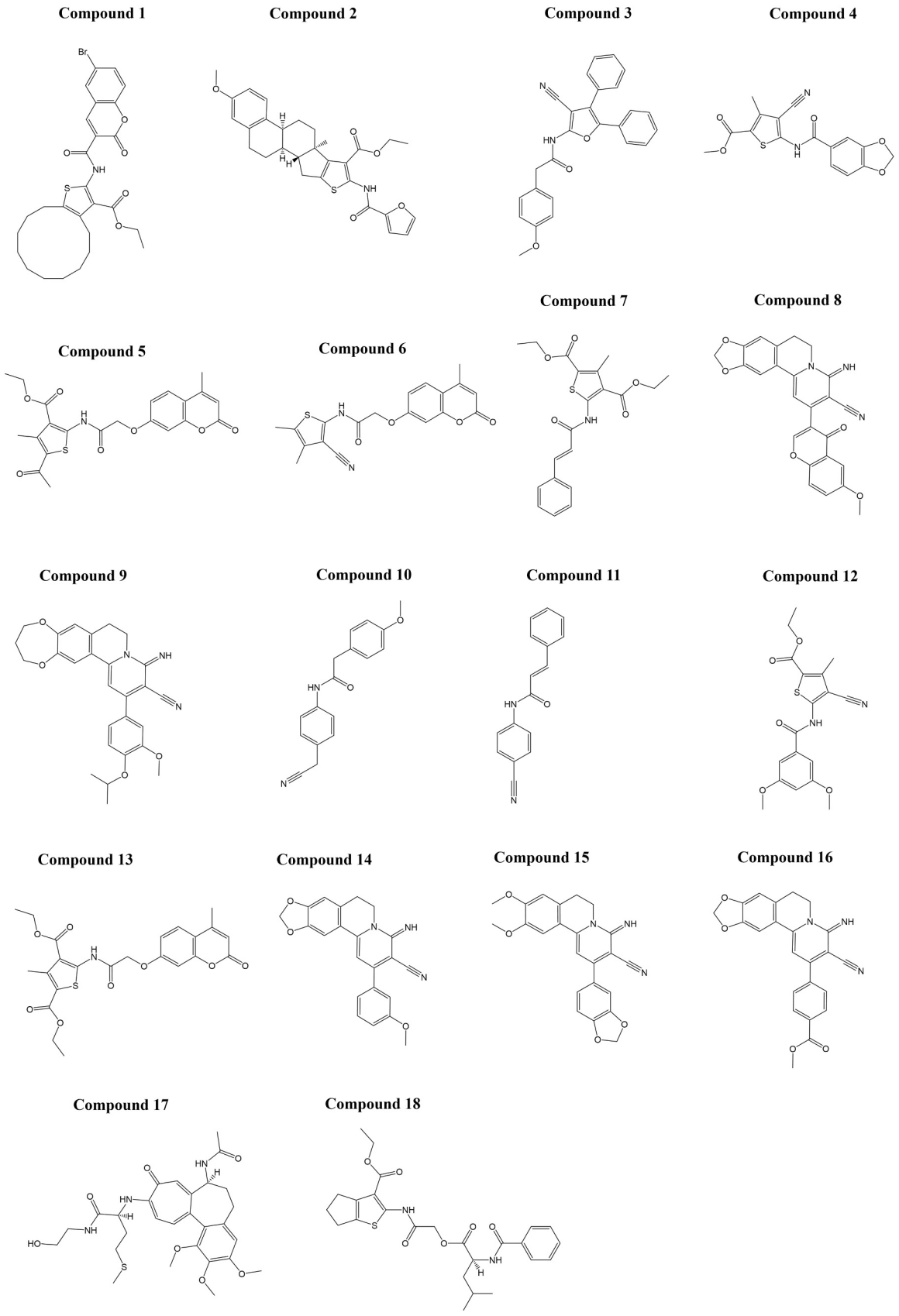

Fig. 1. Chemical structures of the top 18 natural-derived compounds exhibiting the lowest binding energy to the RBD of the SARS-CoV-2 spike protein.

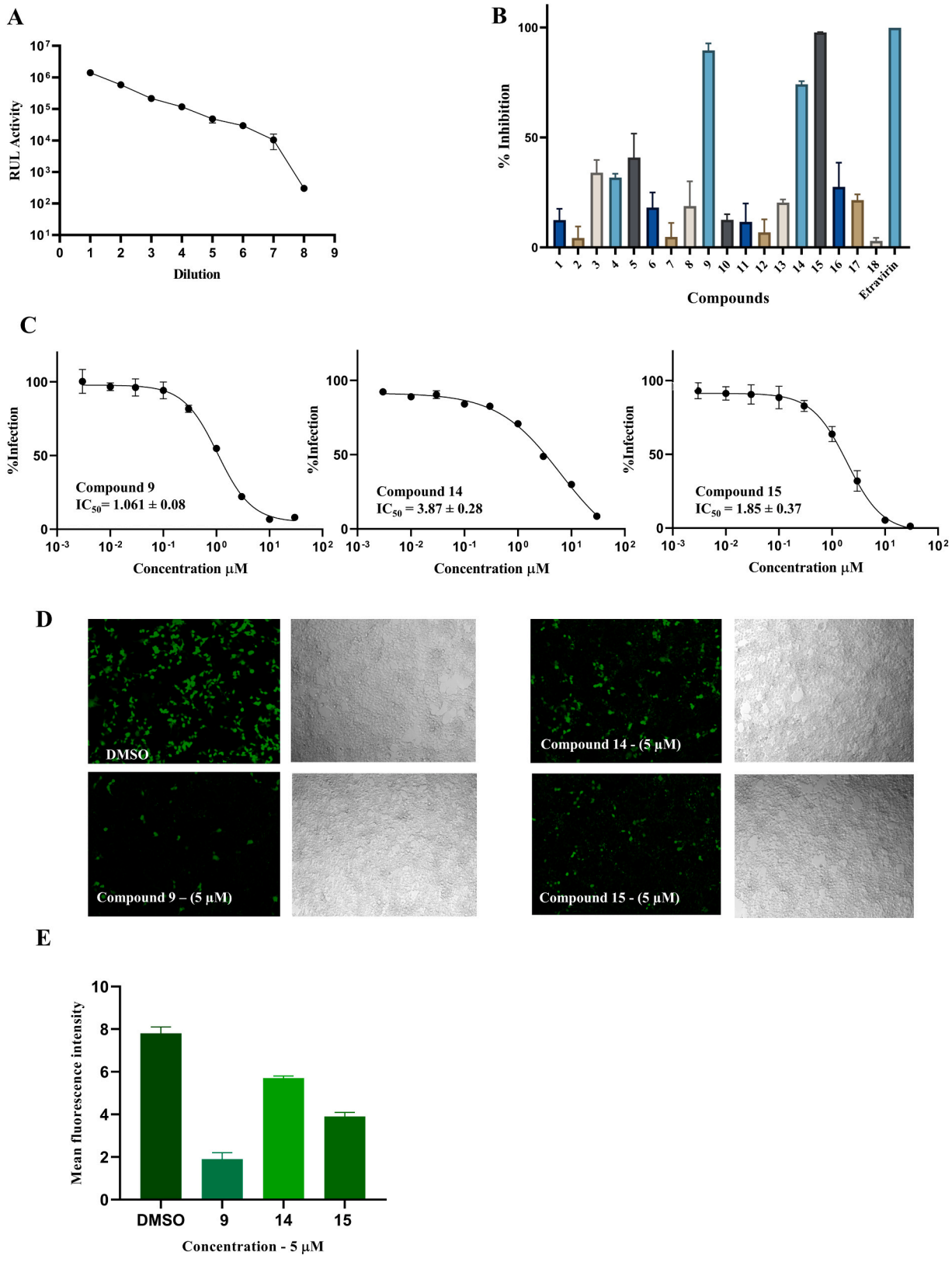

Fig. 2. Identification of entry inhibitors against pseudotyped SARS-CoV-2 lentivirus in HEK-ACE2 cells: A) Titration of the SARS-CoV-2 pseudovirus. Samples were run in duplicates, and the data are shown as mean ± SD. B) Percentage of inhibition of the SARS-CoV-2 pseudovirus in the presence of 18 selected natural-derived compounds and etravirine as a positive control (30 μM). C) Dose-response curves of compounds **9**, **14**, and **15** on the SARS-CoV-2 pseudovirus, IC_{50} values and data points are shown as mean ± SD for three independent replicates. D) fluorescence microscopic images of HEK-ACE2 treated with pseudotyped SARS-CoV-2 lentivirus in the presence of 5 μM of compounds **9**, **14**, and **15**. E) quantification of GFP fluoresces standardized to the mean of fluorescence intensity using Image J, at 5 μM concentration and presented as mean ± S.D of three replicates.

compound **14** had only week effects, which was consistent with the results from the luciferase inhibition assay (Fig. 2D).

3.4. Inhibition of live SARS-CoV-2 replication

The inhibitory activity of compounds **9**, **14**, and **15** towards the live SARS-CoV-2 viruses were assessed in titration experiments in order to calculate the IC_{50} values. Compound **15** effectively blocked SARS-CoV-2 infection at the cellular level with an IC_{50} of 9.32 ± 1.3 μM. Compounds **9** and **14** also showed inhibiting effects against SARS-CoV-2, with IC_{50} values of 22.86 ± 4.3 μM and 26.26 ± 7.38 μM, respectively (Fig. 3).

3.5. Cell viability assay

The cytotoxicity of compounds **9**, **14**, and **15** was tested on human MRC-5 fibroblasts, HEK-ACE2 cells, and Vero E6 cells using the resazurin assay. Compound **9** was cytotoxic towards HEK-ACE2, human MRC-5 fibroblasts, and Vero E6 cells with CC_{50} values of 28.29 ± 1.2, 81.15 ± 0.36, and 99.7 ± 1.5 μM, respectively. Compound **14** was cytotoxic against HEK-ACE2 and Vero E6 cells with CC_{50} values of 38.7 ± 1.5 and 96.8 ± 1.5, respectively, while it did not show toxicity against human MRC-5 fibroblasts. While compound **15** was cytotoxic against HEK-ACE2, with a CC_{50} value of 23.31 ± 3.06 μM, it did not display toxic effects towards human MRC-5 fibroblasts and Vero E6 cells (Fig. 4).

3.6. Sequence alignment

To determine whether our top compounds can bind to the spike protein of various coronavirus family members, sequence alignments were performed to identify the similarity between the receptor-binding domains (RBD) of the spike proteins from different coronavirus family members. The results revealed 89.91 %, 73.42 %, 18.75 %, and 19.81 % identity of the SARS-CoV-2 spike RBD domain to SARS-CoV-2 XBB.1 (Omicron variant), SARS-CoV-1, MERS-CoV, and HCoV-HKU1, respectively. Fig. 5 shows the conserved amino acid residues between the RBD domain of the spike protein of coronaviruses. The dark blue color indicates > 80 % identity, the blue color stands for > 60 %, and the light blue color means > 40 %.

3.7. Microscale thermophoresis

Microscale thermophoresis as a sensitive technology was performed to determine the binding affinity between active compounds and labeled RBD of the spike proteins from different coronavirus species, including different SARS-CoV-2 variants, SARS-CoV-1 and MERS, as well as the endemic strain HCoV-HKU1. For this purpose, the labeled recombinant RBDs of the spike proteins of SARS-CoV-2, SRAS-CoV-2 XBB.1, SARS-CoV-1, MERS-CoV, and HCoV-HKU1 were titrated against different concentrations of selected compounds. Compound **9** was bound to the RBD of spike protein of SARS-CoV-2, SARS-CoV-2 XBB.1, SARS-CoV-1, HCoV-HKU1, and MERS-CoV, with K_d values of 1.38, 3.7, 20.8, 23.3, and 23.3 μM, respectively. Compound **14** was bound to the spike protein of SARS-CoV-2, SARS-CoV-2 XBB.1, SARS-CoV-1, HCoV-HKU1, and MERS-CoV, with K_d values of 1.29, 1.39, 41.5, 50.1, and 63.1 μM, respectively. Finally, compound **15** resulted in K_d values of 1.4, 5.1, 28.4, and 48.3 μM for the spike protein of SARS-CoV-2, SARS-CoV-2 XBB.1, SARS-CoV-1, HCoV-HKU1, and MERS-CoV, respectively (Fig. 6).

3.8. Binding mode of the top candidates

Molecular docking with AutoDock 4.2.6 revealed high binding affinities of compounds **9**, **14**, and **15** to the RBD of spike proteins of SARS-CoV-2, SARS-CoV-2 XBB.1, SARS-CoV-1, MERS-CoV, and HCoV-HKU1, which can block the binding of RBD and ACE2 and thus protect healthy cells and prevent further degeneration in the early stage of infection. The three candidate compounds showed lowest binding energy (LBE) values between − 6.21 and − 8.11 kcal/mol and predicted inhibition constants (pK_i) between 28.22 and 1.14 μM. The amino acid interactions between the three candidate compounds and the proteins of interest are displayed in Fig. 7.

4. Discussion

Up to now, three zoonotic coronaviruses (CoVs) have been identified that cause deadly pneumonia outbreaks in humans, thereby posing a significant threat to public health. The SARS-CoV-1 caused severe acute respiratory syndrome (SARS) first appeared in 2002 and quickly expanded to five continents. MERS-CoV caused the Middle East respiratory syndrome (MERS), leading to high fatality rates at the Arabic peninsula in 2012, and the severe acute respiratory syndrome coronavirus 2 (SARS-CoV-2) rapidly developed to a global pandemic [23].

Several vaccines and antiviral medications have been developed to combat the COVID-19 pandemic. However, the diverse SARS-CoV-2 variants of concern (VOCs), especially Omicron and its sub-lineages, made the current COVID-19 vaccines and therapeutic antibodies less effective [24]. Along with SARS-CoV-2 and MERS-CoV, the four seasonal endemic HCoVs (OC43, HKU1, 229E, and NL63) still cause disease in humans [25]. Moreover, new studies showed that some SARS-related coronaviruses (SARSr-CoVs) in bats have the potential to cause novel coronavirus diseases in humans. Given these facts, a pan-coronavirus (pan-CoV) drug should be developed to prevent infection not only with SARS-CoV-2 and its variants but also with other newly emerging or reemerging HCoVs [26].

From 2010 to 2020, the US FDA has granted approval to at least one medicine containing a nitrile group every year [27]. These

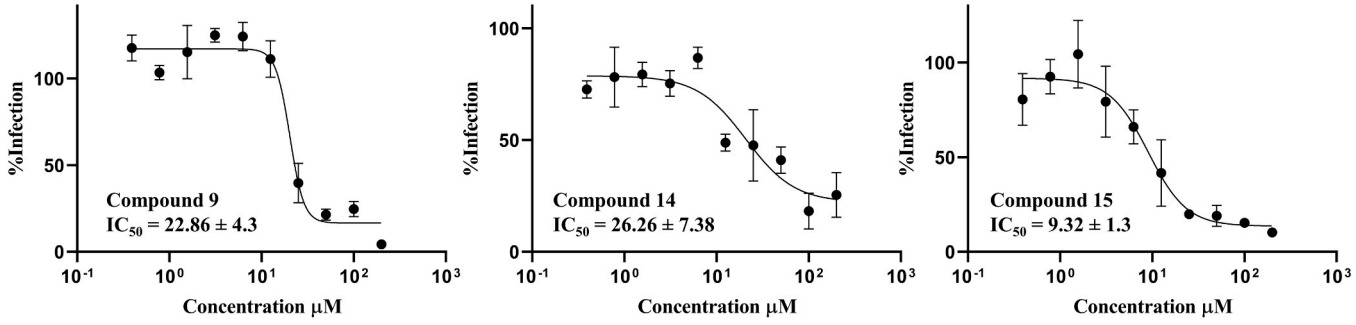

Fig. 3. Inhibition of fully replication-competent SARS-CoV-2. Vero E6 cells were infected with a clinical SARS-CoV-2 isolate for 24 h in the presence of different candidate inhibitors at the indicated concentrations. Infection levels were quantified by in-cell ELISA and normalized to mock-treated control wells (infected, but non-treated). Infection data were fitted with a four parameters inhibitor vs. response function (Y = Bottom + (Top - Bottom)/(1 + (IC_{50} / X) ^ HillSlope) using the statistics software GraphPad prism. Data points show mean ± standard error of the mean, calculated from at least three independent titrations of each compound.

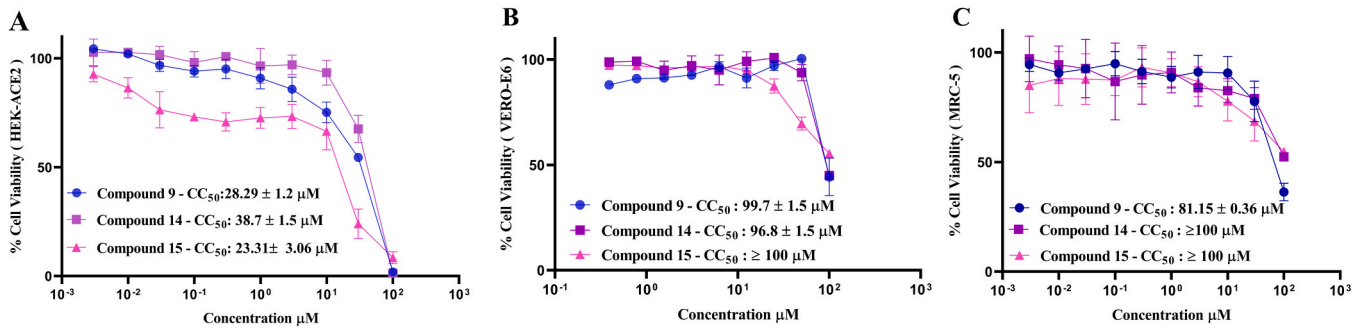

Fig. 4. Cytotoxic effects of compounds **9**, **14**, and **15** against A) HEK-ACE2, B) MRC-5, and C) Vero E6 cell lines. The cytotoxicity was assessed using the resazurin method. Each data point represents the mean value ± SD of three independent experiments with six replicates each.

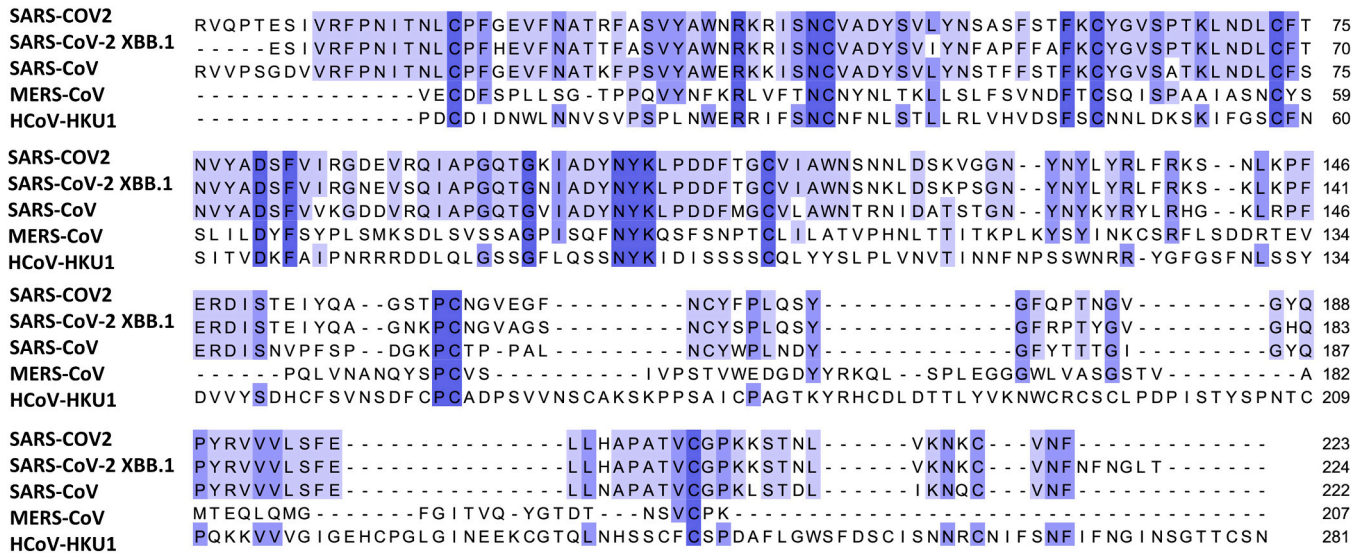

Fig. 5. Sequence alignments of the RBD of spike proteins of SARS-CoV-2, SARS-CoV-2 XBB.1, SARS-CoV-1, MERS-CoV, and HCoV-HKU1. The dark blue color indicates that residues show > 80 % identity with the consensus residues; the blue color indicates > 60 %; the light blue color indicates > 40 %; and the white color indicates < 40 % identity.

nitrile-containing drugs target a variety of diseases such as heart failure, cancer, inflammation, as well as fungal, bacterial, viral infections, and others [28]. Nitrile-containing antiviral drugs were broadly used during the past decades. For instance, etravirine, rilpivirine, and doravirin were employed to inhibit the human immunodeficiency virus (HIV). Remdesivir was first developed for use against the Ebola virus. Since the middle of the year 2020, it has been employed to treat COVID-19 caused by SARS-CoV-2. Nirmatrelvir was developed against SARS-CoV-2 too. The prevalence of nitrile-containing drugs confirms that they may exert better pharmacokinetic and pharmacological effects in comparison to other drugs exhibiting similar therapeutic effects [27].

From the metabolic perspective, the nitrile group is stable and non-toxic, and usually remains unchanged after passing through the human body [29]. Nitrile-containing compounds usually have lower clog *P*-values, which improves their solubilities [28]. Chemically, the nitrile group consists of a nitrogen atom that has a free pair of electrons and is connected to an sp^3-hybridized carbon atom, which gives the nitrile group a linear shape. The molecular volume of the nitrile group is approximately one-eighth the size of the methyl group. This relationship, together with the linear shape, is regarded as a significant factor contributing to the ability of the nitrile group to fit well into binding pockets and to exhibit a high tolerance towards different target mutations.

Natural products and herbal medicines represent a valuable source for drug development [30]. Previous investigations suggest that natural products may provide novel drug candidates against viral infections [31, 32]. Hence, with the aim of finding novel pan-coronaviral compounds we focused on nitrile- and sulfur-containing natural products in this study. We screened a library of 143 sulfur- and nitrile-containing natural products and their derivatives against the RBD of the spike protein of SARS-CoV-2 using AutoDock Vina in the PyRx software package. As a result of this initial screening, the 84 top compounds based on their lowest binding energies were selected and subjected to molecular docking using AutoDock 4.2.6 to validate the virtual screening results. Finally, 18 compounds obtained from the computer-based screening were selected for further *in vitro* experiments. Research on SARS-CoV-2 as a novel human pathogen is restricted to high-level biosafety laboratories, which usually do not have the necessary instrumentation for the large-scale screening of antiviral compounds. Thus, we first used a pseudovirus technology to overcome this challenge and facilitate the screening of active compounds against the viral entry process in a biosafety level 2 laboratory. The pseudovirus inhibition assay revealed that compounds **9**, **14**, and **15** strongly inhibit the cellular pseudovirus entry, with low micromolar IC_{50} values and a high selectivity index of 26.6, 10 and 12.6 respectively. These finding were confirmed using inhibition of live SARS-CoV-2 replication, where the compounds showed inhibition with higher IC_{50} values with the selectivity index of 4.3 and 3.6 for compounds **9** and **14**, likely due to the low titer of pseudovirus compared to the live viruses. It was remarkable that the cell viability assays evidenced that compounds **9**, **14**, and **15** exerted only moderate

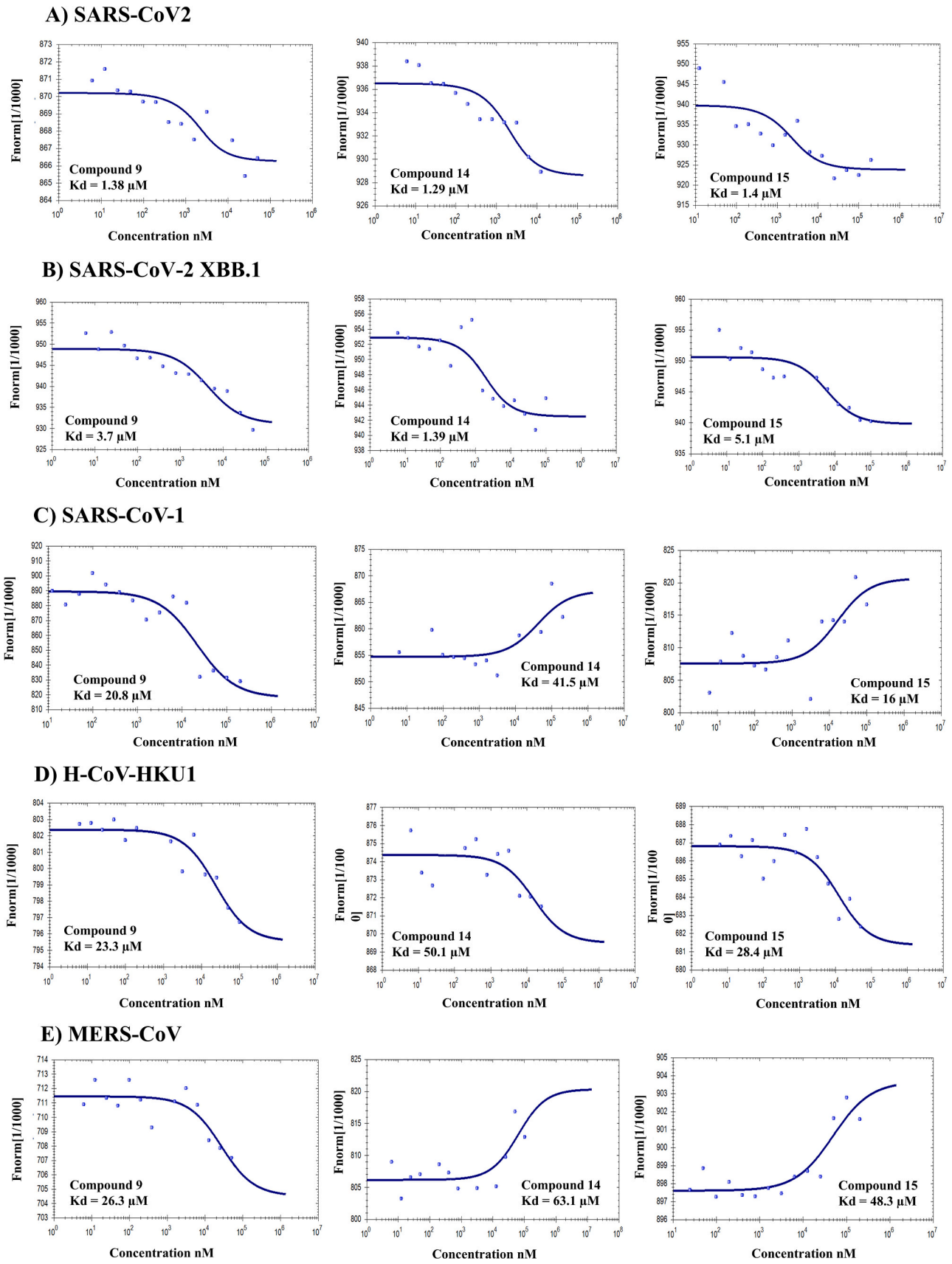

Fig. 6. Microscale thermophoresis analysis of compounds **9**, **14**, and **15** with the RBD of spike protein of: A) SARS-CoV-2, B) SARS-CoV-2 XBB.1, C) SARS-CoV-1, D) H-CoV-HKU1, and E) MERS-CoV.

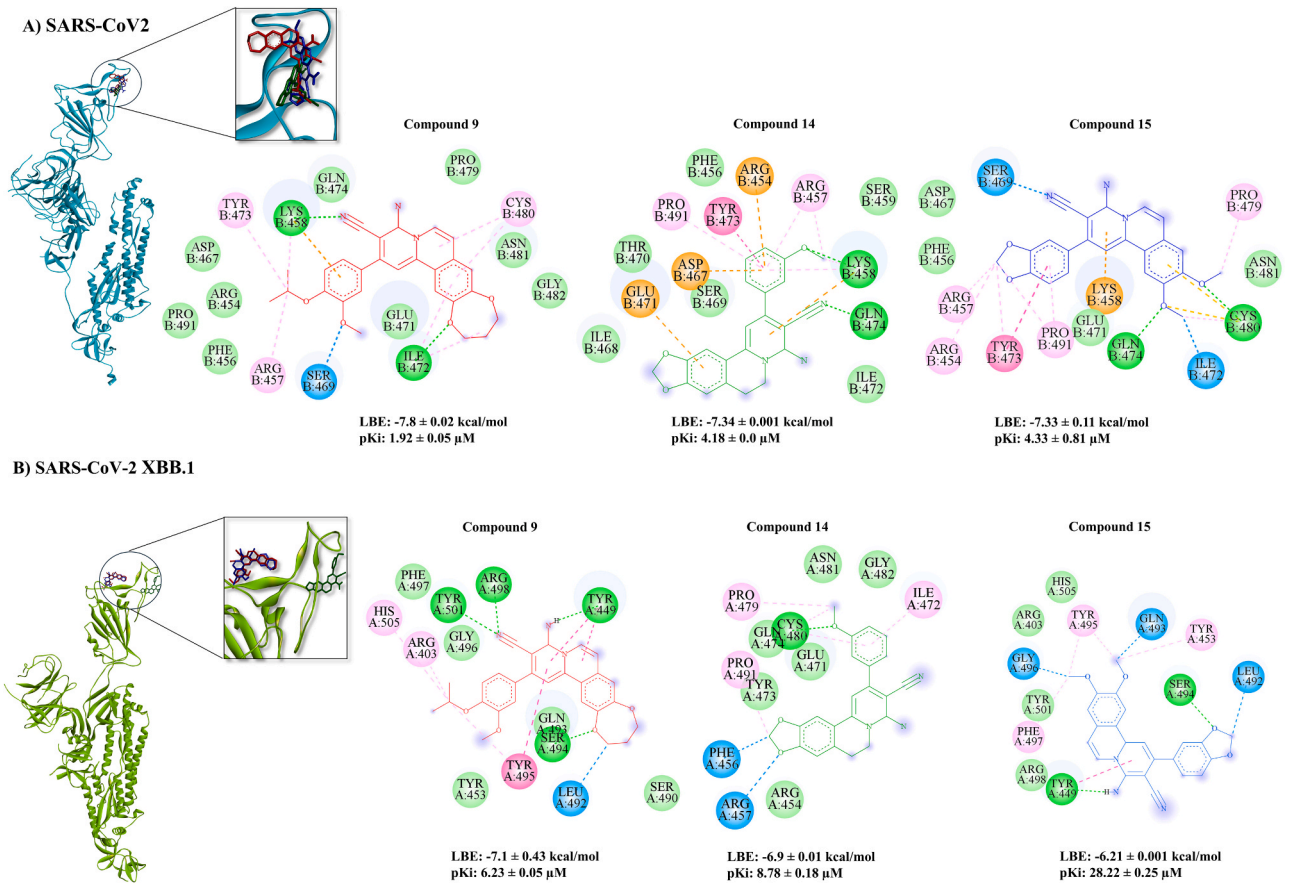

Fig. 7. The binding mode and 2D representation of compounds **9**, **14**, and **15** with the RBD of spike protein of: A) SARS-CoV-2 (PDB ID: 7bnn), B) SARS-CoV-2 XBB.1 (PDB ID: 8iou), C) SARS-CoV1 (PDB ID: 6acd), D) MERS-CoV (PDB ID: 6nb03), and E) HCoV-HKU1 (PDB ID: 8opo). These visualizations were generated using Discovery Studio Visualizer software (version v.24.1.0.23298). The lowest binding energies (LBE) and the predicted inhibition constant (pKi) of each compound were calculated using AutoDock 4.2.6.

cytotoxicity against HEK-ACE2, and slight toxicities were also observed against human fetal MRC-5 lung fibroblasts and Vero E6 cells.

Compounds **9**, **14**, and **15**, as also compound **16**, are structurally related to each other. Among these four compounds, **16** showed the weakest activity (less than 50 % of inhibition). Structurally, it is the only one with an electron-withdrawing group on the phenyl substituent in the "south" (bottom): a carboxymethyl (*i.e.*, a methyl ester) group. A much better activity was found for compound **14**. It has an electron-donating methoxy group (-OMe) on that phenyl substituent in the “south”. This fits significantly with the fact that the two highest activities are exhibited by compounds **9** and **15**, which both have even two electron-donating alkoxy groups on that “southern” phenyl ring. The “north-western” (upper-left) part of the molecule is electronically less differentiated. All four structures have two oxygen functions there. The difference between the two best compounds, **9** and **15**, is given by the alkyl (or alkylidene) substituents on the two oxygens on the left upper side of the molecule, and on the two oxygens on the bottom side. On the left upper (“north-western”) side, compound **9** has a large, 7-membered ring, which is more voluminous than the two methoxy groups on the left upper side of compound **15**. Also, on the “southern” phenyl substituent, the combination of a methoxy and an isopropyloxy group, as in compound **9**, is larger than the small 5-membered methylene acetal ring on the “southern” phenyl ring of compound **15**. Apart from the aspect of mere molecular size, however, these groups are not only voluminous for compound **9** and smaller for compound **15** on both sides, but the larger ones on compound **9** are also more lipophilic in both cases. Thus, it seems that not only the molecular shape influences the inhibitory activity but also the lipophilicity.

Compounds **9**, **14**, **15**, and **16** have more in common than the presence of the mentioned nitrile and alkoxy groups. They are, all of them, tetracyclic (or even pentacyclic in the case of the cyclic ether/acetal in the isoquinoline part) heterocycles, which are generally addressed as fused isoquinolines (more exactly as benzo[*a*]quinolizine-4-imines). They are not natural products as such, but are directly derived from a natural product, *viz.* from the natural alkaloid 1-methyl-6,7-dihydroxy-3,4-dihydroisoquinoline [33,34]or from the respective ethers. From these natural products, they are semi-synthetically built up, in a single step, by reaction with malodinitrile and the respective benzaldehyde. Thus, they are easily available by an efficient, natural product-based one-pot semi-synthesis [35,36]. The parent compound, 1-methyl-6,7-dihydroxy-3,4-dihydroisoquinoline, belongs to a group of catecholic isoquinolines, isolated, *i.a.*, from *Portulaca oleracea* L. (plant family: Portulacaceae), also known as common purslane [37]. This is a cosmopolitan succulent plant with a broad spectrum of bioactivities, among them neuroprotective, anti-inflammatory, anti-cancer, and also anti-viral effects [38]. Plant extracts and polysaccharide fractions of *P. oleracea* have been reported to inhibit the porcine epidemic diarrhea virus (PEDV, α-coronavirus), the porcine rotavirus (Reoviridae, double-stranded RNA virus), the influenza A virus, the hepatitis C virus (HCV, Flaviviridae, single-stranded RNA virus), and the herpes simplex virus 2 (HSV-2, Herpesviridae, double-stranded DNA virus) [39–43]. In a commercial SARS-CoV-2 inhibitor screening assay kit, *P. oleracea* extract also inhibited SARS-CoV-2 [44]. Several isoquinoline alkaloids have been shown to inhibit SARS-CoV-2 [45].

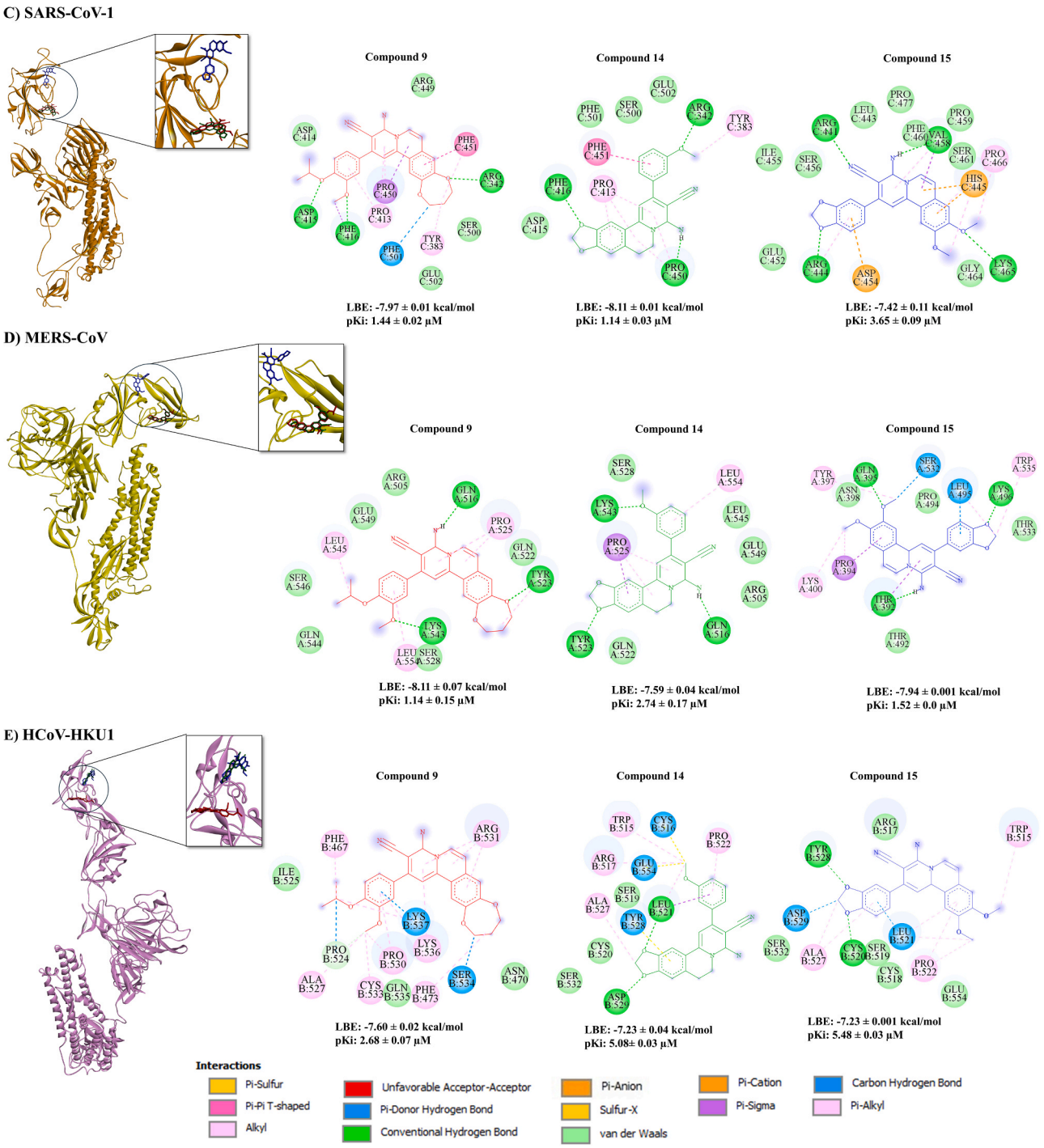

Fig. 7. (*continued*).

To the best of our knowledge, the three active compounds that we identified in the present investigation have not been reported before to inhibit the spike protein in a pseudovirus model of a clinical SARS-CoV-2 isolate. Up to now, numerous investigations have concentrated on the discovery of natural compounds binding to the spike protein of SARS-CoV2 and preventing the viral infection. For instance, H69C2 had a binding affinity (K_d value) of 0.0947 µM for the RBD of SASRS-CoV2 and an inhibitory effect with an IC_{50} value of 85.75 µM against the native live virus [46]. Two organic dyes (Congo red and direct violet 1) were found to bind to the RBD and inhibited pseudovirus entry and cell infection with IC_{50} values of 27.4 and 16.4 µM, respectively, that were higher than the IC_{50} values of compounds **9**, **14**, and **15** [6]. Although different peptides and small molecules were developed as pan-coronavirus inhibitors against the spike protein in the past, they all targeted the fusion peptide of the spike protein and inhibited the cellular entry of coronaviruses through the inhibition of membrane fusion at low micromolar IC_{50} values [47–49].

With the aim of developing a pan-coronaviral inhibitors targeting the RBD domain of the spike protein, we first performed a sequence alignment for the RBD of SARS-CoV2, SARS-CoV-2 XBB.1 (Omicron variant), SARS-CoV-1, MERS-CoV, and HCoV-HKU1. The Omicron variant showed the highest and MERS-CoV the lowest homology to wild-type SARS-CoV-2. We then performed microscale thermophoresis to investigate whether these three active compounds can bind to the RBD of the

spike protein of other coronavirus family members. Indeed, all three active compounds bound to the RBD of the spike protein of SARS-CoV2, SARS-CoV-2 XBB.1, SARS-CoV-1, MERS-CoV, and HCoV-HKU1. Their binding affinities decreased with their sequence homology identified by sequence alignment with a good correlation (R = -0.88, -0.91, -0.93 and *p*-value = 0.04, 0.03, 0.02 for Compounds **9**, **14** and **15** respectively).

According to previous studies, there were some residues on the RBD of SARS-CoV2 considered as hotspot residues for protein-protein or protein-ligand binding, including R402, N439, N440, L441, K433, V444, G446,Y449, Y453, L452, L455, F456, T4790, E471, I472, N481, E484, F486, N487,Y489, F490, Q493, Q498, P499, T500, N501, and Y505 [46, 50]. A pharmacophore analysis based on the docking simulation revealed that compounds **9**, **14**, and **15** interacted with some of these hotspot residues, including F456, T470, E471, and N481. Thus, the compounds may interfere with the interaction between these residues and ACE2. The Omicron and wild-type RBDs shared similar overall structures, while the RBD of Omicron demonstrated higher binding affinity for the ACE2 compared to the wild-type RBD [50]. Our molecular docking analysis revealed that the three active compounds, **9**, **14**, and **15**, interacted with some of the hot spot residues in the RBDs of SARS-CoV2, SARS-CoV-2 XBB.1, *i.e.*, F456, R498, S496, Y501, and H505 that may interfere with the interaction between RBD and ACE2. While previous studies demonstrated that the N501Y mutation allows the virus to escape from monoclonal antibodies, convalescent plasma, and vaccines [46,51], our molecular docking results showed that mutations in this residue do not affect binding of the active compounds **9**, **14**, and **15**. Moreover, molecular docking revealed that compounds **9**, **14**, and **15** may inhibit the HCoV-HKU1 virus entry through the interaction with the R531, R517, Y528, and D529 hotspot residues [52]. Although compounds **9**, **14,** and **15** did not interact with the hotspot residues of SARS-CoV-1 and MERS-CoV, they still exerted high affinities to the RBD based on their LBE of molecular docking and K_d values of microscale thermophoresis studies. Thus, the inhibitory effects of these compounds towards SARS-CoV-1 and MERS-CoV could take place by conformational changes of the RBD [53].

In summary, we report here on a group of nitrile-containing natural product-derived compounds as broad-spectrum coronaviral entry inhibitors with low toxicity. Initially starting with a focus on nitrile- and/or sulfur-containing structures as the prime criterion, our strategy has led to no less than three highly promising and easy-to-synthesize agents, remarkably all of them with nitrile groups, but none with sulfur. Likewise remarkable is the fact that all of them have an isoquinoline-derived structure, despite the broad plethora of the other ZINC-derived starting structures. This shows the efficiency and specificity of the chosen selection pathway, which, out of a very large number of starting structures picks out this promising class of heterocycles. These compounds effectively protect the cells from infection with both SARS-CoV-2 pseudoviruses and live viruses. Moreover, *in silico* and *in vitro* studies revealed that they bind to the RBD of SARS-CoV-2 XBB.1, SARS-CoV-1, MERS-CoV, and HCoV-HKU1 with high affinities. We thus conclude that these compounds may be interesting candidates to develop novel potent pan-coronavirus entry inhibitors, in particular compound **15**, which had the highest antiviral activity. Further investigations including *in vivo* studies are required.

CRediT authorship contribution statement

Sara Abdelfatah: Conceptualization. **Nasim Shahhamzehei:** Writing – review & editing, Writing – original draft, Methodology, Formal analysis, Conceptualization. **Kathrin Sutter:** Methodology. **Hannah S. Schwarzer-Sperber:** Methodology. **Gerhard Bringmann:** Writing – review & editing, Writing – original draft, Conceptualization. **Rümeysa Yücer:** Methodology. **Thomas Efferth:** Writing – review & editing, Conceptualization. **Roland Schwarzer:** Writing – review & editing.

Declaration of Competing Interest

The authors declare that they have no known competing financial interests or personal relationships that could have appeared to influence the work reported in this paper.

Data availability

Data will be made available on request.

Acknowledgement

We are grateful to the financial support of Marc Strobel, Frankfurt a. M., Germany and CVC Philanthropy, Jersey.

Conflict of interest

The authors declare that there is no conflict of interest.

References

[1] J. Zhang, T. Xiao, Y. Cai, B. Chen, Structure of SARS-CoV-2 spike protein, Curr. Opin. Virol. 50 (2021) 173–182, https://doi.org/10.1016/j.coviro.2021.08.010.
[2] S. Xia, L. Wang, Y. Zhu, L. Lu, S. Jiang, Origin, virological features, immune evasion and intervention of SARS-CoV-2 Omicron sublineages, Signal Transduct. Target Ther. 7 (2022), https://doi.org/10.1038/s41392-022-01105-9.
[3] S. Moreno, B. Alcázar, A. Antela, C. Dueñas, J.G. Del Castillo, J. Olalla, Use of antivirals in SARS-CoV-2 infection. Critical review of the role of remdesivir, Drug Des. Dev. Ther. 16 (2022) 827–841, https://doi.org/10.2147/DDDT.S356951.
[4] L.D. Saravolatz, S. Depcinski, M. Sharma, Molnupiravir and nirmatrelvir-ritonavir: oral coronavirus disease 2019 antiviral drugs, Clin. Infect. Dis. 76 (2023) 165–171, https://doi.org/10.1093/cid/ciac180.
[5] M.G. Cox, T.P. Peacock, W.T. Harvey, J. Hughes, D.W. Wright, B.J. Willett, E. Thomson, R.K. Gupta, S.J. Peacock, D.L. Robertson, A.M. Carabelli, SARS-CoV-2 variant evasion of monoclonal antibodies based on in vitro studies, Nat. Rev. Microbiol. 21 (2023) 112–124, https://doi.org/10.1038/s41579-022-00809-7.
[6] D. Bojadzic, O. Alcazar, J. Chen, S.T. Chuang, J.M. Condor Capcha, L.A. Shehadeh, P. Buchwald, Small-molecule inhibitors of the coronavirus spike: ACE2 protein-protein interaction as blockers of viral attachment and entry for SARS-CoV-2, ACS Infect. Dis. 7 (2021) 1519–1534, https://doi.org/10.1021/acsinfecdis.1c00070.
[7] Y. Huang, C. Yang, X. feng Xu, W. Xu, S. wen Liu, Structural and functional properties of SARS-CoV-2 spike protein: potential antivirus drug development for COVID-19, Acta Pharm. Sin. 41 (2020) 1141–1149, https://doi.org/10.1038/s41401-020-0485-4.
[8] C. Zhao, K.P. Rakesh, L. Ravidar, W.Y. Fang, H.L. Qin, Pharmaceutical and medicinal significance of sulfur (SVI)-containing motifs for drug discovery: a critical review, Eur. J. Med. Chem. 162 (2019) 679–734, https://doi.org/10.1016/j.ejmech.2018.11.017.
[9] S. Kim, R. Kubec, R.A. Musah, Antibacterial and antifungal activity of sulfur-containing compounds from Petiveria alliacea L, J. Ethnopharmacol. 104 (2006) 188–192, https://doi.org/10.1016/j.jep.2005.08.072.
[10] L.G. Bahrin, M.O. Apostu, L.M. Birsa, M. Stefan, The antibacterial properties of sulfur containing flavonoids, Bioorg. Med. Chem. Lett. 24 (2014) 2315–2318, https://doi.org/10.1016/j.bmcl.2014.03.071.
[11] O.-G. Nh, F.F. Fleming, Nitrile-containing natural products, n.d.
[12] X. Wang, Y. Wang, X. Li, Z. Yu, C. Song, Y. Du, Nitrile-containing pharmaceuticals: target, mechanism of action, and their SAR studies, RSC Med. Chem. 12 (2021) 1650–1671, https://doi.org/10.1039/d1md00131k.
[13] C. Scotti, J.W. Barlow, Natural products containing the nitrile functional group and their biological activities, Nat. Prod. Commun. 17 (2022), https://doi.org/10.1177/1934578X221099973.
[14] M. Zeino, M.E.M. Saeed, O. Kadioglu, T. Efferth, The ability of molecular docking to unravel the controversy and challenges related to P-glycoprotein – a well-known, yet poorly understood drug transporter, Invest. New Drugs 32 (2014) 618–625, https://doi.org/10.1007/s10637-014-0098-1.
[15] K.H.D. Crawford, R. Eguia, A.S. Dingens, A.N. Loes, J.D. Bloom, K. Crawford, Pseudotyping lentiviral particles with SARS-CoV-2 spike protein for neutralization assays V.2 coronavirus method development community, Viruses (2021), https://doi.org/10.17504/protocols.io.br44m8yw.
[16] S.A. Almahboub, A. Algaissi, M.A. Alfaleh, M.Z. ElAssouli, A.M. Hashem, Evaluation of neutralizing antibodies against highly pathogenic coronaviruses: a detailed protocol for a rapid evaluation of neutralizing antibodies using vesicular stomatitis virus pseudovirus-based assay, Front. Microbiol. 11 (2020), https://doi.org/10.3389/fmicb.2020.02020.
[17] R.K.L. Lee, T.N. Li, S.Y. Chang, T.L. Chao, C.H. Kuo, M.Y.C. Pan, Y.T. Chiou, K. J. Liao, Y. Yang, Y.H. Wu, C.H. Huang, H.F. Juan, H.P. Hsieh, L.H.C. Wang, Identification of entry inhibitors against delta and omicron variants of SARS-CoV-2, Int. J. Mol. Sci. 23 (2022), https://doi.org/10.3390/ijms23074050.
[18] C.S. Heilingloh, U.W. Aufderhorst, L. Schipper, U. Dittmer, O. Witzke, D. Yang, X. Zheng, K. Sutter, M. Trilling, M. Alt, E. Steinmann, A. Krawczyk, Susceptibility

of SARS-CoV-2 to UV irradiation, Am. J. Infect. Control 48 (2020) 1273–1275, https://doi.org/10.1016/j.ajic.2020.07.031.
[19] L. Schöler, V.T.K. Le-Trilling, M. Eilbrecht, D. Mennerich, O.E. Anastasiou, A. Krawczyk, A. Herrmann, U. Dittmer, M. Trilling, A novel in-cell ELISA assay allows rapid and automated quantification of SARS-CoV-2 to analyze neutralizing antibodies and antiviral compounds, Front. Immunol. 11 (2020) 1–11, https://doi.org/10.3389/fimmu.2020.573526.
[20] V. Kuete, A.T. Mbaveng, E.C.N. Nono, C.C. Simo, M. Zeino, A.E. Nkengfack, T. Efferth, Cytotoxicity of seven naturally occurring phenolic compounds towards multi-factorial drug-resistant cancer cells, Phytomedicine 23 (2016) 856–863, https://doi.org/10.1016/j.phymed.2016.04.007.
[21] M. Jerabek-Willemsen, C.J. Wienken, D. Braun, P. Baaske, S. Duhr, Molecular interaction studies using microscale thermophoresis, Assay. Drug Dev. Technol. 9 (2011) 342–353, https://doi.org/10.1089/adt.2011.0380.
[22] E.-J. Seo, T. Efferth, Interaction of antihistaminic drugs with human translationally controlled tumor protein (TCTP) as novel approach for differentiation therapy, Oncotarget (2016). ⟨https://www.impactjournals.com/oncotarget⟩.
[23] M.M. Kesheh, P. Hosseini, S. Soltani, M. Zandi, An overview on the seven pathogenic human coronaviruses, Rev. Med. Virol. 32 (2022), https://doi.org/10.1002/rmv.2282.
[24] X. Lin, X. Li, X. Lin, A review on applications of computational methods in drug screening and design, Molecules 25 (2020) 1–17, https://doi.org/10.3390/molecules25061375.
[25] I. Trifonova, N. Korsun, I. Madzharova, P. Velikov, I. Alexsiev, L. Grigorova, S. Voleva, R. Yordanova, I. Ivanov, T. Tcherveniakova, I. Christova, Prevalence and clinical impact of mono- and co-infections with endemic coronaviruses 229E, OC43, NL63, and HKU-1 during the COVID-19 pandemic, Heliyon 10 (2024) e29258, https://doi.org/10.1016/j.heliyon.2024.e29258.
[26] R. Geng, P. Zhou, Severe acute respiratory syndrome (SARS) related coronavirus in bats, Anim. Dis. 1 (2021) 1–8, https://doi.org/10.1186/s44149-021-00004-w.
[27] X. Wang, Y. Wang, X. Li, Z. Yu, C. Song, Y. Du, Nitrile-containing pharmaceuticals: target, mechanism of action, and their SAR studies, RSC Med. Chem. 12 (2021) 1650–1671, https://doi.org/10.1039/d1md00131k.
[28] X. Wang, Y. Wang, X. Li, Z. Yu, C. Song, Y. Du, Nitrile-containing pharmaceuticals: target, mechanism of action, and their SAR studies, RSC Med. Chem. 12 (2021) 1650–1671, https://doi.org/10.1039/d1md00131k.
[29] V. Bonatto, R.F. Lameiro, F.R. Rocho, J. Lameira, A. Leitão, C.A. Montanari, Nitriles: an attractive approach to the development of covalent inhibitors, RSC Med. Chem. 14 (2022) 201–217, https://doi.org/10.1039/d2md00204c.
[30] B. Chopra, A.K. Dhingra, Natural products: a lead for drug discovery and development, Phytother. Res. 35 (2021) 4660–4702, https://doi.org/10.1002/ptr.7099.
[31] R. Sharma, M. Bhattu, A. Tripathi, M. Verma, R. Acevedo, P. Kumar, V.D. Rajput, J. Singh, Potential medicinal plants to combat viral infections: a way forward to environmental biotechnology, Environ. Res. 227 (2023) 115725, https://doi.org/10.1016/j.envres.2023.115725.
[32] N. Nasim, I.S. Sandeep, S. Mohanty, Plant-derived natural products for drug discovery: current approaches and prospects, Nucleus 65 (2022) 399–411, https://doi.org/10.1007/s13237-022-00405-3.
[33] T.Y. Jin, S.Q. Li, C.R. Jin, H. Shan, R.M. Wang, M.X. Zhou, A.L. Li, L.Y. Li, S.Y. Hu, T. Shen, L. Xiang, Catecholic isoquinolines from portulaca oleracea and their anti-inflammatory and β 2 -adrenergic receptor agonist activity, J. Nat. Prod. 81 (2018) 768–777, https://doi.org/10.1021/acs.jnatprod.7b00762.
[34] X.F. Shang, C.J. Yang, S.L. Morris-Natschke, J.C. Li, X.D. Yin, Y.Q. Liu, X. Guo, J. W. Peng, M. Goto, J.Y. Zhang, K.H. Lee, Biologically active isoquinoline alkaloids covering 2014–2018, Med. Res. Rev. 40 (2020) 2212–2289, https://doi.org/10.1002/med.21703.
[35] L. Li, H. Zhang, M. Zhang, M. Zhao, L. Feng, X. Luo, Z. Gao, Y. Huang, O. Ardayfio, J.H. Zhang, Y. Lin, H. Fan, Y. Mi, G. Li, L. Liu, L. Feng, F. Luo, L. Teng, W. Qi, J. Ottl, A. Lingel, D.E. Bussiere, Z. Yu, P. Atadja, C. Lu, E. Li, J. Gu, K. Zhao, Discovery and molecular basis of a diverse set of polycomb repressive complex 2 inhibitors recognition by EED, PLoS One 12 (2017) 1–18, https://doi.org/10.1371/journal.pone.0169855.
[36] T.A. Abdallah, H.A. Abdelhadi, A.A. Ibrahim, H.M. Hassaneen, Reactivity of 1-methylisoquinoline. One pot synthesis of benzo[a]-quinolizine derivatives, Synth. Commun. 32 (2002) 581–589, https://doi.org/10.1081/SCC-120002405.
[37] Z.Z. Jiao, S. Yue, H.X. Sun, T.Y. Jin, H.N. Wang, R.X. Zhu, L. Xiang, Indoline amide glucosides from Portulaca oleracea: isolation, structure, and DPPH radical scavenging activity, J. Nat. Prod. 78 (2015) 2588–2597, https://doi.org/10.1021/acs.jnatprod.5b00524.
[38] Y.X. Zhou, H.L. Xin, K. Rahman, S.J. Wang, C. Peng, H. Zhang, Portulaca oleracea L.: a review of phytochemistry and pharmacological effects, BioMed Res. Int. 2015 (2015), https://doi.org/10.1155/2015/925631.
[39] C.X. Dong, K. Hayashi, J.B. Lee, T. Hayashi, Characterization of structures and antiviral effects of polysaccharides from Portulaca oleracea L, Chem. Pharm. Bull. 58 (2010) 507–510, https://doi.org/10.1248/cpb.58.507.
[40] S. Noreen, I. Hussain, M.I. Tariq, B. Ijaz, S. Iqbal, Qamar-Ul-Zaman, U.A. Ashfaq, T. Husnain, Portulaca oleracea L. as a prospective candidate inhibitor of hepatitis C virus NS3 serine protease, Viral Immunol. 28 (2015) 282–289, https://doi.org/10.1089/vim.2014.0079.
[41] Y.H. Li, C.Y. Lai, M.C. Su, J.C. Cheng, Y.S. Chang, Antiviral activity of Portulaca oleracea L. against influenza A viruses, J. Ethnopharmacol. 241 (2019) 112013, https://doi.org/10.1016/j.jep.2019.112013.
[42] Y. Liu, L. Zhao, Y. Xie, Z. Chen, S. Yang, B. Yin, G. Li, H. Guo, S. Lin, J. Wu, Antiviral activity of Portulaca oleracea L. extracts against porcine epidemic diarrhea virus by partial suppression on myd88/NF-κb activation in vitro, Microb. Pathog. 154 (2021) 104832, https://doi.org/10.1016/j.micpath.2021.104832.
[43] X. Zhou, Y. Li, T. Li, J. Cao, Z. Guan, T. Xu, G. Jia, G. Ma, R. Zhao, Portulaca oleracea L. polysaccharide inhibits porcine rotavirus in vitro, Animals 13 (2023), https://doi.org/10.3390/ani13142306.
[44] D.A. Al-Quwaie, A. Allohibi, M. Aljadani, A.M. Alghamdi, A.A. Alharbi, R.S. Baty, S.H. Qahl, O. Saleh, A.O. Shakak, F.S. Alqahtani, O.S.F. Khalil, M.T. El-Saadony, A. M. Saad, Characterization of Portulaca oleracea whole plant: evaluating antioxidant, anticancer, antibacterial, and antiviral activities and application as quality enhancer in yogurt, Molecules 28 (2023), https://doi.org/10.3390/molecules28155859.
[45] M. Valipour, A. Hosseini, A. Di Sotto, H. Irannejad, Dual action anti-inflammatory/antiviral isoquinoline alkaloids as potent naturally occurring anti-SARS-CoV-2 agents: a combined pharmacological and medicinal chemistry perspective, Phytother. Res. 37 (2023) 2168–2186, https://doi.org/10.1002/ptr.7833.
[46] L. Wang, Y. Wu, S. Yao, H. Ge, Y. Zhu, K. Chen, W. zhang Chen, Y. Zhang, W. Zhu, H. yang Wang, Y. Guo, P. xiang Ma, P. xuan Ren, X. lei Zhang, H. qiong Li, M.A. Ali, W. qing Xu, H. liang Jiang, L. ke Zhang, L. li Zhu, Y. Ye, W. juan Shang, F. Bai, Discovery of potential small molecular SARS-CoV-2 entry blockers targeting the spike protein, Acta Pharm. Sin. 43 (2022) 788–796, https://doi.org/10.1038/s41401-021-00735-z.
[47] L. Guo, S. Lin, Z. Chen, Y. Cao, B. He, G. Lu, Targetable elements in SARS-CoV-2 S2 subunit for the design of pan-coronavirus fusion inhibitors and vaccines, Signal Transduct. Target Ther. 8 (2023), https://doi.org/10.1038/s41392-023-01472-x.
[48] Q. Lan, L. Wang, F. Jiao, L. Lu, S. Xia, S. Jiang, Pan-coronavirus fusion inhibitors to combat COVID-19 and other emerging coronavirus infectious diseases, J. Med. Virol. 95 (2023), https://doi.org/10.1002/jmv.28143.
[49] S. Xia, L. Yan, W. Xu, A.S. Agrawal, A. Algaissi, C.T.K. Tseng, Q. Wang, L. Du, W. Tan, I.A. Wilson, S. Jiang, B. Yang, L. Lu, A pan-coronavirus fusion inhibitor targeting the HR1 domain of human coronavirus spike, Sci. Adv. 5 (2019), https://doi.org/10.1126/sciadv.aav4580.
[50] J. Lan, X. He, Y. Ren, Z. Wang, H. Zhou, S. Fan, C. Zhu, D. Liu, B. Shao, T.Y. Liu, Q. Wang, L. Zhang, J. Ge, T. Wang, X. Wang, Structural insights into the SARS-CoV-2 omicron RBD-ACE2 interaction, Cell Res. 32 (2022) 593–595, https://doi.org/10.1038/s41422-022-00644-8.
[51] D. Hattab, M.F.A. Amer, Z.M. Al-Alami, A. Bakhtiar, SARS-CoV-2 journey: from alpha variant to omicron and its sub-variants, Infection 2 (2024), https://doi.org/10.1007/s15010-024-02223-y.
[52] L. Xia, Y. Zhang, Q. Zhou, Structural basis for the recognition of HCoV-HKU1 by human TMPRSS2, Cell Res. (2024), https://doi.org/10.1038/s41422-024-00958-9.
[53] S.R. Tzeng, C.G. Kalodimos, Protein activity regulation by conformational entropy, Nature 488 (2012) 236–240, https://doi.org/10.1038/nature11271.

Use of AI-Tools:

AI tool	Used for	Why	When
Quill Bot	Reformation of my draft text	Help for grammatical correction and increase fluency	First and second research papers
ChatGPT	Reformation of my draft text	Help for grammatical correction and increase fluency	Third research paper and introduction of thesis

Nasim Shahhamzehei

PhD. Student

Germany | +49 15772173624 | nshahham@uni-mainz.de

Overview:

Molecular pharmacologist with over five years of expertise in drug discovery, specializing in lentiviruses, and high-throughput small molecule screening. Proven success in identifying coronavirus pan-inhibitors, optimizing HPC-driven workflows, and publishing high-impact research. Skilled in BSL-2 lab practices, interdisciplinary collaboration, and computational drug discovery. Eager to contribute to innovative academic research and foster knowledge advancement.

Education:

Ph.D. in Pharmaceutical Biology

Johannes Gutenberg University of Mainz, Institute of Pharmaceutical and Biomedical Sciences, Germany.

M.Sc. in Clinical Biochemistry

Tarbiat Modares University, Iran.

B.Sc. Biology

Kharazmi University, Iran

Skills:

- DNA cloning
- Viral vector production (Lentivirus)
- Molecular biology techniques
- Experiment Design and research methodology
- Analytical and Critical Thinking
- Organization and Time Management
- Training and mentoring

Work History:

Quality Assurance Specialist, CinnaGen

Sep 2017 - Mar 2019

• Ensured GMP compliance and data integrity for pharmaceutical products, improving audit readiness.

• Conducted regular audits and inspections, achieving zero major regulatory findings.

Research And Development Specialist, Rojan Azma

Jul 2014 - Jul 2017

• Developed and optimized protocols for rapid diagnostic tests (e.g., PSA and Cardiac biomarkers), ensuring accuracy and reliability in point of diagnostics.

• Conducted regular audits and inspections, achieving zero major regulatory findings.

Languages:

• **English**: C1

• **German**: B1

• **Persian**: Native